Central Eyre Iron Project
Environmental Impact Statement

APPENDIX R
CAPE HARDY COASTAL MODELLING

Cape Hardy Coastal Modelling Report

IRON ROAD

E-F-34-RPT-0030 | Rev0

11 Dec 2014

Document history and status

Revision	Date	Description	By	Review	Approved
A	15/05/2014	DRAFT for comment	Jess Ryan / Sam Watkin	Athol Cummin	Nick Bull
B	19/11/2014	Final	Jess Ryan / Sam Watkin	Nick Bull	Sam Watkin

Distribution of copies

Revision	Issue approved	Date issued	Issued to	Comments
0	N Bull	19/11/2014	Iron Road Limited	
0	N Bull	11/12/2014	Iron Road Limited	

JACOBS

EIS Coastal Modelling Report

Project no:	VE23730
Document title:	EIS Coastal Modelling Report
Document no:	E-F-34-RPT-0030
Revision:	Rev0
Date:	11 December 2014
Client name:	Iron Road Limited
Client no:	EF69CTR0003
Project manager:	Nick Bull
Author:	Jess Ryan & Sam Watkin
File name:	E-F-34-RPT-0030_0 (EIS Coastal Modelling Report)

Jacobs Group (Australia) Pty Limited
ABN 37 001 024 095
Level 5, 33 King William Street
Adelaide SA 5000 Australia
PO Box 8291
T +61 8 8424 3800
F +61 8 8424 3810
www.jacobs.com

Contents

List of Figures

List of Tables

Executive Summary

Coastal modelling studies were carried out to inform the Environmental Impact Statement of potential impacts associated with the construction of the proposed maritime infrastructure for the Central Eyre Iron Project. The infrastructure at Cape Hardy includes a reclaimed causeway with a Module Offload Facility (MOF), a tug mooring facility, as well as a jetty and wharf structure.

The coastal climate in the vicinity of Cape Hardy was evaluated to provide an overview of the coastal processes at the site. Hydrodynamic and wave models were developed for both the baseline scenario and infrastructure scenario to assess the potential impact of the infrastructure on the prevailing tidal and wave climates at the proposed site. Results from the models were also analysed to estimate the relative impact of the infrastructure on the bed shear stress. Finally, littoral drift models were run to assess the potential impact of the proposed marine infrastructure on the longshore sediment transport regime in the region.

Results from the hydrodynamic models indicate that changes to the nearshore and offshore current regimes are minor and localised. Changes in the offshore currents are predominately affected by the high piling density along the wharf, jetty, and berthing dolphins. Changes in nearshore currents are a result of current interaction with the reclaimed causeway and MOF infrastructure, causing some minor changes in current circulation patterns in the northern and southern bays. Depending on the prevailing current direction, the reclaimed causeway structure also provides some sheltering from the incoming current for areas north and south of the infrastructure. Bed shear stress results indicate that current regime is unlikely to have a significant impact on sediment transport at the site, with the current induced bed shear stress falling below the threshold of motion.

The spectral wave model results indicate that the construction of the proposed infrastructure causes some minor changes to the nearshore wave climate. The orientation of the proposed causeway is head on to the predominant wave direction and therefore the wave climate in the bays remains relatively unchanged during regular events; however there are low occurrence directional events where the structure will shelter the wave climate in the bays. Offshore wave conditions in the region remain relatively unchanged after construction of the proposed infrastructure. Bed shear stress results indicate that nearshore sediment transport is likely to be induced by the prevailing wave climate at the site which was investigated further with a longshore sediment transport investigation.

Results from the littoral drift models indicate that the changes to the longshore sediment transport rates at Cape Hardy are minor. Prior to construction of the proposed infrastructure, sediment drift across the headlands is restricted, with low net and gross longshore drift rates calculated for the corresponding cross shore profiles. This indicates that the headlands act as terminal groynes, restricting the sediment transport past the headland into the adjacent bay. The construction of the causeway structure at the central headland accentuates these effects, further restricting the sediment drift past this point. Hence the model results indicate that the northern and southern bays act predominately as closed cell beaches, both prior to and after construction, with negligible amounts of sediment being transferred between the adjacent bays.

In summary the results from the hydrodynamic, spectral wave, and littoral drift models indicate that the construction of the proposed maritime infrastructure will not have a significant impact on the local current, wave, and sediment transport processes at Cape Hardy.

1. Introduction

1.1 Purpose

This document reports on the coastal modelling studies carried out to inform the Environmental Impact Statement (EIS) of the Central Eyre Iron Project (CEIP). The coastal modelling studies focus primarily on the assessment of the potential impact of the proposed marine port infrastructure on the coastal processes. This includes the assessment of the impact on wave, tidal current and sediment transport processes.

1.2 Port Infrastructure

The location of the Port Marine works for the Central Eyre Iron Project (CEIP) is offshore from Cape Hardy on the eastern coast of the Eyre Peninsula in Spencer Gulf, South Australia. Cape Hardy is approximately 70km north of Port Lincoln and 10km south of Port Neill.

The proposed CEIP port infrastructure is shown in Figure 1-1 below. The infrastructure includes a 350m long causeway reclamation, a tug mooring facility, a Module Offload Facility (MOF), a 600m long jetty and a 400m long wharf with berthing arrangements for up to two 210,000 DWT capesize bulk carrier vessels.

16	Causeway - Reclamation with rock revetment edge protection
17	Causeway and Module Landing Area – Reclamation with rock revetment edge protection
18	Tug Mooring Facility – Floating pontoon and mooring arrangement.
20	Wharf – Piled Suspended Deck Structure
31	Jetty – Piled suspended deck structure
45	Module Offload Facility

Figure 1-1 Locality Plan of proposed CEIP Port Infrastructure facilities at Cape Hardy

1.3 Objectives

The objective of this report is to assess the potential impact of the proposed marine port infrastructure on the coastal processes. This can be further broken down into the objectives shown below in Table 1-1 which are addressed and reported in separate sections of this document.

Table 1-1 EIS Coastal Modelling Report Objectives and Structure

Report Section		Objective
2.	**Coastal Climate**	Provide an overview of the coastal processes in the vicinity of Cape Hardy
3.	**Hydrodynamic Modelling**	Assess the tidal current regime in the vicinity of Cape Hardy and assess the potential impact of the proposed marine infrastructure.
4.	**Wave Modelling**	Assess the wave climate in the vicinity of Cape Hardy and assess the potential impact of the proposed marine infrastructure.
5.	**Bed Shear Stress Analysis**	Assess the bed shear stress in the vicinity of Cape Hardy and assess the potential impact of the proposed marine infrastructure.
6.	**Sediment Transport Assessment**	Assess the longshore sediment transport in the vicinity of Cape Hardy and assess the potential impact of the proposed marine infrastructure.

2. Coastal Climate

2.1 Tidal Levels

The water levels at Cape Hardy are primarily driven by the astronomical tides. These tides are predominantly semi-diurnal with two high and low tides each day. There is also a marginal diurnal component during the neap cycles.

Following the National Tidal Centre (NTC) approved methodology; Hydro Survey Australia deployed a tidal gauge at a site approximately 2km south of Cape Hardy to capture a full lunar cycle of tidal data. The tide gauge recorded 34 days of tidal water level data. The data was then analysed by the NTC to produce tidal planes at Cape Hardy which are summarised in Table 2-1 below.

Table 2-1 Tidal Levels at Cape Hardy

Tidal level	Acronym	Levels relative to chart datum (mCD)
Highest Astronomical Tide	HAT	2.25
Mean High Water Springs	MHWS	1.82
Mean High Water Neap	MHWN	1.30
Mean Sea Level	MSL	1.08
Mean Low Water Neap	MLWN	0.86
Mean Low Water Springs	MLWS	0.34
Lowest Astronomical Tide	LAT	0.06
Chart Datum	CD	0.00

Detailed tidal constituents were obtained from the NTC for key locations around the Spencer Gulf. The tidal constituents were adopted to generate a time-series of predicted tidal levels at key locations to force and calibrate the hydrodynamic model (reported in section 3 of this report).

2.2 Wind Conditions

2.2.1 2012 Offshore Wind Dataset

Wind speed and directional time-series data at the Spencer Gulf was obtained from the Bureau of Meteorology (BOM). The data indicates that winds predominantly occur from the southerly quadrants with the majority of wind events being less than 20m/s. Winds from the westerly quadrants are generally stronger than winds from the easterly quadrants. Appendix A summarises wind data for the year 2012 which has been extracted from the BOM AUSWAVE model. Details regarding these wind datasets are further summarised in section 4.2.3.

2.3 ADCP Measurements

SKM commissioned the collection of field data at a single point approximately 1200m offshore from Cape Hardy (34°11'22.29"S 136°19'54.55"E) in a water depth of approximately 21m. The location of the deployment is shown in

Figure 2-1 (MGA-53 projection).

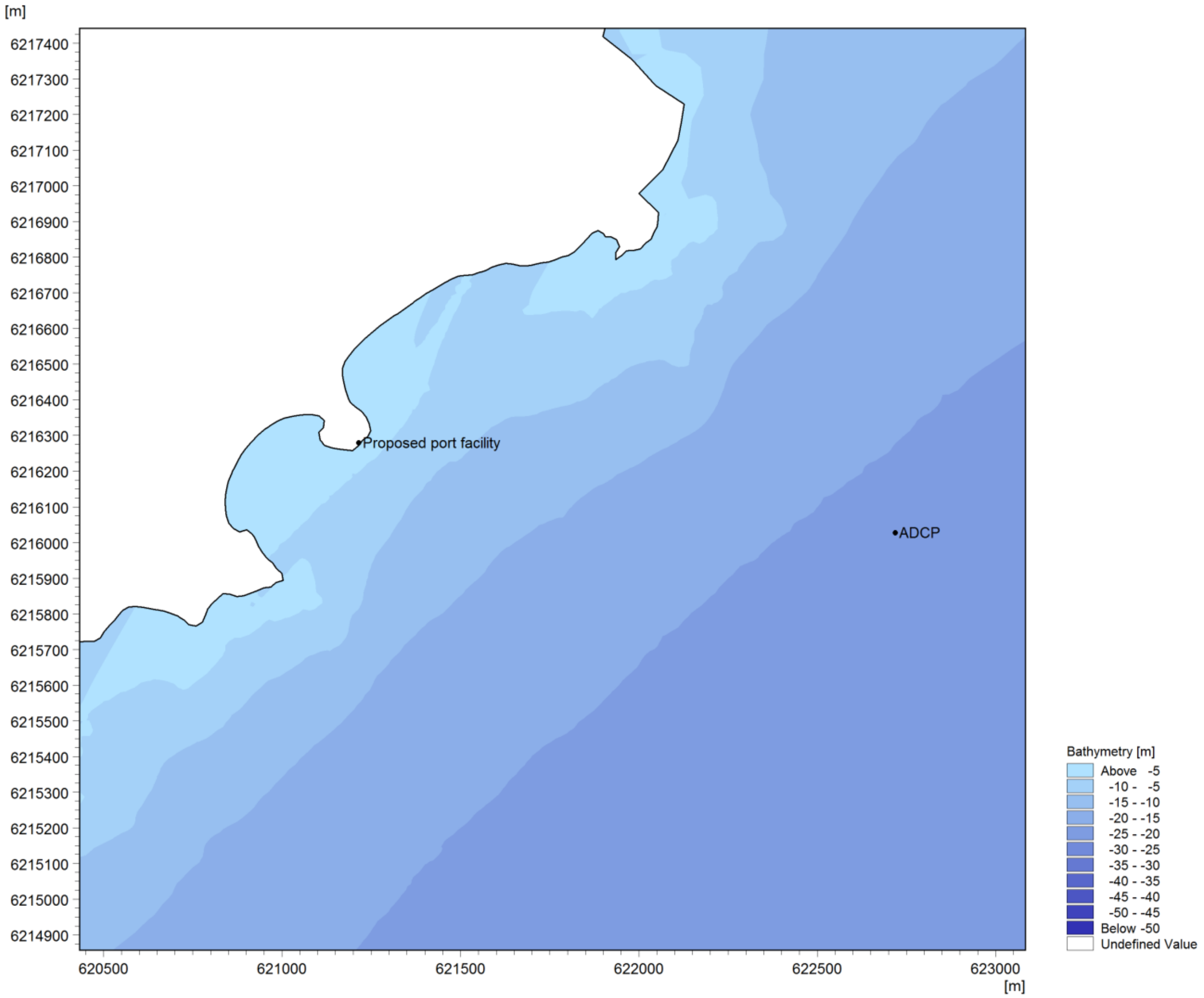

Figure 2-1 Location of ADCP deployment in relation to the proposed port facility

The field data collection included the deployment of a Teledyne Sentinel Workhorse Acoustic Doppler Current Profiler (ADCP) which was deployed three times during the period from 31/01/2012 to 21/09/2012. During this deployment period the ADCP collected data for a total of 191 days (Refer to Table 2-2 below). This period of data contains numerous spring and neap tidal cycles across various seasons, and therefore is considered adequate for model calibration and verification purposes.

Table 2-2 ADCP Deployment Summary

Deployment	Period	Duration
Deployment 1	31/01/12 to 30/03/12	59 Days
Deployment 2	07/04/12 to 16/06/12	70 Days
Deployment 3	21/07/12 to 21/09/12	62 Days

The ADCP recorded measurements of water level, current speed and direction, as well as wave height, period, and direction during this period. A summary of this data is provided in Appendix B and is referred to throughout this report for model calibration and verification.

2.4 Wave Conditions

A review of the wave data recorded by the ADCP device at Cape Hardy identified that the site is exposed to both ocean swell and wind generated sea waves. The swell wave energy appears to approach Cape Hardy from the south-south-east while the sea conditions can approach from a wider directional sector. It was also observed that the site can experience large wind generated wave heights, generally associated with south easterly storms. The wind, sea and swell components of the wave climate at Cape Hardy are all considered in the wave modelling study which is reported in section 4 of this report.

3. Hydrodynamic modelling

Hydrodynamic modelling was undertaken to assess the baseline tidal currents at the proposed port site and any relative change to the currents as a result of the development of port infrastructure. Results from the hydrodynamic modelling will inform the EIS.

3.1 Model Description

Hydrodynamic modelling was carried out using DHI's MIKE 21 HD numerical model. This model is commonly used to simulate water level variation and flow, including current direction and speed, over estuaries, bays, and coastal areas. MIKE 21 HD resolves the water levels and flows on a flexible mesh covering the area of interest. The model is based on the numerical solution of the 2D incompressible Reynolds averaged Navier-Stokes equations subject to the assumptions of Boussinesq and hydrostatic pressure (DHI, 2011).

3.2 Setup

A hydrodynamic model of the Spencer Gulf was developed using the MIKE 21 software over the domain shown below in Figure 3-1. This model extends from Taylor's Landing/Pondalowie Bay in the south to Franklin Harbour/Wallaroo in the north. All figures are displayed in MGA-53 projection.

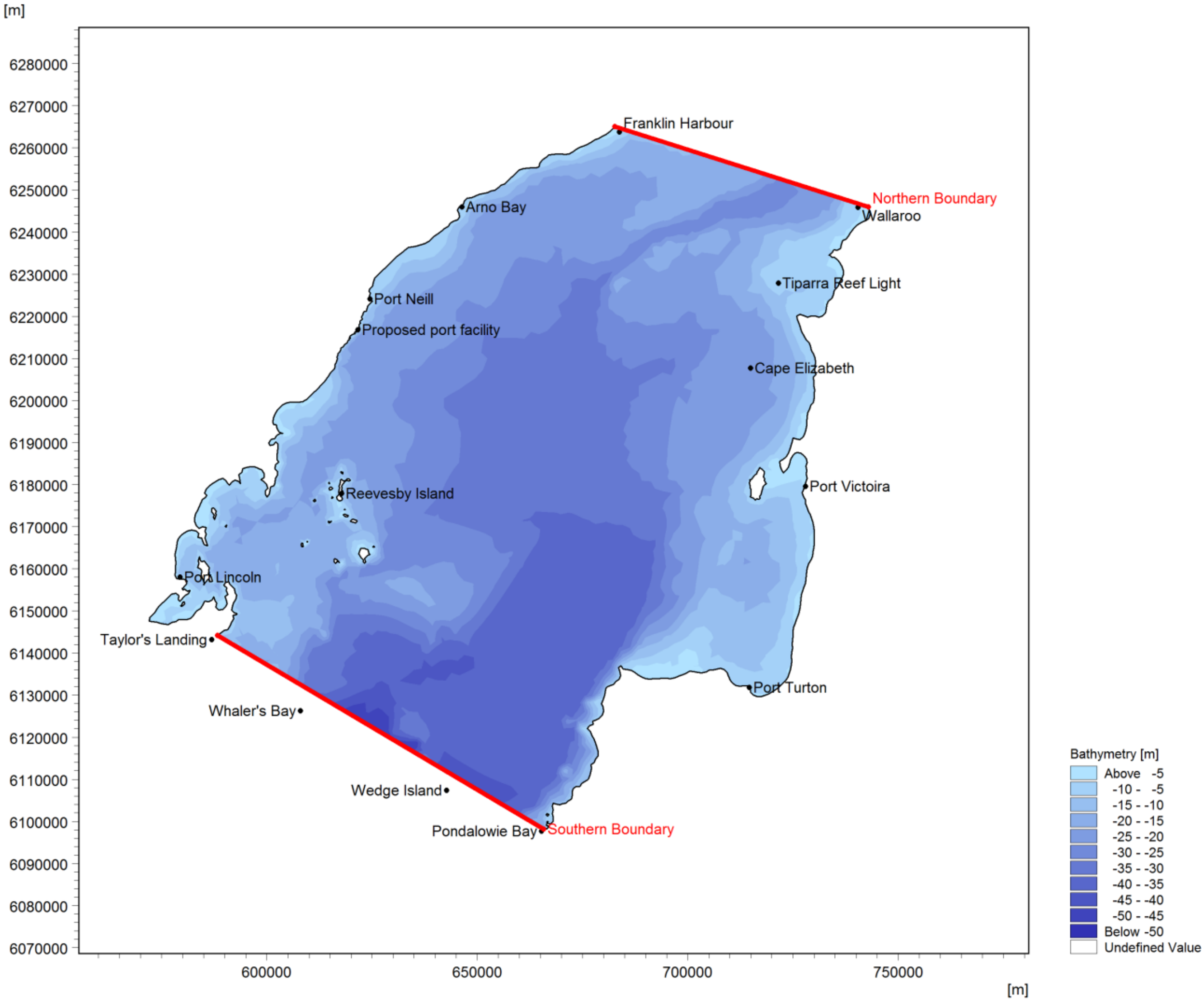

Figure 3-1 Extents of the SKM Spencer Gulf hydrodynamic model

3.2.1 Model Boundary Conditions

A northern and a southern boundary were defined within the hydrodynamic model as shown in **Figure 3-1**. The northern boundary extends from the entrance of Franklin Harbour to Wallaroo, whilst the southern boundary extends from Taylors Landing to Pondalowie Bay. Tidal constituents were obtained from the NTC in order to generate tidal height prediction levels at the port site in close proximity to the model boundary. These tidal levels were interpolated between the adjacent ports to generate tidal levels and drive the tidal flows across the model boundaries.

3.2.2 Bathymetry

Digitised bathymetric data of the Spencer Gulf was procured from the Department of Environment, Water and Natural Resources (DEWNR). This was supplemented with detailed hydrographic data obtained from the Cape Hardy bathymetric survey which was conducted by Hydro Survey, registered hydrographic surveyors commissioned by Iron Road in February 2012. The bathymetry at the Iron Road site is shown in Figure 3-2.

The resolution of the mesh varies within the model domain to enable finer resolution around areas of interest and complex bathymetric features. Figure 3-3 shows the model mesh over the entire model domain. The triangular mesh elements surrounding the project area decrease gradually to a grid resolution of approximately 20m at the project site. This approach has been undertaken to maximise the computation efficiency of the model without compromising the accuracy in close proximity to the project site.

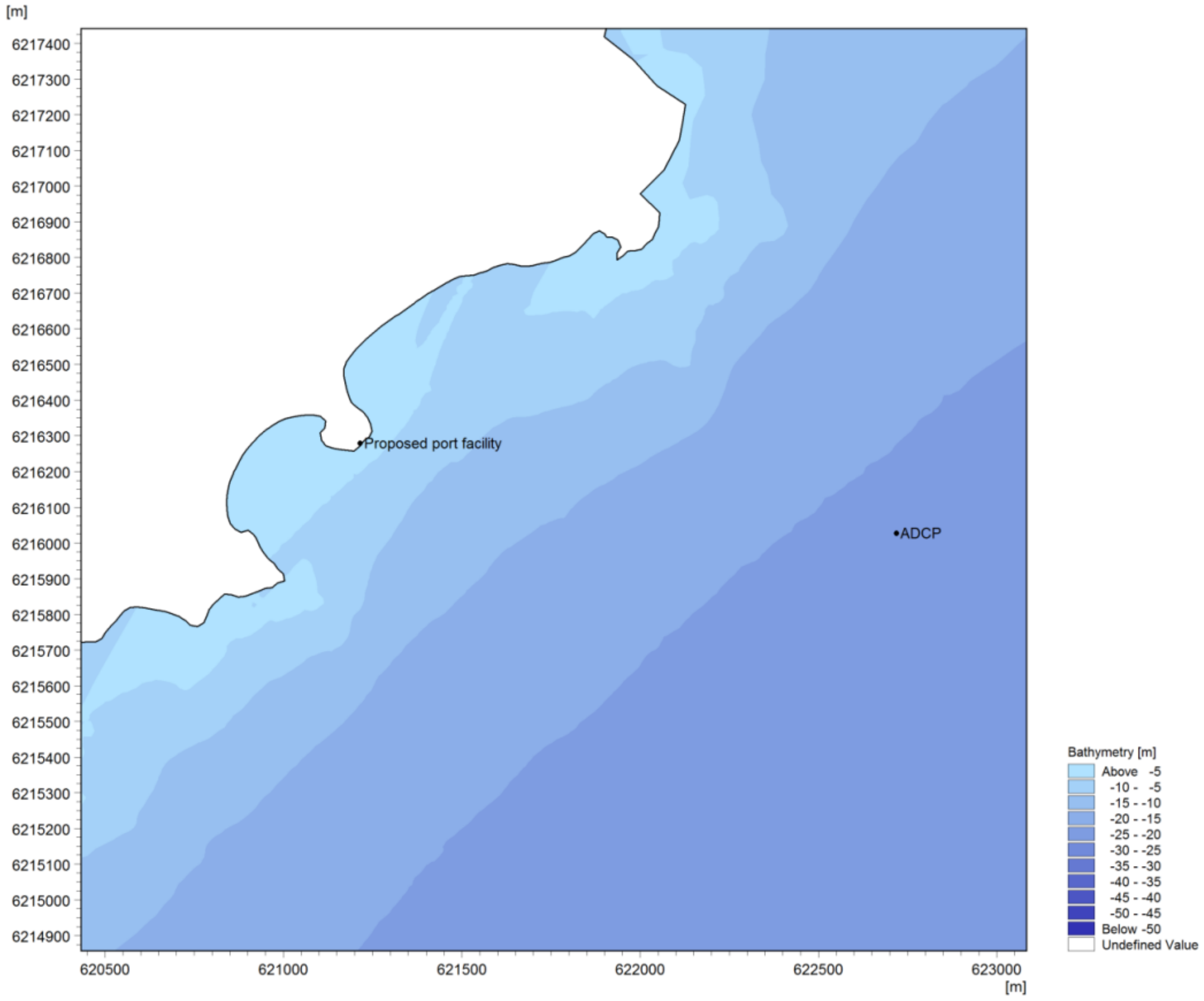

Figure 3-2 Model bathymetry in proximity to the proposed Iron Road port site at Cape Hardy

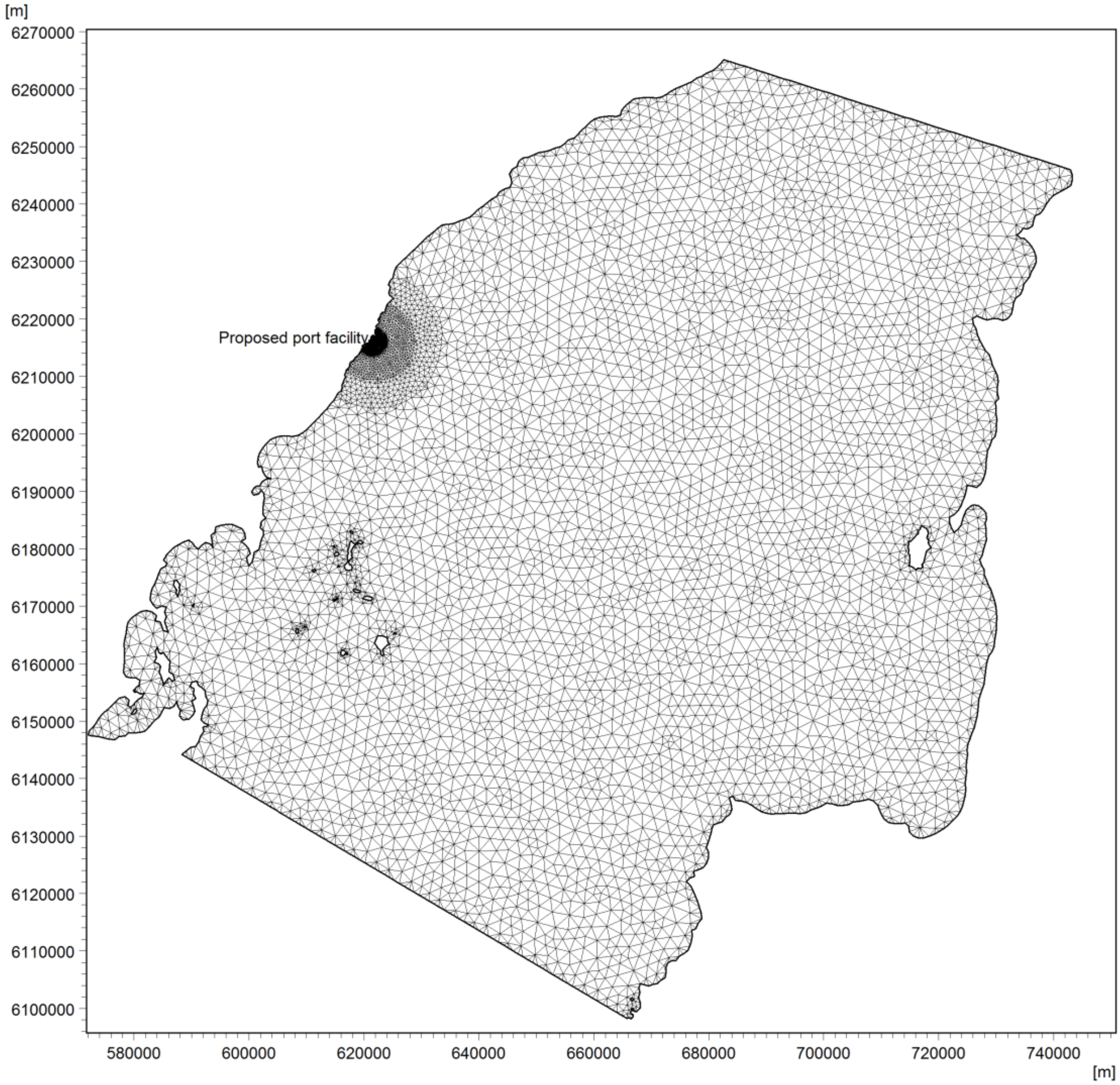

Figure 3-3 Hydrodynamic model mesh over the entire model domain

3.3 Calibration

3.3.1 Water Level Calibration

Tidal constituents from the NTC were used to generate tidal height predictions for the ports shown in Figure 3-1. These predictions were compared against the modelled tidal level fluctuations for a representative spring and neap cycle taken from within the period of the ADCP measurements (see section 2.3).

Figure **3-4** and Figure 3-5 show the calibration plots against water levels at Arno Bay and Port Victoria respectively. The plots illustrate that the phasing and amplitude of the modelled and predicted water levels are well correlated, indicating that the model is well calibrated.

The root-mean-square-error (RMSE) plots give an indication of the accuracy of the model. The ratio of the RMSE to the maximum predicted tidal amplitude (Amp.) indicates that the differences between the modelled and predicted water level are minimal, with only a 3% difference at Arno Bay and a 9% difference at Port Victoria. Whilst Port Neill is the closest port to the project site, the number of constituents available at this location is limited and the tidal station is sheltered by existing maritime structures. Therefore it is believed that the modelled tidal levels at this location are inaccurate and hence are not shown below.

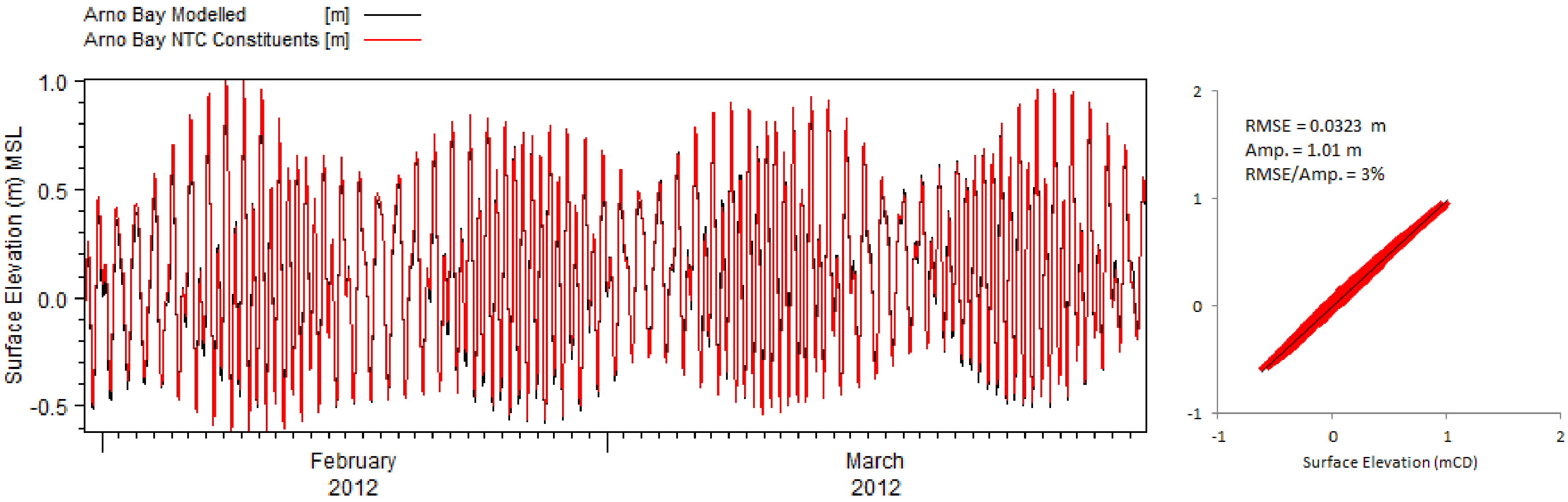

Figure 3-4 Modelled vs NTC predicted water levels at Arno Bay

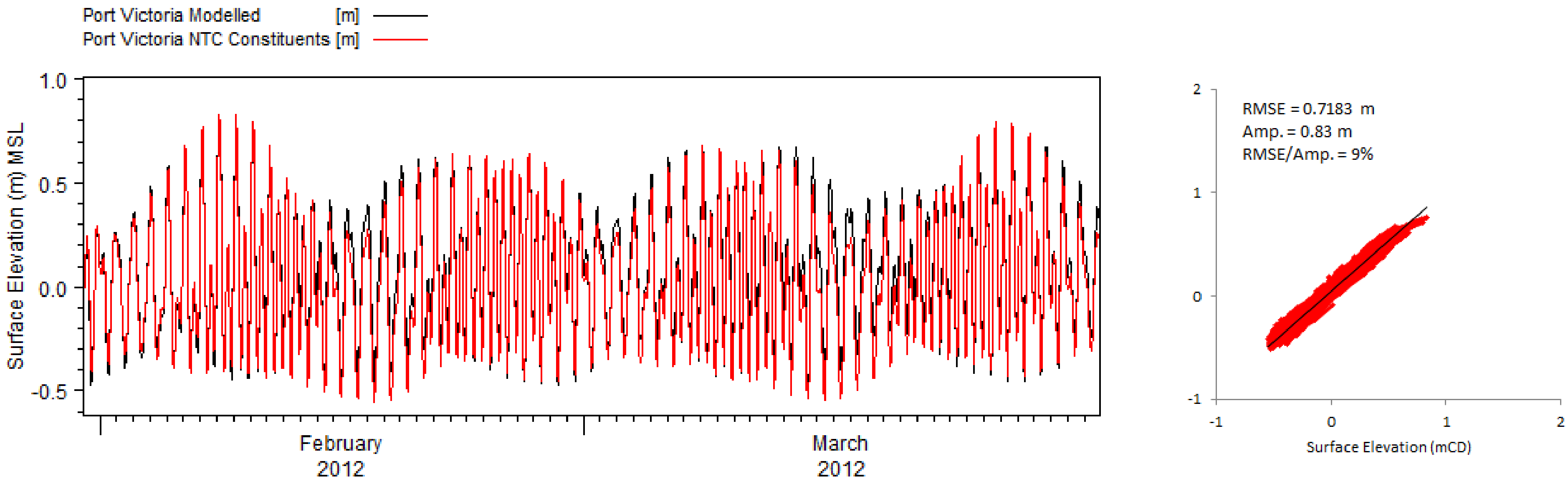

Figure 3-5 Modelled vs NTC predicted water levels at Port Victoria

3.3.2 ADCP Calibration

Current data was recorded with an ADCP in three deployments between 31/01/2012 and 21/09/2012 (refer to section 2.3). The approximate location of the ADCP deployment is shown in Figure 3-2. Data was extracted from the hydrodynamic model at the ADCP deployment location to validate the accuracy of the model. Comparison plots of the ADCP measured and modelled current and water level data are shown below in Figure 3-6 to Figure 3-8. The phasing and amplitude between the modelled and measured data correlates well which demonstrates that the model is representative of the actual tidal currents at the site.

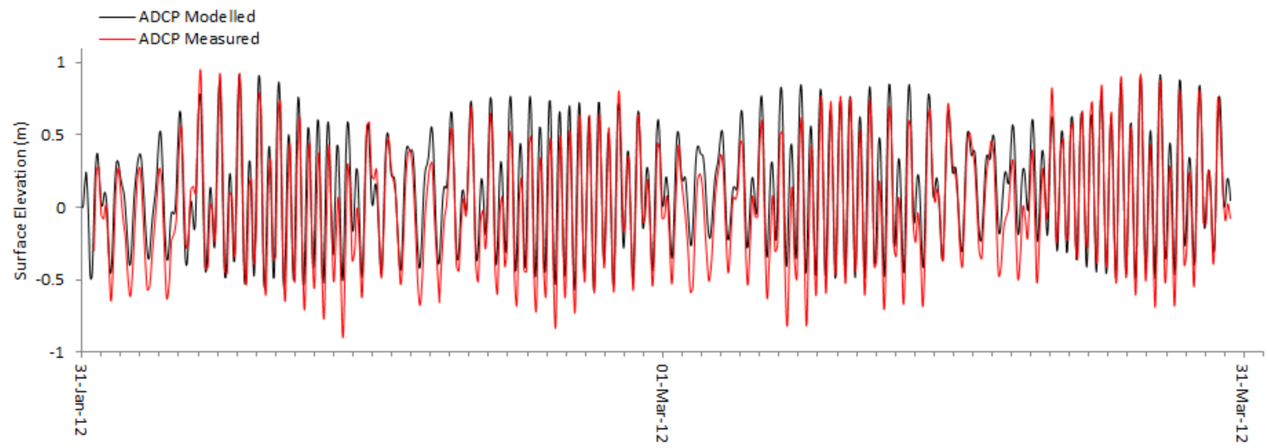

Figure 3-6 Modelled vs measured ADCP water levels

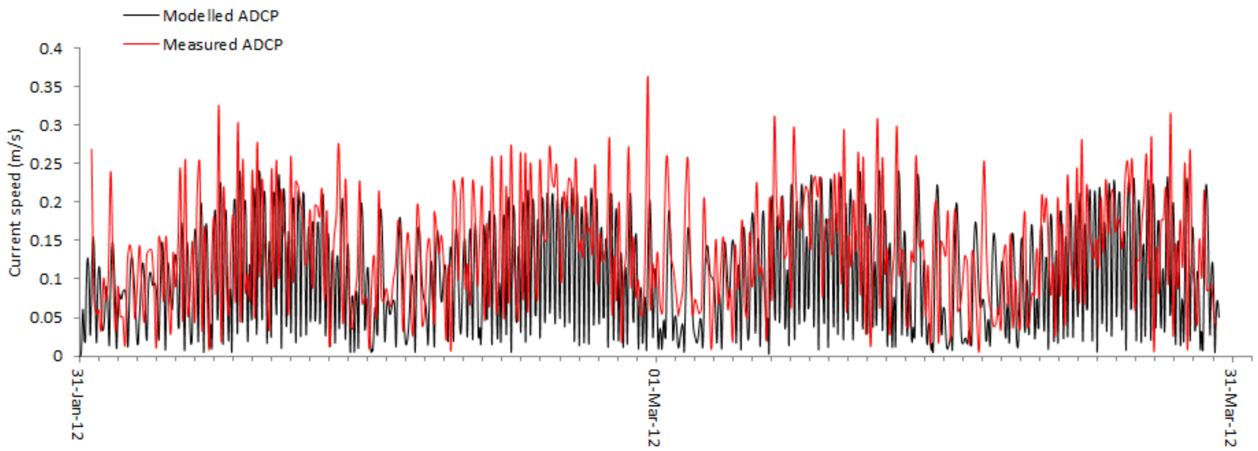

Figure 3-7 Modelled vs measured ADCP current speed

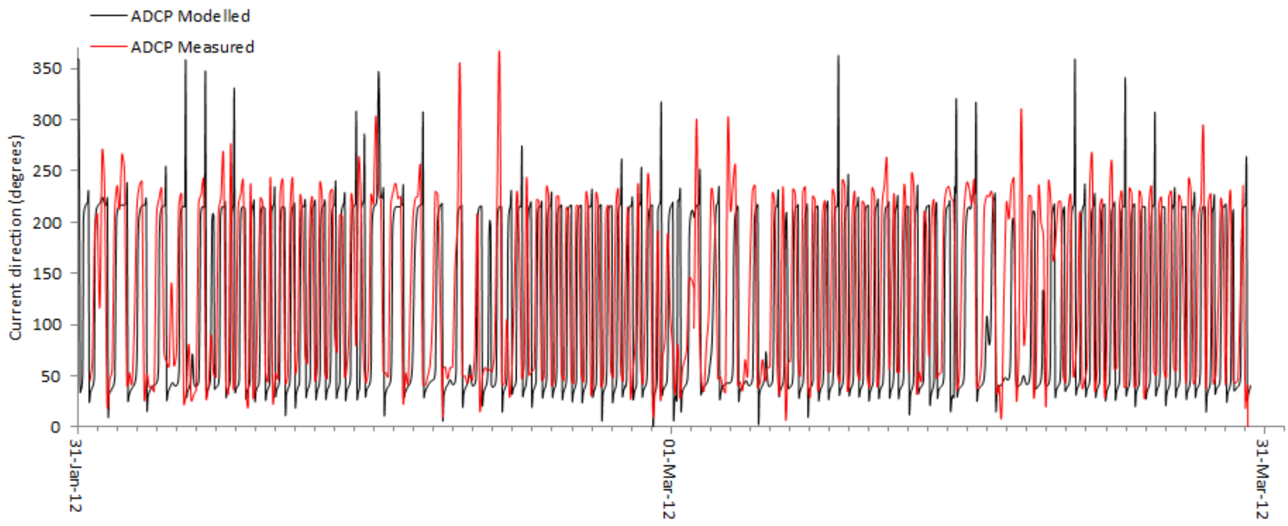

Figure 3-8 Modelled vs measured ADCP current direction

3.4 Base Case Hydrodynamics

A spring and neap tidal cycle occurring over the period of February and March 2012 was selected as the base case scenario and is representative of the tidal conditions experienced at the Iron Road site. The base case is the basis for comparison with the model runs incorporating the proposed maritime infrastructure at Cape Hardy. The period was selected from the dates of the ADCP measurements to ensure that the modelled data was calibrated and validated against the measured ADCP data at the site.

3.4.1 Results

The maximum base case current speeds at the Iron Road site are shown in Figure 3-9 to Figure 3-12 for the flood and ebb spring and neap tide cycles respectively. For the period selected, the maximum current speed in the region during a spring tide is above 0.35m/s (Figure 3-9 and Figure 3-10). The maximum current speed for the neap tides is approximately 0.25m/s to 0.35m/s as shown in Figure 3-11 and Figure 3-12.

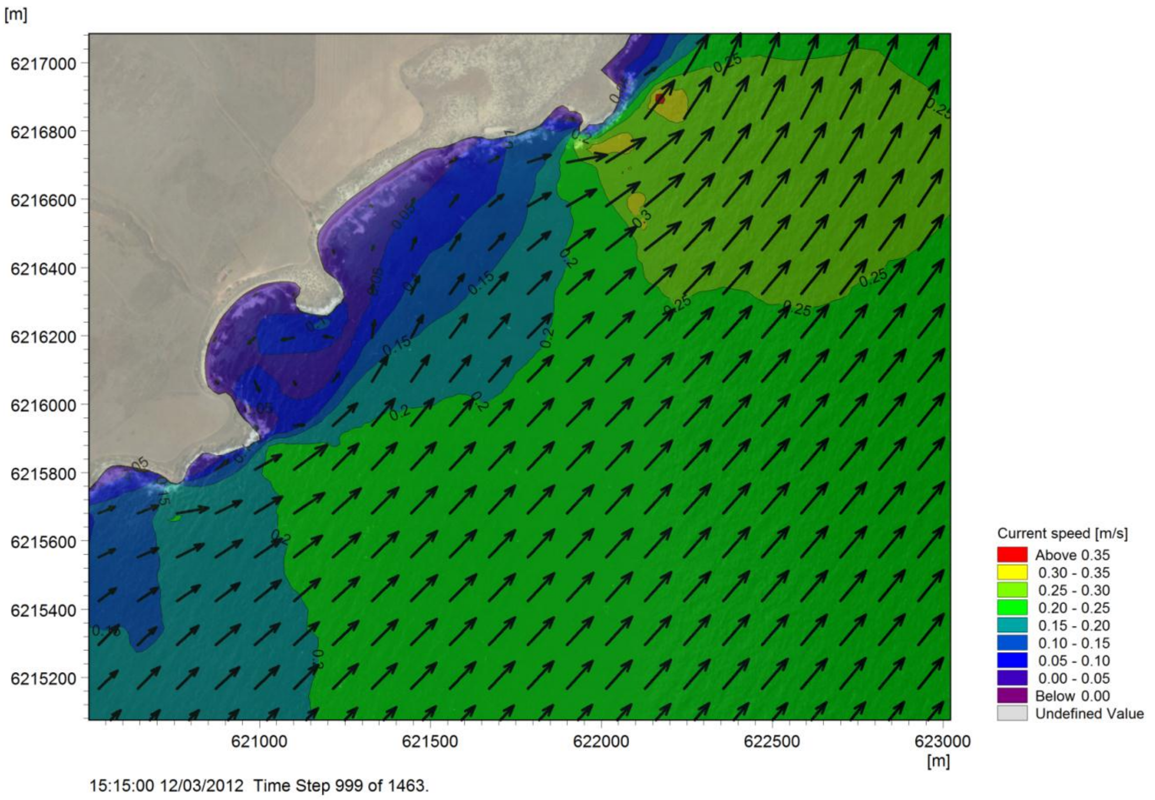

Figure 3-9 Maximum current speed for spring flood tide

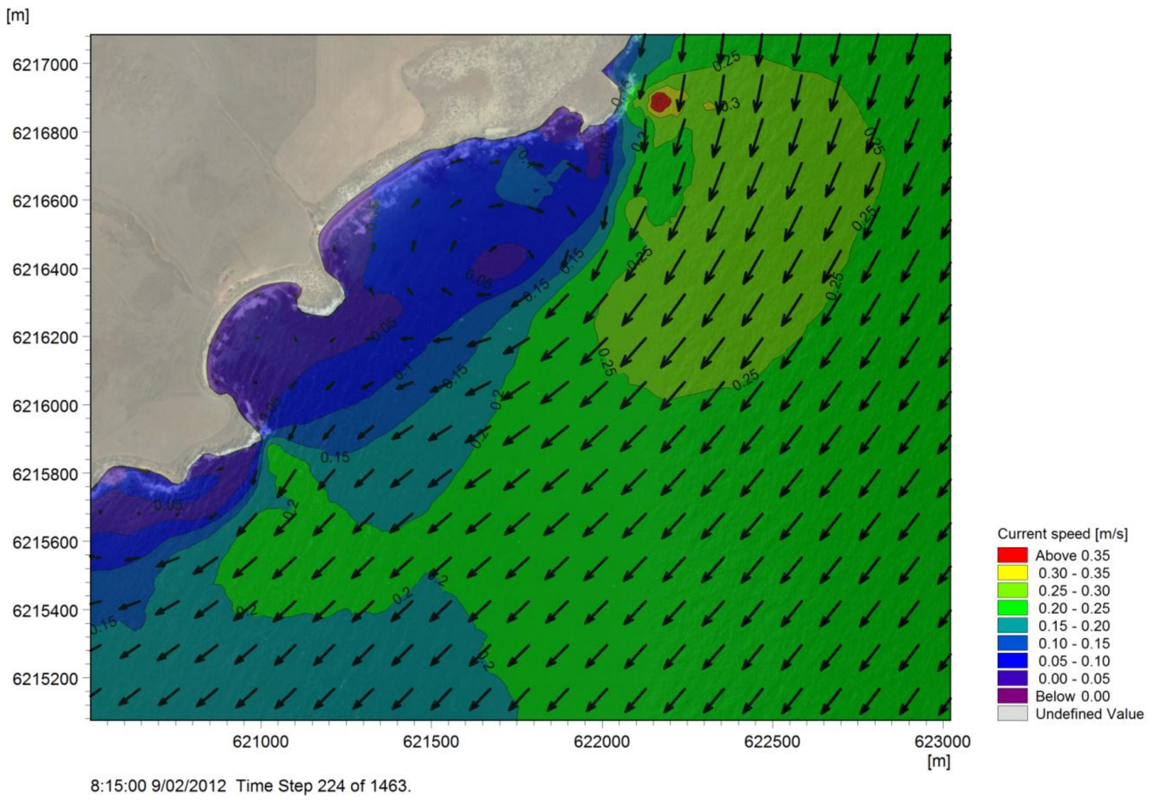

Figure 3-10 Maximum current speed for spring ebb tide

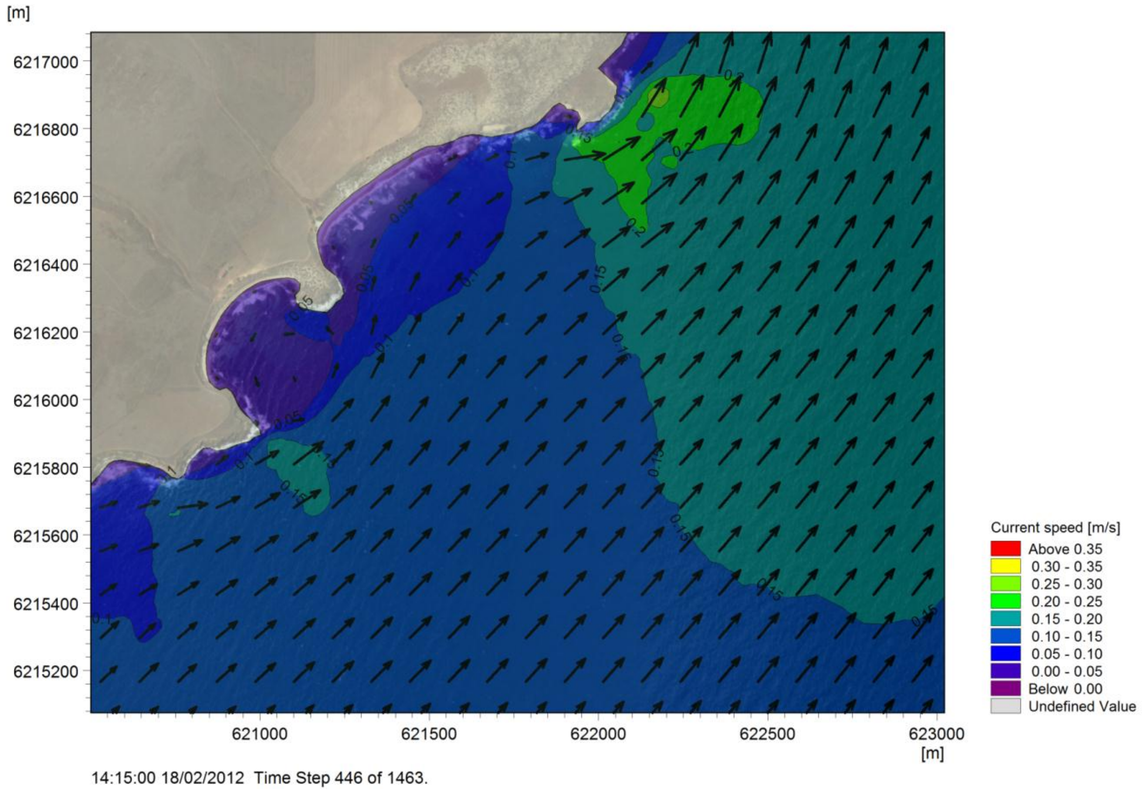

Figure 3-11 Maximum current speed for neap flood tide

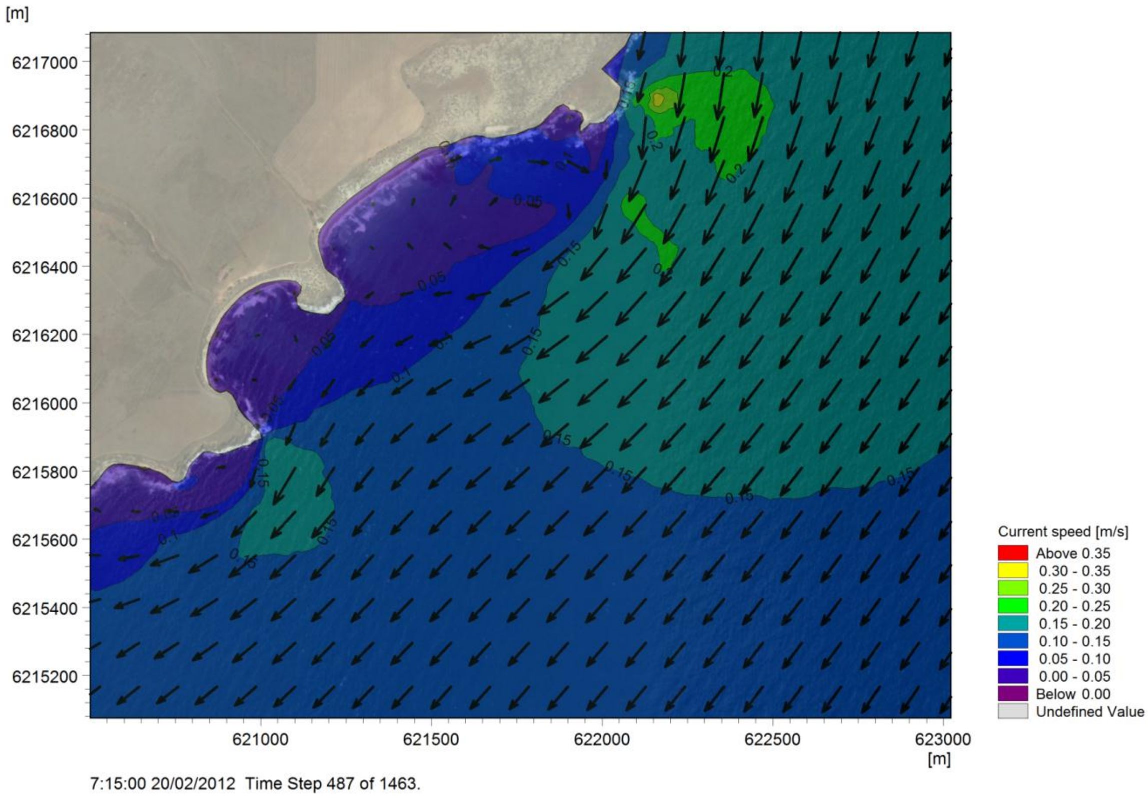

Figure 3-12 Maximum current speed for neap ebb tide

3.4.2 Discussion

The results for the sample spring flood and ebb tides indicate that current speeds exceeding 0.35m/s are generated at the northern headland (Figure 3-9 and Figure 3-10). Both the northern and southern bays are relatively sheltered from strong currents, with current speeds reduced to below 0.15m/s in this region. The predominant current direction is parallel to the shoreline, with the exception of currents in the bays where the nearshore currents are deflected around the northern and southern headlands. During the spring flood tide the currents follow a circulating pattern after deflecting around the southern headland whilst during a spring ebb tide the currents are deflected around the northern headland resulting in current circulation patterns in the northern bay.

The hydrodynamic results for a sample neap flood and ebb tides (Figure 3-11 and Figure 3-12) indicate that maximum current speeds between 0.25m/s to 0.30m/s are generated in close proximity to the northern headland. Similar to the spring tides, the direction of the offshore currents is parallel to the shoreline following the bathymetry contours with lower nearshore currents within the bays. During neap flood tides the currents deflect around the southern headland resulting in current speeds below 0.05m/s to 0.1m/s within the southern bay. During ebb tides the currents deflect around the northern headland resulting in current speeds below 0.05m/s to 0.1m/s within the northern bay.

3.5 Development scenario

The hydrodynamic model was further developed to investigate the relative changes to the currents as a result of the inclusion of the proposed infrastructure at the port site. Effects of the MOF and causeway reclamation, as well as the piling associated with the jetty, wharf, and berthing dolphins were assessed in this scenario.

3.5.1 Proposed infrastructure

The extent of the causeway, MOF, jetty, and wharf is shown below in Figure 3-13. The causeway and MOF reclamation levels were added to the baseline mesh to account for the footprint and armoured slopes of the proposed causeway structure (see Figure 3-14 and Figure 3-15). This allowed the majority of the mesh elements to remain unchanged, providing an accurate comparison of the results between the base case and infrastructure scenarios.

The jetty, wharf, and dolphin piles were added as sub-grid structures with the properties and distribution as shown in Table 3-1. The piles were represented as a rough surface structure (Cd=1.05), assuming a marine growth of 0.1m on the piles below MSL.

Table 3-1 Pile distribution

Section	Number of Piles	Diameter including marine growth	Spacing	Length of Section
Jetty	55	1.3m	2 piles/bent @ 24m c-c	576m
Wharf	54	1.3m	3 piles/bent @ 24m c-c	408m
Dolphins	86	1.6m	Northern side of wharf: 6 piles/pair @ 48m c-c Southern side of wharf: 4 piles/pair @ 48 c-c	392m

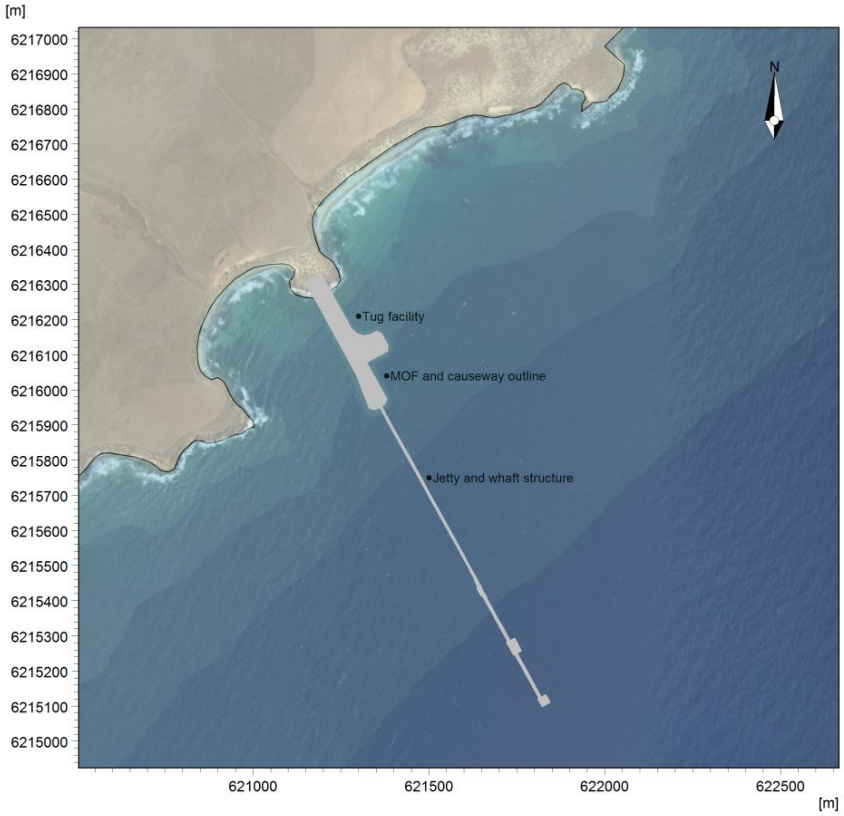

Figure 3-13 Extents of the proposed maritime infrastructure

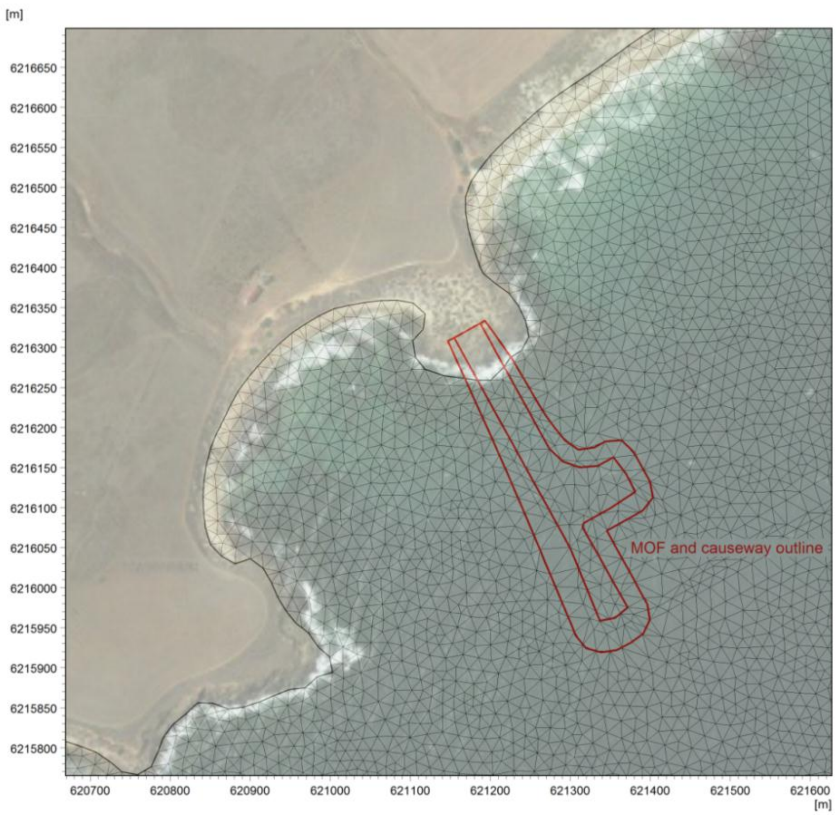

Figure 3-14 Hydrodynamic model mesh resolution at the Iron Road site

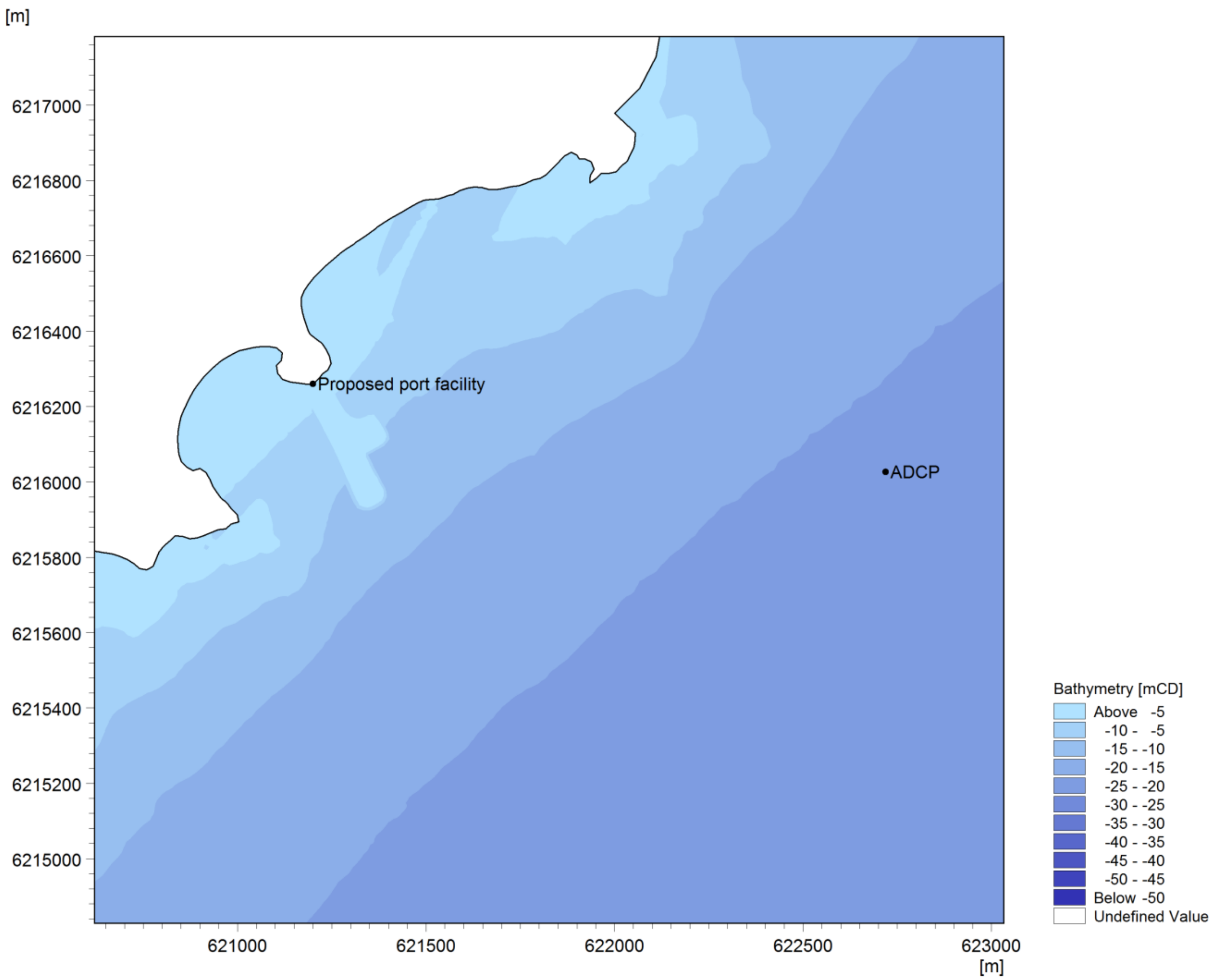

Figure 3-15 Infrastructure scenario bathymetry incorporating the proposed infrastructure

3.5.2 Results

A comparison of the current velocities before and after the inclusion of the proposed infrastructure are shown below in Figure 3-17 to Figure 3-23 for the flood and ebb spring and neap tide cycles.

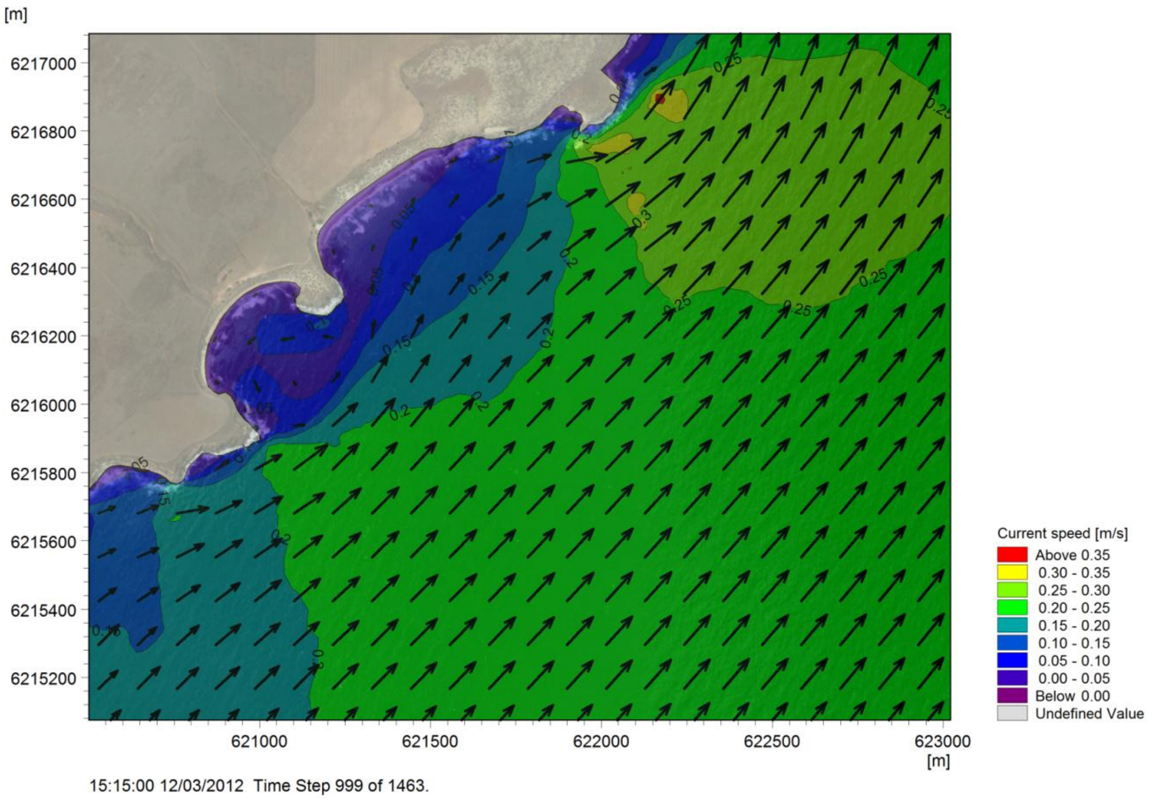

Figure 3-16 Maximum current speed for spring flood tide

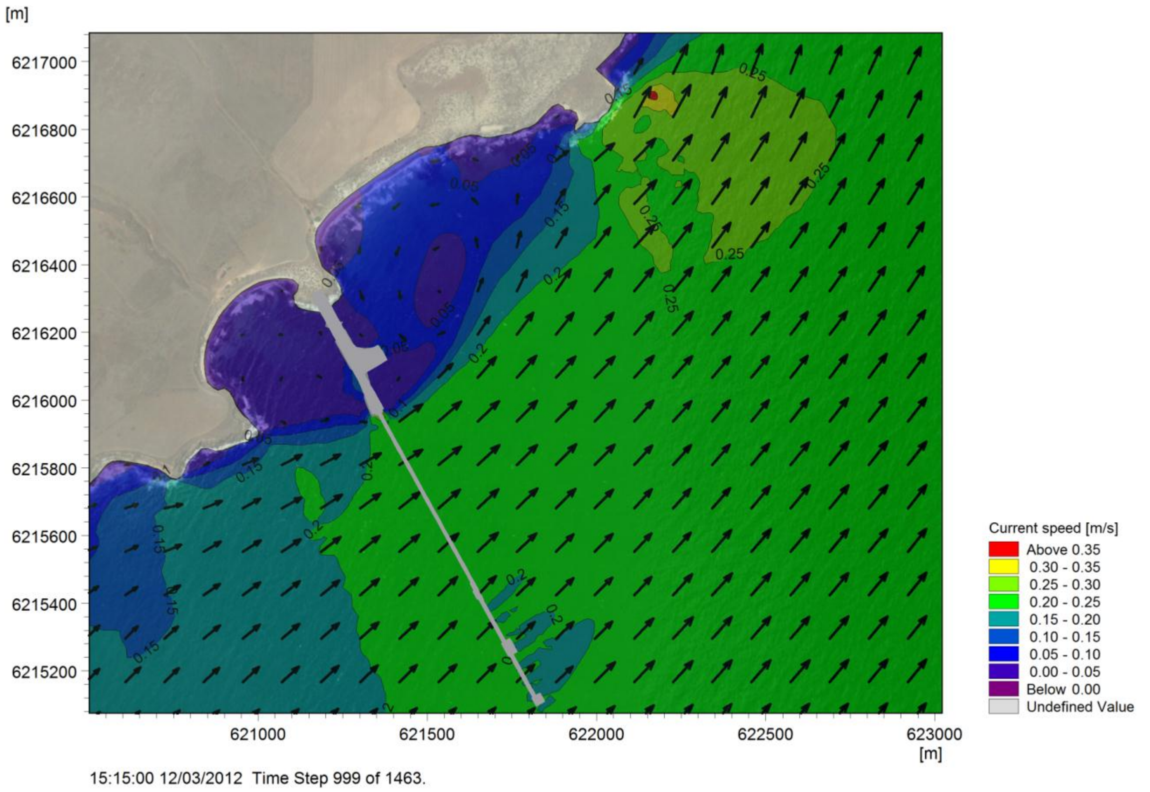

Figure 3-17 Maximum current speed for spring flood tide (infrastructure scenario)

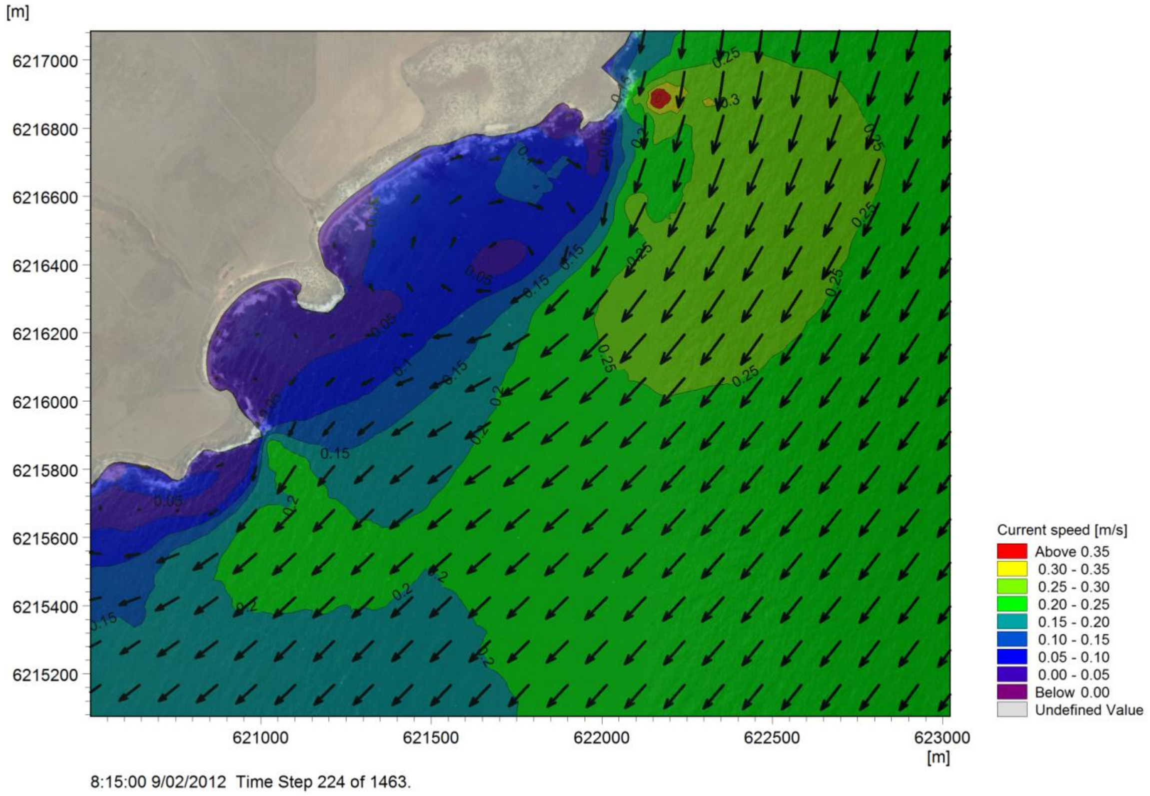

Figure 3-18 Maximum current speed for spring ebb tide

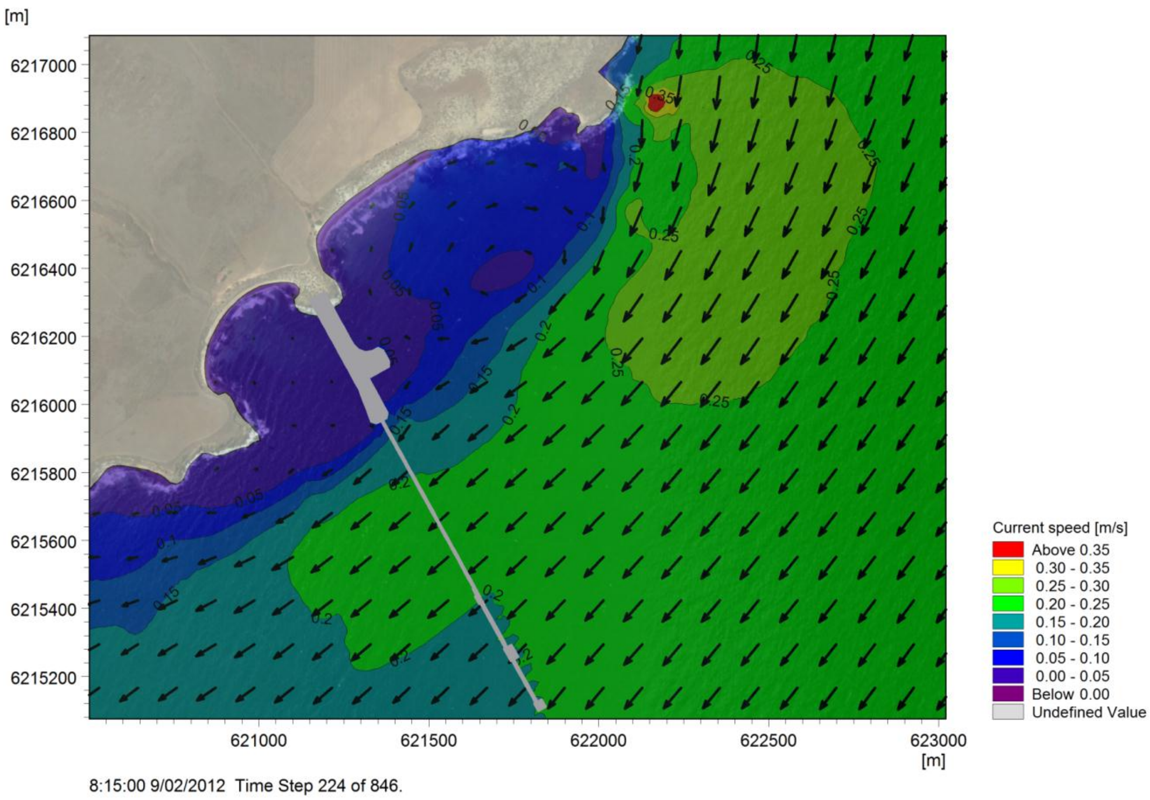

Figure 3-19 Maximum current speed for spring ebb tide (infrastructure scenario)

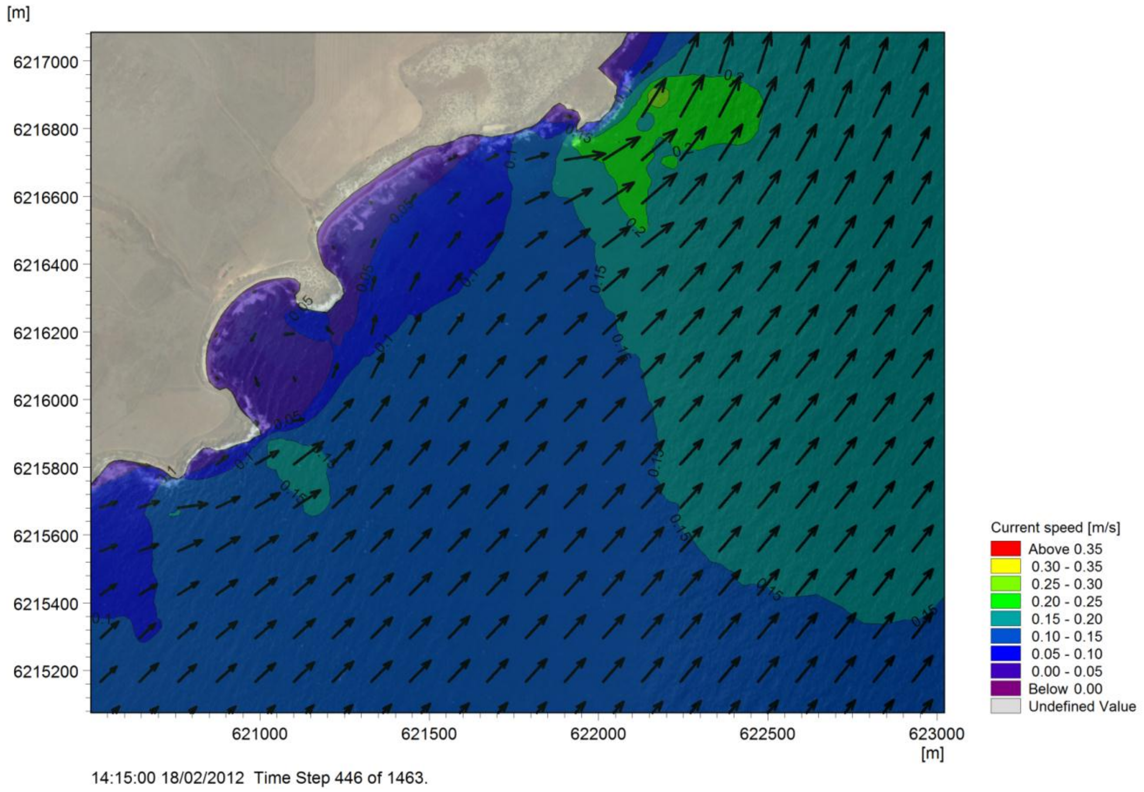

Figure 3-20 Maximum current speed for neap flood tide

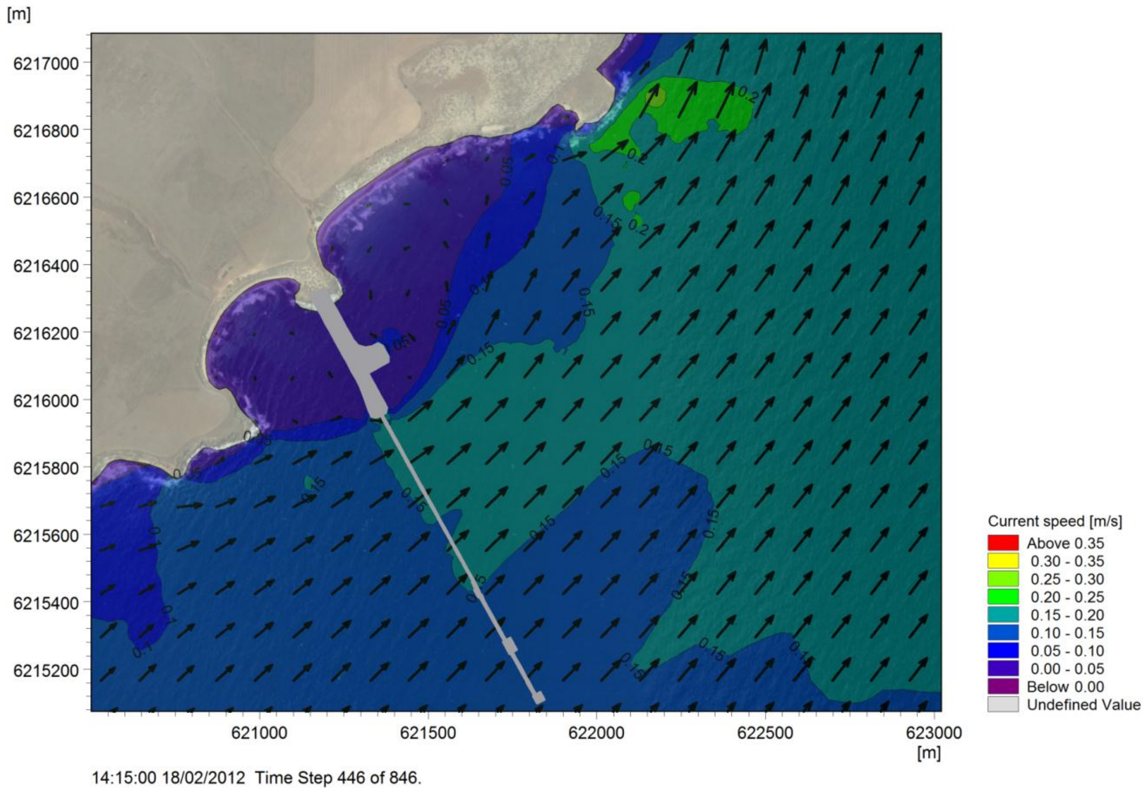

Figure 3-21 Maximum current speed for neap flood tide (infrastructure scenario)

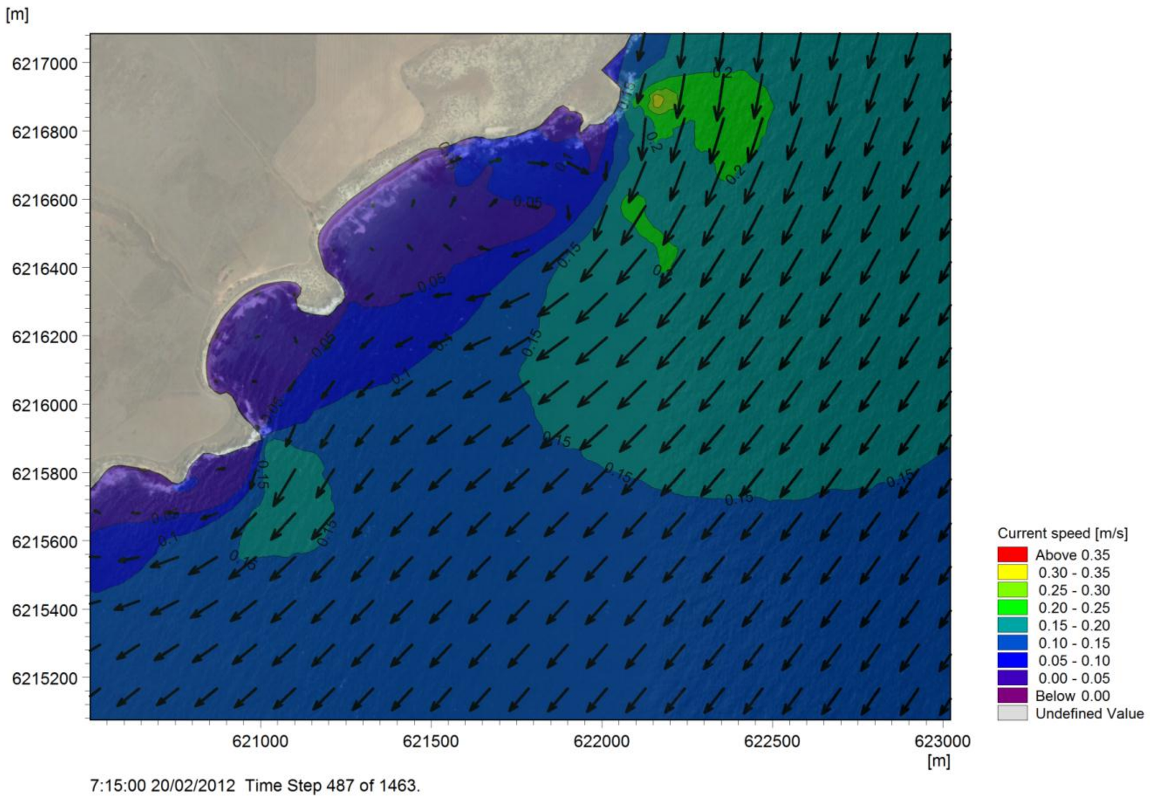

Figure 3-22 Maximum current speed for neap ebb tide

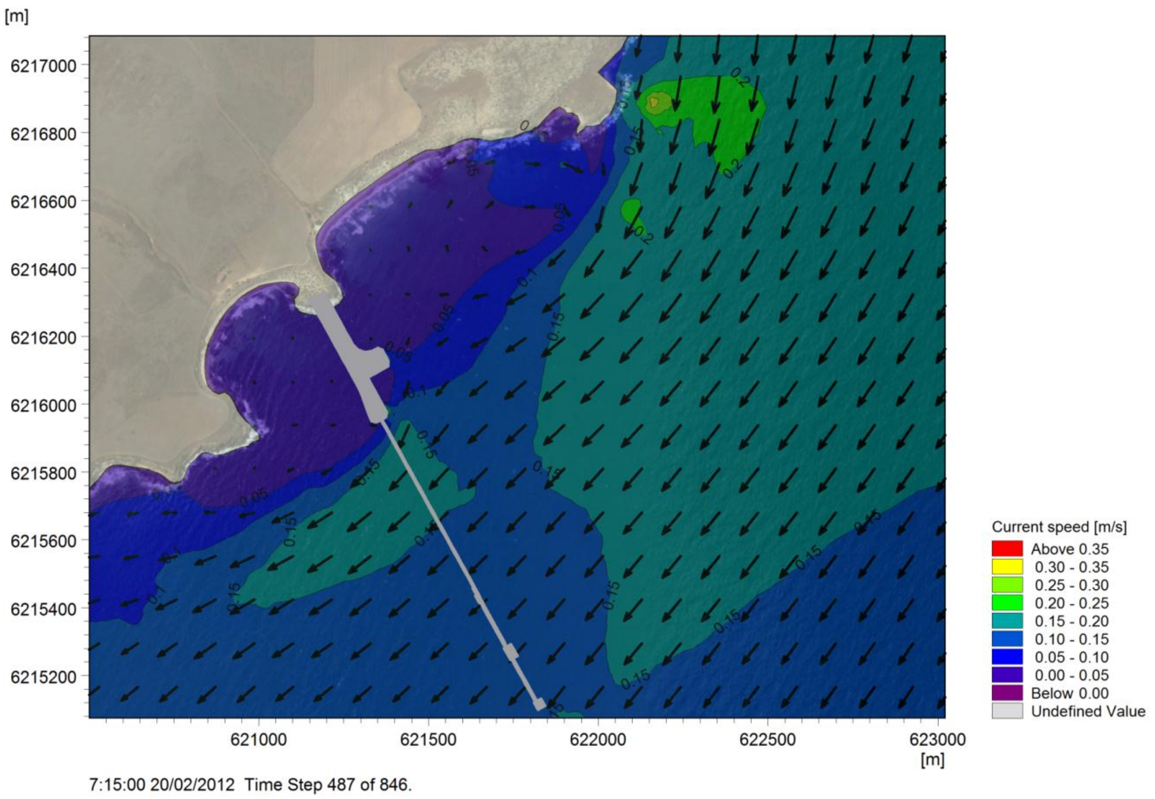

Figure 3-23 Maximum current speed for neap ebb tide (infrastructure scenario)

3.6 Hydrodynamic Comparison Discussion

3.6.1 Spring Flood Current

Figure 3-16 and Figure 3-17 illustrate the changes in the spring flood currents after construction of the proposed causeway structure. Observations between the basecase and infrastructure scenario include:

- Generally the offshore currents continue to travel shore parallel,
- The maximum current speed is located at the northern headland and remains above 0.35m/s
- Currents closer to shore interact with the reclaimed area resulting in a change in the current circulation patterns generated in the northern bay as well as a marginal decrease in current speed in the southern bay.
- The increased piling density at the wharf structure results in a slight shadowing effect reducing the current speeds in the lee of the structure from 0.25-0.30m/s to 0.20-0.25m/s.

3.6.2 Spring Ebb Current

Figure 3-18 and Figure 3-19 illustrate the changes in the spring ebb currents after construction of the proposed causeway structure. Observations between the basecase and infrastructure scenario include:

- In a similar manner to the base case scenario, after construction the predominant offshore current direction remains parallel to the shore with some current circulation in the northern bay.
- The reclamation does provide some additional sheltering effects to the southern bay generating a circulation in the bay.
- Within the southern bay the causeway structure reduces the current speeds from 0.20-0.25m/s in the base case to 0.00-0.05m/s in the infrastructure scenario.
- The largest currents within the northern bay are reduced from 0.1-0.15m/s to 0.05-0.1m/s due to the addition of the causeway structure.
- The current vectors and speeds around the northern headland are not significantly altered by the marine infrastructure.

3.6.3 Neap Flood Current

Figure 3-20 and Figure 3-21 illustrate the changes in the neap flood currents after construction of the proposed causeway structure. Observations between the basecase and infrastructure scenario include:

- After construction of the proposed infrastructure the neap flood currents are directed around the tip of the causeway, generating current circulations in the northern bay.
- Current speeds are increased by approximately 0.05m/s as they are directed around the tip of the causeway and interact with the jetty piles.
- Current circulation patterns continue to be generated in the southern bay
- The increased extent of the causeway results in a slight reduction in the maximum current at the southern headland from 0.15-0.20m/s to 0.10-0.15m/s.

3.6.4 Neap Ebb Current

Figure 3-22 and Figure 3-23 illustrate the changes in the neap ebb currents after construction of the proposed causeway structure. Observations between the base case and infrastructure scenario include:

- The construction of the MOF and causeway structure leads to a decrease in neap ebb current velocities in both the northern and southern bays.

- The addition of the infrastructure increases the extent of current circulation, particularly in the southern bay.
- The presence of the causeway causes the currents to be directed around the structure, resulting in a localised 0.05m/s increase in current speeds.
- The currents speeds generated at the tip of the southern headland are reduced from 0.15m/s-0.20m/s to less than 0.05m/s due to the sheltering effect of the causeway structure.

3.7 Conclusions

A hydrodynamic model was utilised to assess the potential changes and impacts on the tidal currents at the site resulting from the construction of the proposed causeway and MOF infrastructure. The results indicate that:

- Generally, the offshore hydrodynamics change minimally due to the addition of the proposed infrastructure. There is a slight change in current speed as the currents interact with the berthing dolphin piles due to the increased piling density. However, it is predicted that these changes in current speed are within ±0.1m/s. Currents are also increased by a similar magnitude as they are diffracted around the tip of the causeway structure.
- The orientation of the proposed causeway structure shelters the southern bay and headland during ebb tides, reducing the current speeds to below 0.05m/s. The structure also provides some sheltering of the northern bay during flood tides, with current speeds reduced to below 0.1m/s.
- Prior to construction of the proposed infrastructure, current circulation occurs in the northern bay during ebb tides and the southern bay during flood tides. The addition of the MOF and causeway structure generates current circulation in both bays during flood and neap tides as currents are deflected around the proposed infrastructure.
- The main impact to the hydrodynamic regime is as a result of the construction of the proposed causeway and MOF infrastructure. However in general any changes to the nearshore current regime are minor and localised.

4. Wave modelling

Wave transformation modelling was undertaken to assess the baseline wave climate at the proposed port site and any relative change to the wave conditions as a result of the development of port infrastructure. Results from the wave modelling will inform the EIS.

4.1 Model Description

Wave modelling was carried out with the MIKE 21 Spectral Wave (SW) numerical model. This model simulates the growth, decay and transformation of wind generated waves and swells in offshore and coastal areas. The model can be modified to provide a suitable resolution at the area of interest, accounting for any local bathymetry features at the site. Effects of refraction and shoaling are accounted for in the model, as well as local wind generation and energy dissipation due to bottom friction and wave breaking. Wave parameters such as the significant wave height, wave period, and wave direction are generated across the model domain and can be extracted as output from the model.

4.2 Wave parameter description

Table 4-1 summarises the wave parameters used to describe the wave climate at the proposed site location.

Table 4-1 Description of main wave parameters

Parameter	Abbreviation	Units	Description
Significant wave height	Hs	m	Average height of the highest one-third of the waves for a given sea state.
Peak wave period	Tp	s	The wave period determined by the inverse of the frequency at which the wave energy spectrum reaches a maximum.
Mean wave direction	MWD	Degrees	Mean direction of the waves to true north

4.3 Setup

The extent of the spectral wave model developed for the Spencer Gulf is shown in Figure 4-1. The model extends across the entrance of the Spencer Gulf in the south, to Port Augusta in the north.

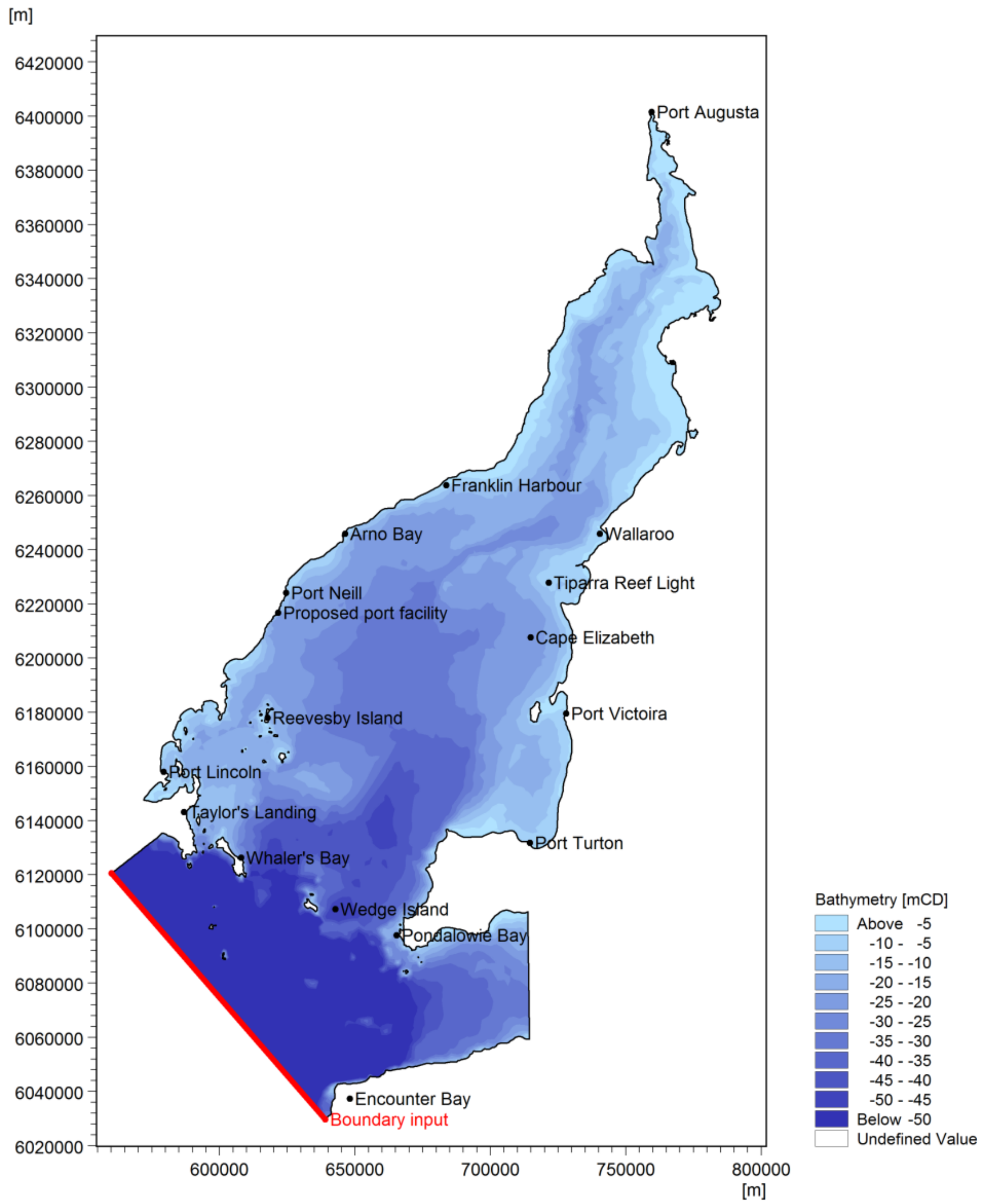

Figure 4-1 Extents of the SKM Spencer Gulf spectral wave model

4.3.1 Bathymetry

The bathymetry for the wave model was developed using the same bathymetric dataset as the hydrodynamic modelling (see section 3.2.2). The bathymetric dataset includes digitised bathymetric data procured from DEWNR, as well as the hydrographic data obtained from the Cape Hardy bathymetric survey commissioned by Iron Road in February 2012. Digitised chart data was also used to supplement bathymetric data where any data gaps existed.

A finer mesh resolution was used around the proposed site to ensure computation accuracy at the location of interest. The mesh used for comparison with the infrastructure scenario varied from a maximum grid resolution of approximately 2500m down to 20m at the site location as shown in Figure 4-2.

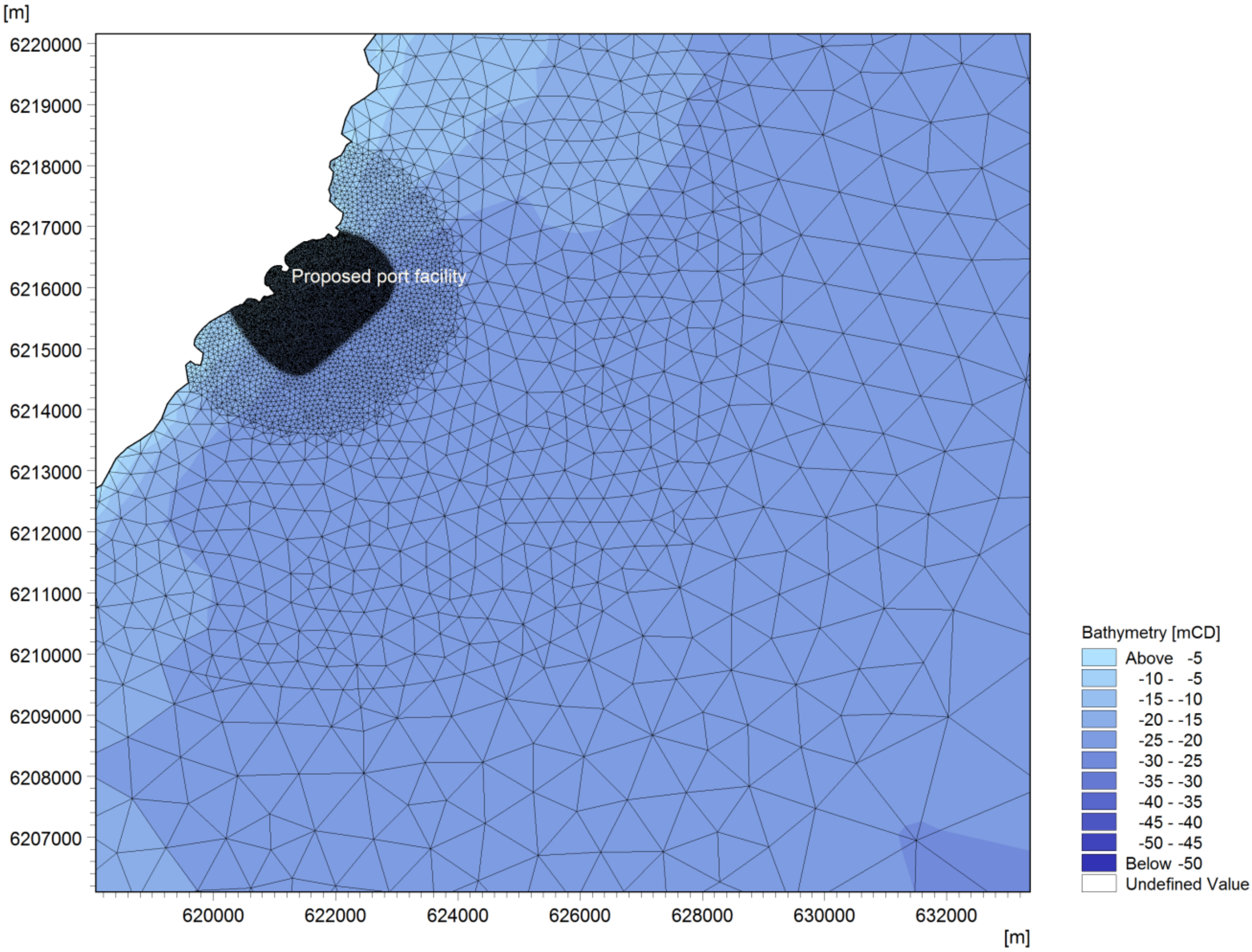

Figure 4-2 Spectral wave model mesh resolution surrounding the proposed port facilities

4.3.2 Input Wave Conditions

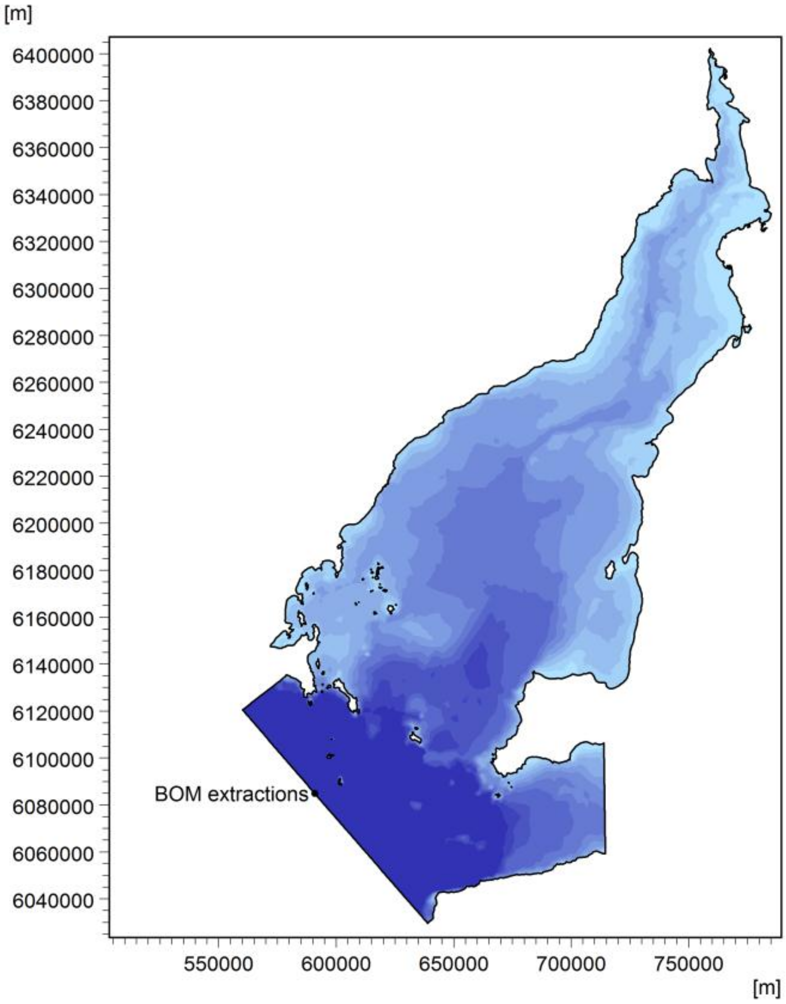

Figure 4-3 BOM model data extraction point

Two datasets were adopted as input to the Spencer Gulf wave model. The first wave dataset covered a period of 30 years (1979 to 2009) which was transformed in the model to determine the dominant wave conditions at the site. The wave data was extracted from the BOM WAVEWATCH III model.

A second 2012 annual wave dataset was adopted to capture the period of the ADCP deployment for calibration of the wave model. Wave data for this model was extracted from the BOM 2012 AUSWAVE dataset.

Both datasets were extracted at the same offshore location (Figure 4-3) and applied along the boundary as shown in Figure 4-1. These offshore wave datasets are described in more detail in Appendix C of this report.

4.3.3 Input Wind Conditions

Wind datasets were also extracted from both of the BOM models at the location shown in Figure 4-3.

The 30 year time-series of wind speed and directional data extracted from the BOM WAVEWATCH III model is summarised in Figure 4-4. The 2012 annual dataset extracted from the BOM AUSWAVE model for a period of 12 months is summarised in the wave rose shown in Figure 4-5.

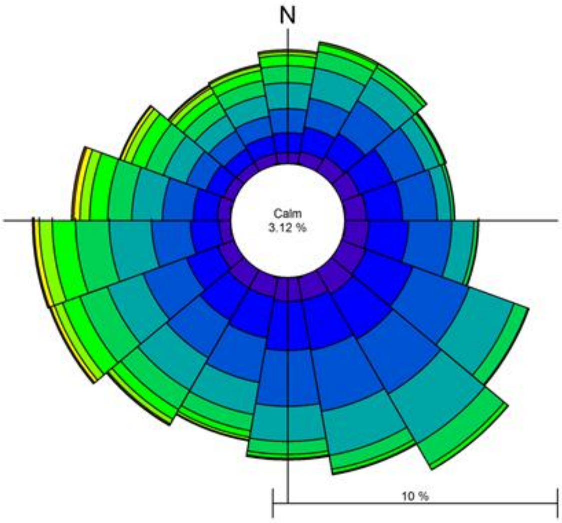

Figure 4-4 BOM WAVEWATCH III dataset wind rose (1979 to 2009)

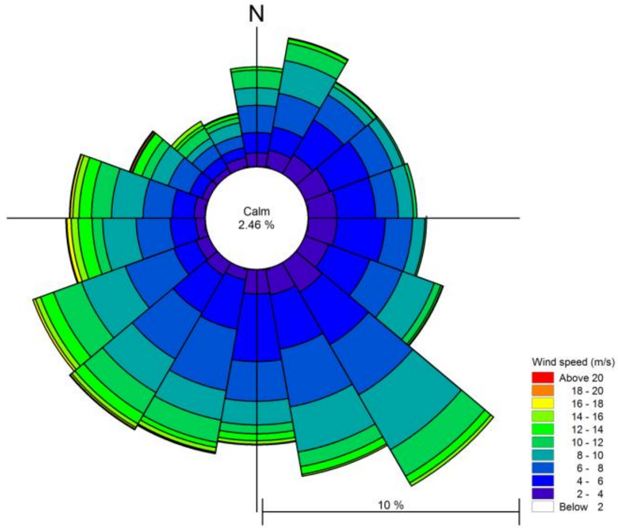

Figure 4-5 BOM AUSWAVE dataset wind rose (2012)

Both datasets were applied across the domain of the respective spectral wave model, concurrently with the offshore wave conditions at the boundary, to generate fetch limited waves within the Spencer Gulf. The water level within the model was run at the Mean Sea Level (MSL) at the site, 1.08mCD.

4.4 Calibration

4.4.1 ADCP Wave Calibration

To validate the accuracy of the numerical model, wave data was extracted from the model at the location of the ADCP. A comparison plot of the ADCP measured and modelled significant wave height (Hs) can be seen below in Figure 4-6. The root-mean-square-error (RMSE) plot in Figure 4-7 indicates that the difference between the modelled and measured Hs is within 12%.

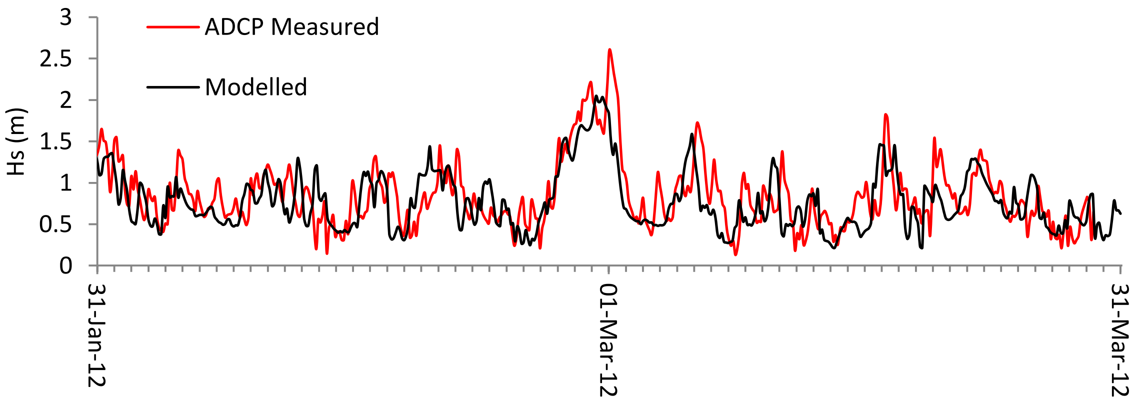

Figure 4-6 Modelled vs measured ADCP wave heights

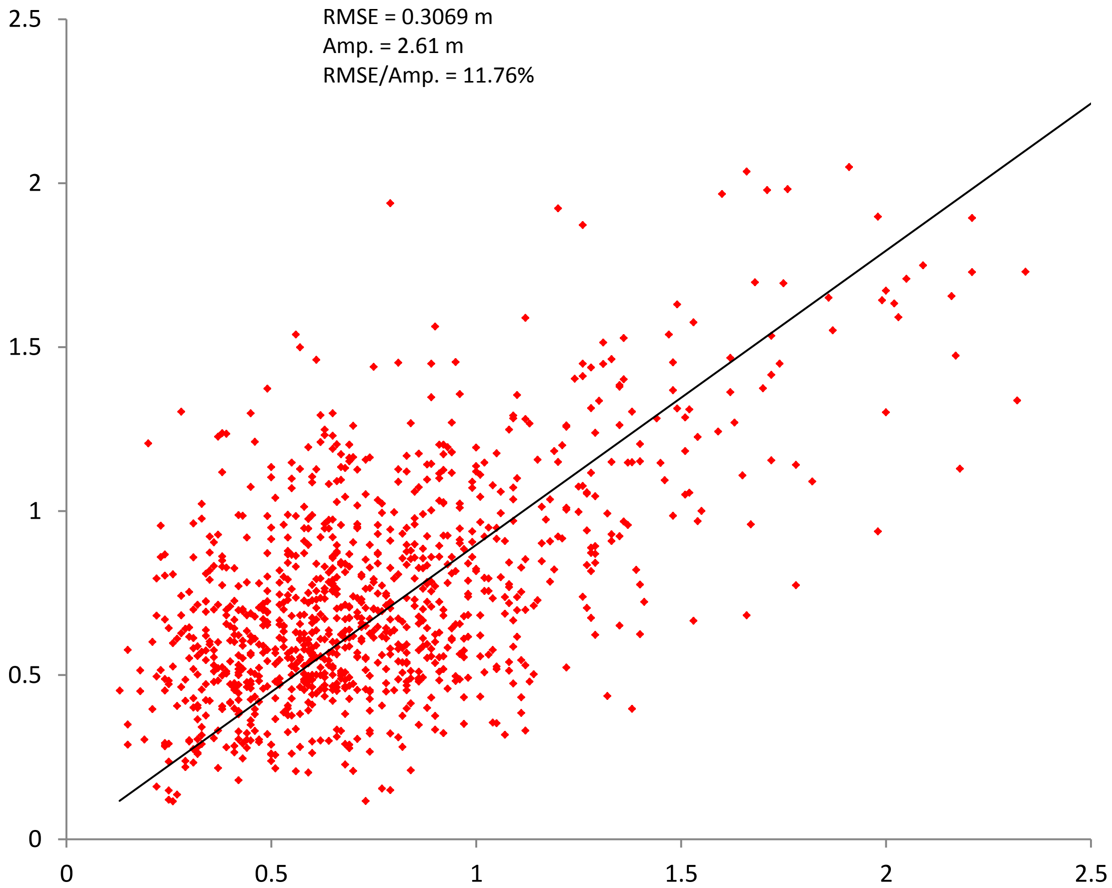

Figure 4-7 RMSE plot for modelled vs measured ADCP wave heights

4.5 Base case wave modelling

Wave data was extracted from the 30 year spectral wave model at the location shown in Figure 4-8 to obtain an indication of the predominant wave conditions. The extracted significant wave height (Hs) and peak period (Tp) datasets are summarised as a wave rose plot in Figure 4-9, indicating that the waves predominately occur from the south easterly quadrant.

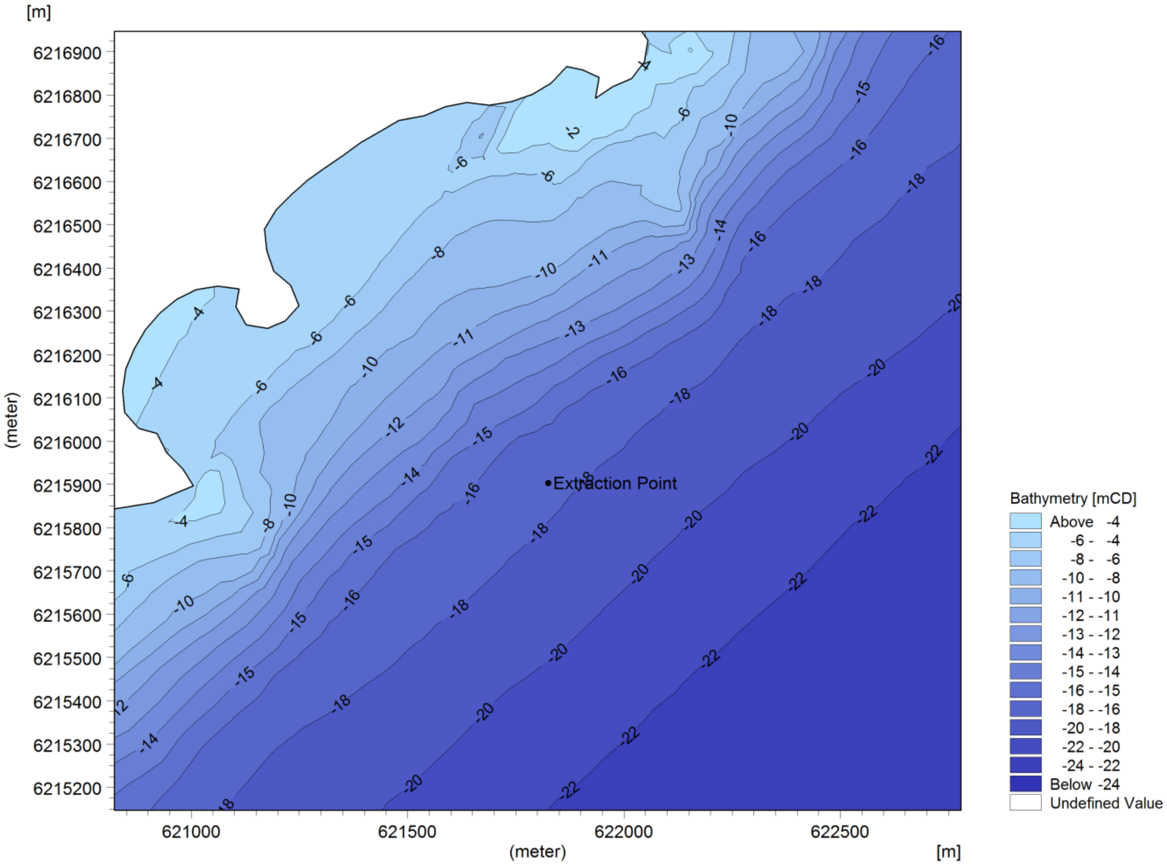

Figure 4-8 30 year wave model extraction location

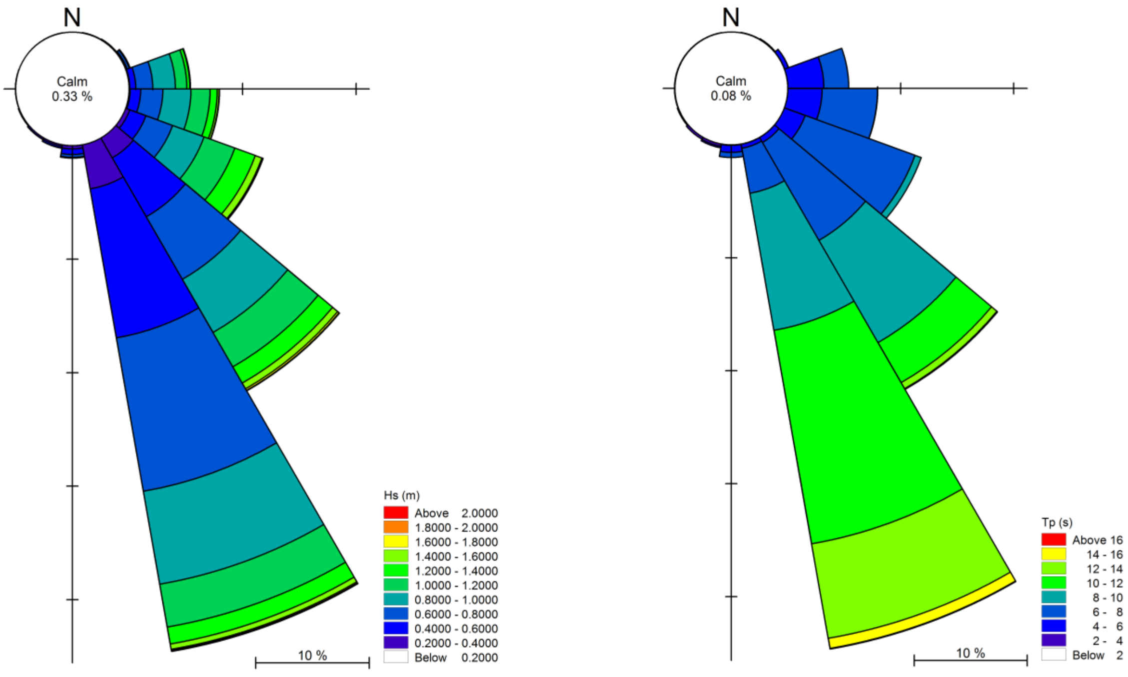

Figure 4-9 Significant wave height (Hs) and peak period (Tp) roses for the 30 year dataset

Occurrence tables of the data are contained in Appendix D. These tables indicate that:

- the most prominent conditions occur within the 140°-160° range, with Hs conditions of 0.6-0.8m and Tp 10-12s.
- wave conditions over Hs=1.8m are also produced within the predominant directional range

To identify changes in the wave climate due to the addition of the proposed infrastructure, the base case and infrastructure scenario were compared for typical and worst case wave conditions at the site location. These wave conditions were identified from the occurrence tables in Appendix D. Results for the corresponding conditions were then extracted from the 2012 spectral wave model. Table 4-2 summarises these conditions selected for comparison. This includes typical wave conditions from the south, easterly, and south easterly quadrants, as well as maximum wave conditions which were identified as propagating from the south east.

Table 4-2 Wave conditions selected for base case and infrastructure comparison

Mean wave direction (degrees)	Hs (m)	Tp (s)	Comment
SE (140-160)	0.6-0.8	10-12	Typical south easterly wave conditions
SE (140-160)	>1.8	8-12	High south easterly wave conditions
S (170-190)	0.4-0.6	6-10	Typical southerly wave conditions
E (80-100)	0.8-1.0	6-8	Typical easterly wave conditions

4.5.1 Results

The results for the four representative wave conditions shown in Table 4-2 are shown in Figure 4-10 to Figure 4-13.

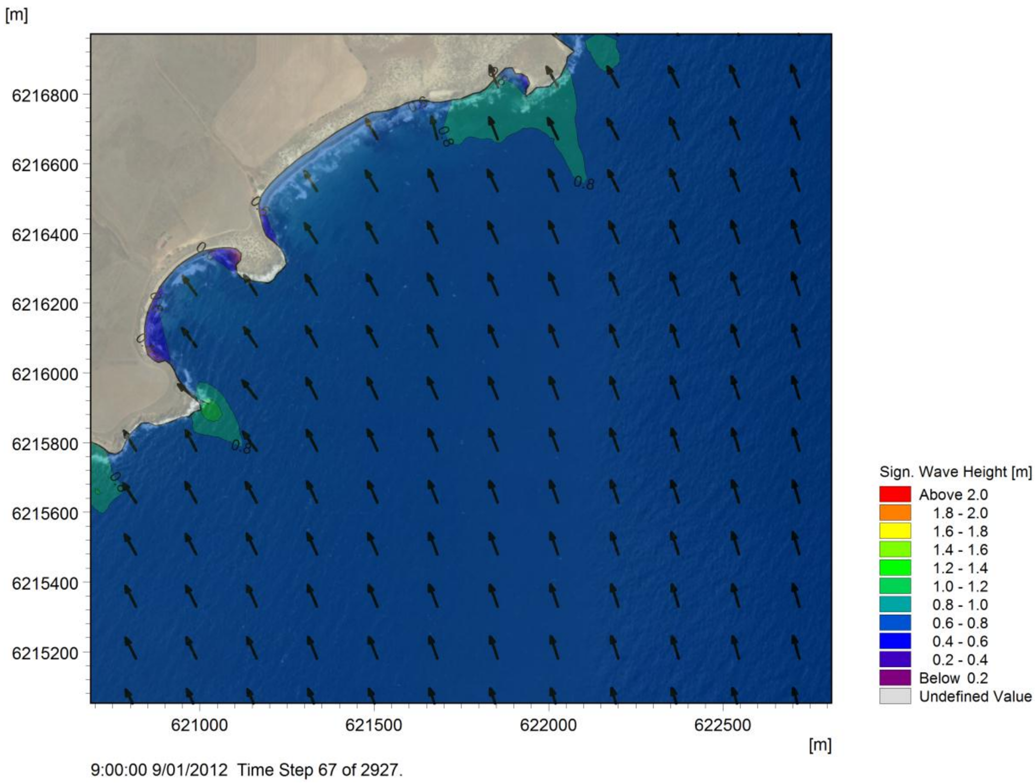

Figure 4-10 Typical south easterly wave conditions

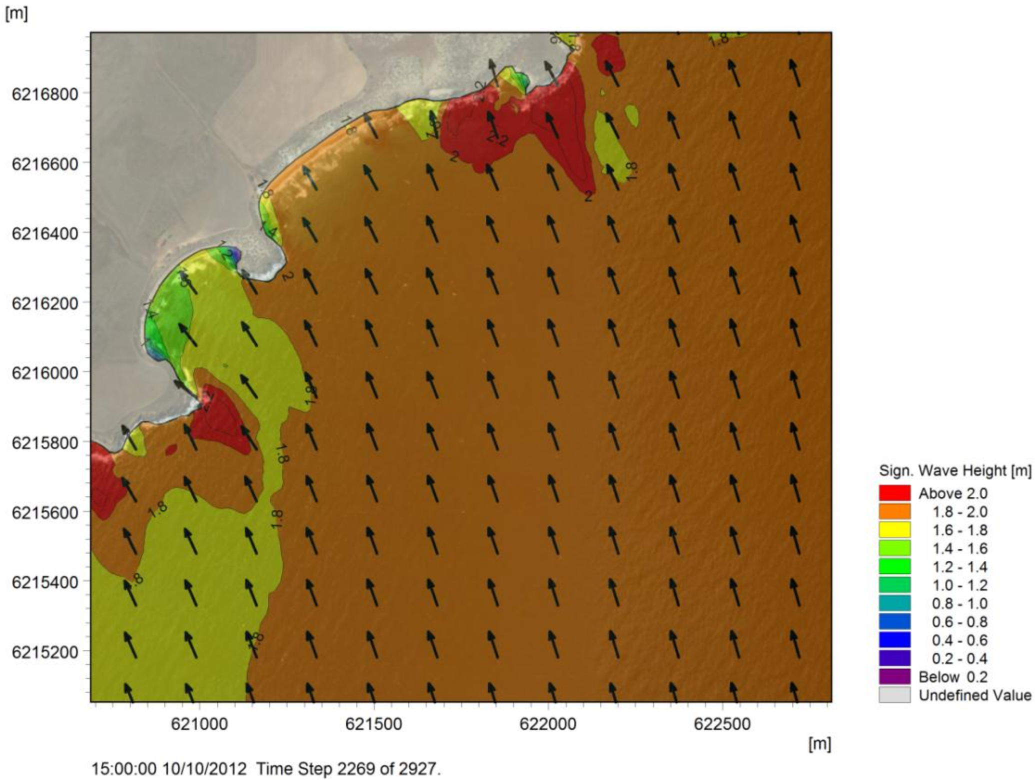

Figure 4-11 High south easterly wave conditions

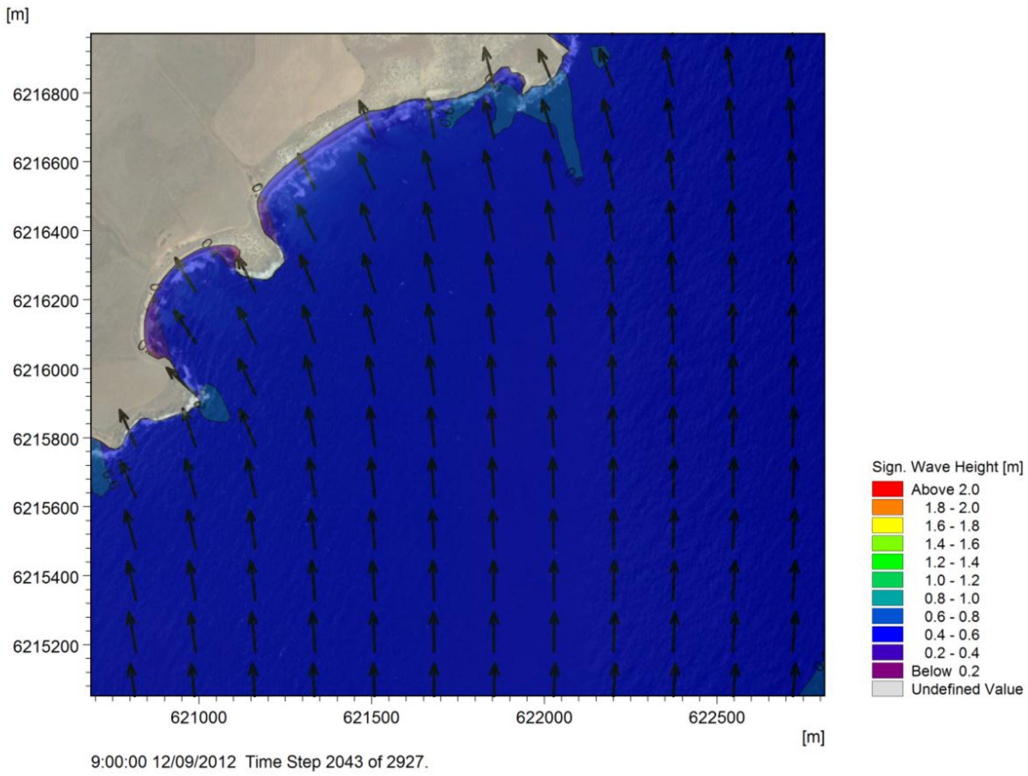

Figure 4-12 Typical southerly wave conditions

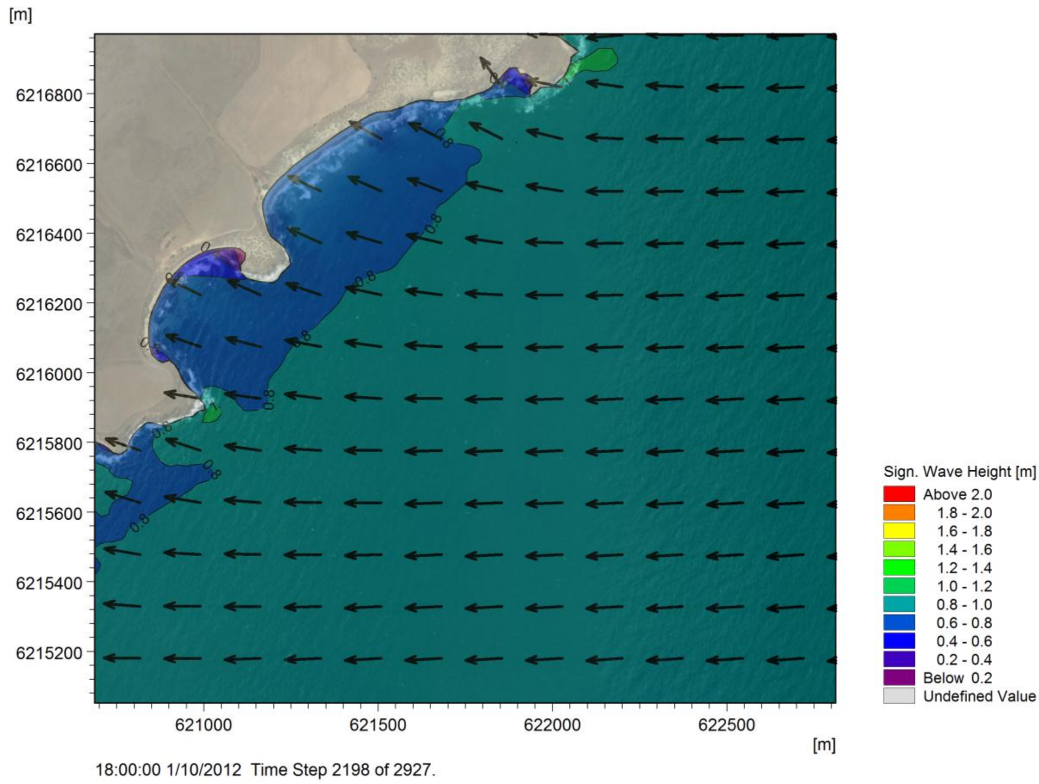

Figure 4-13 Typical easterly wave conditions

4.5.2 Discussion

The resulting wave climate at the proposed site location for typical south easterly wave conditions is shown in Figure 4-10. The orientation of the coastline is approximately perpendicular to the direction of the incoming wave climate, and hence a Hs=0.6-0.8m propagates directly into both the northern and southern bays. The wave conditions increase at the northern and southern headlands, with a maximum Hs=1.0-1.2m generated at the southern headland and Hs=0.8-1.0m generated at the northern headland.

Figure 4-11 illustrates the resulting wave conditions at the proposed site location for high south easterly wave conditions. Offshore wave conditions propagating from the south east are approximately 0.2m less than those propagating directly offshore from the site location. Hence the resulting wave conditions in the northern bay are marginally larger than those in the southern bay. There is an increase in the wave conditions at both the southern and northern headlands, with wave heights of greater than Hs=2.0m being generated at these locations.

Typical southerly wave conditions at the site location are shown in Figure 4-12. The incoming wave conditions of Hs=0.4-0.6m are refracted directly into the northern and southern bays. Marginally larger wave conditions of Hs=0.6-0.8m are generated at both the northern and southern headlands.

The wave climate at the site location for a typical easterly wave climate is shown in Figure 4-13. The results indicate that as the waves propagate into the northern and southern bays the wave climate is reduced by approximately 0.2m. The wave conditions at both the northern and southern headlands are marginally larger with Hs=1.0-1.2m.

4.6 Development scenario

The proposed marine infrastructure was included in the wave model to investigate the relative changes to the wave climate as a result of the inclusion of the proposed infrastructure at the port site. The reclaimed MOF and causeway structure, as well as the piling for the jetty, wharf, and dolphins, were assessed in this scenario.

4.6.1 Proposed Infrastructure

The mesh developed for the base case was used to create the infrastructure scenario. The bathymetry was artificially altered to incorporate the proposed causeway and MOF infrastructure in the model. The bathymetry of the infrastructure scenario is shown in Figure 4-14 below. Piles were included as sub-grid structures in the MIKE setup file with the same properties and distribution used in the hydrodynamic model (see section 3.5.1).

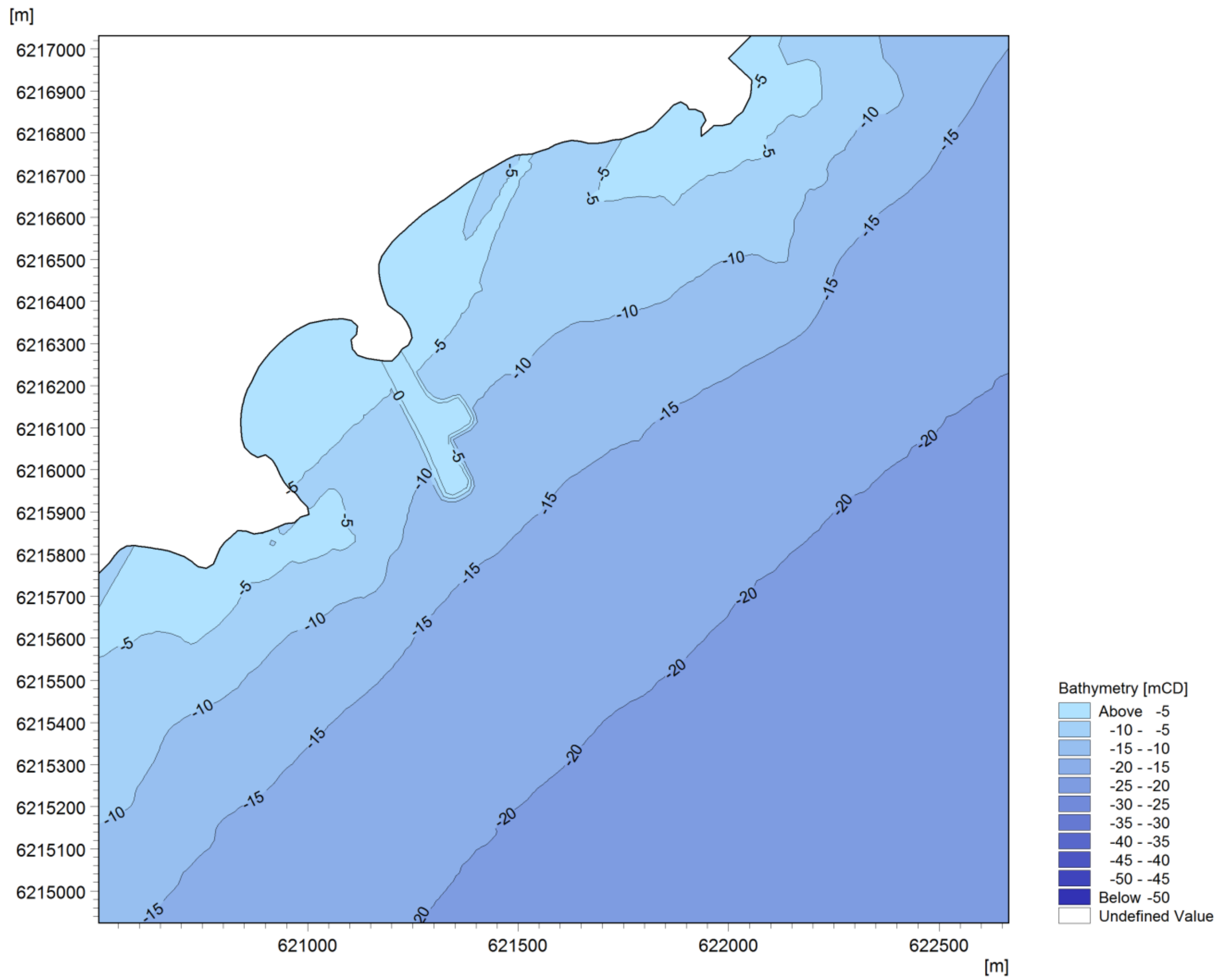

Figure 4-14 Bathymetry incorporating proposed MOF and causeway

4.6.2 Results

A comparison of the wave conditions before and after the construction of the proposed maritime infrastructure are shown in Figure 4-15 to Figure 4-22 for the key wave condition scenarios reported for the base case scenario (refer Table 4-2).

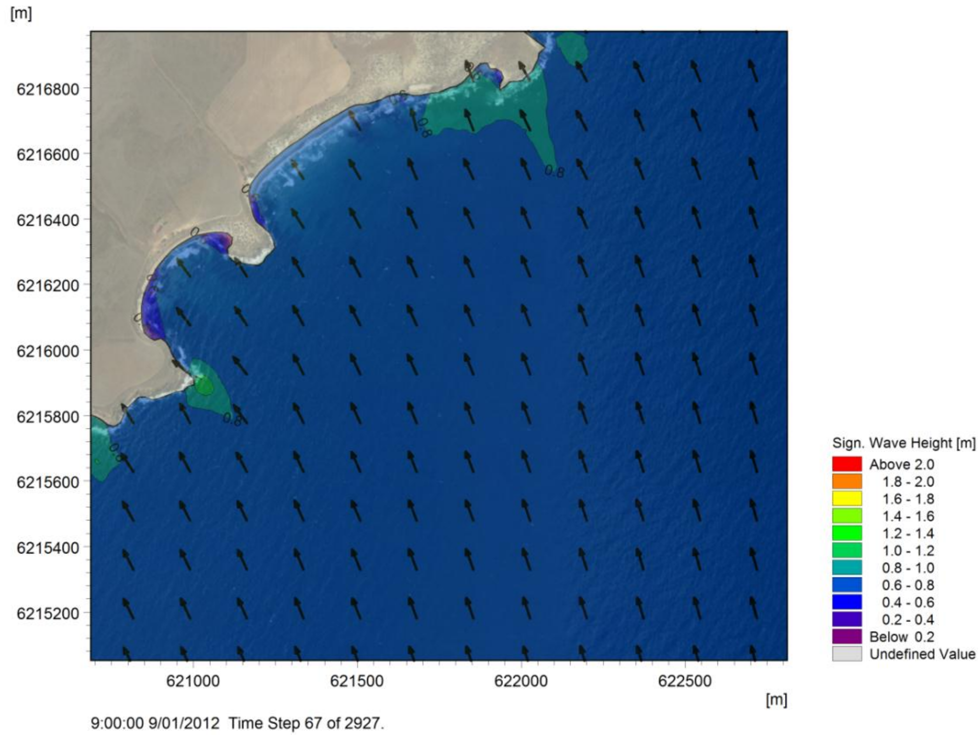

Figure 4-15 Typical south easterly wave conditions

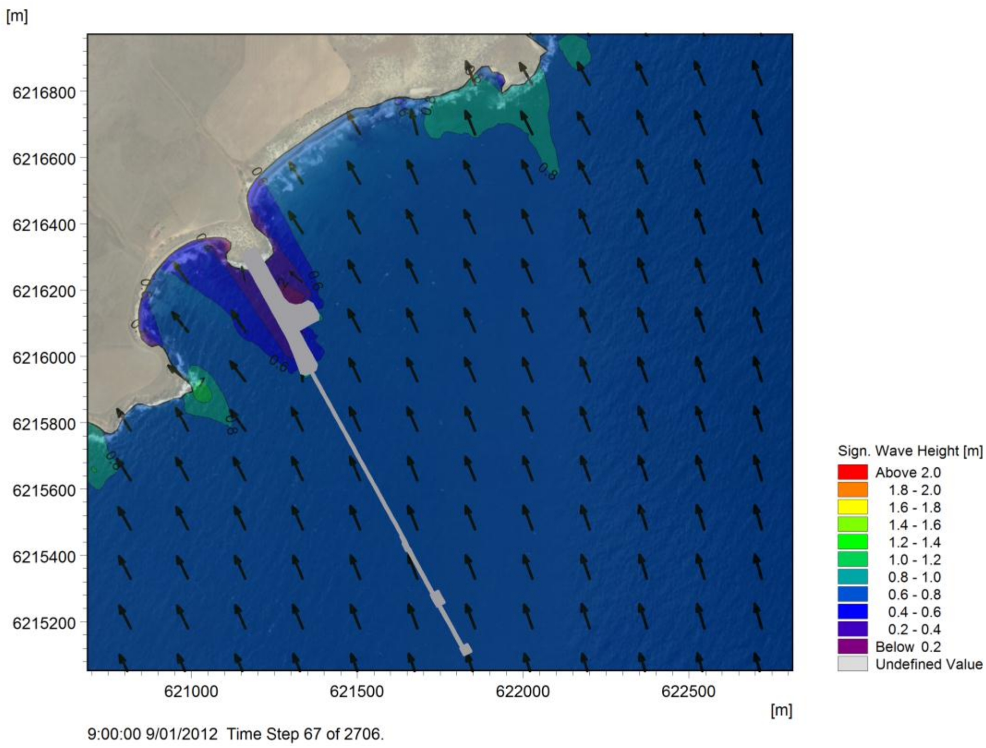

Figure 4-16 Typical south easterly wave conditions for infrastructure scenario

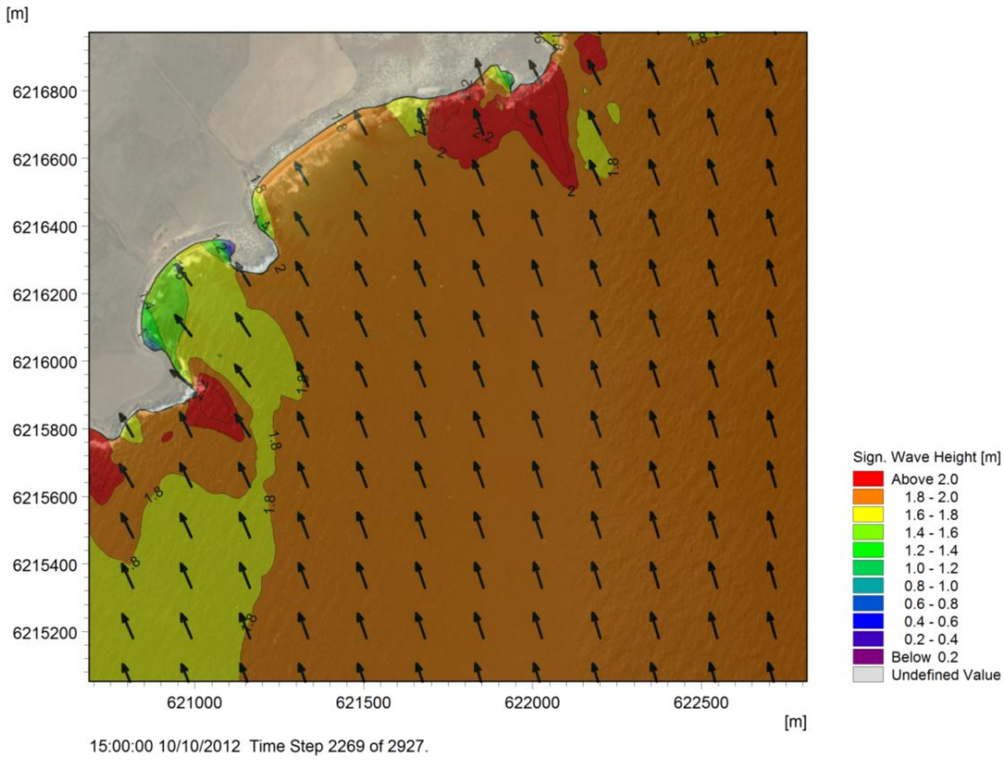

Figure 4-17 High south easterly wave conditions

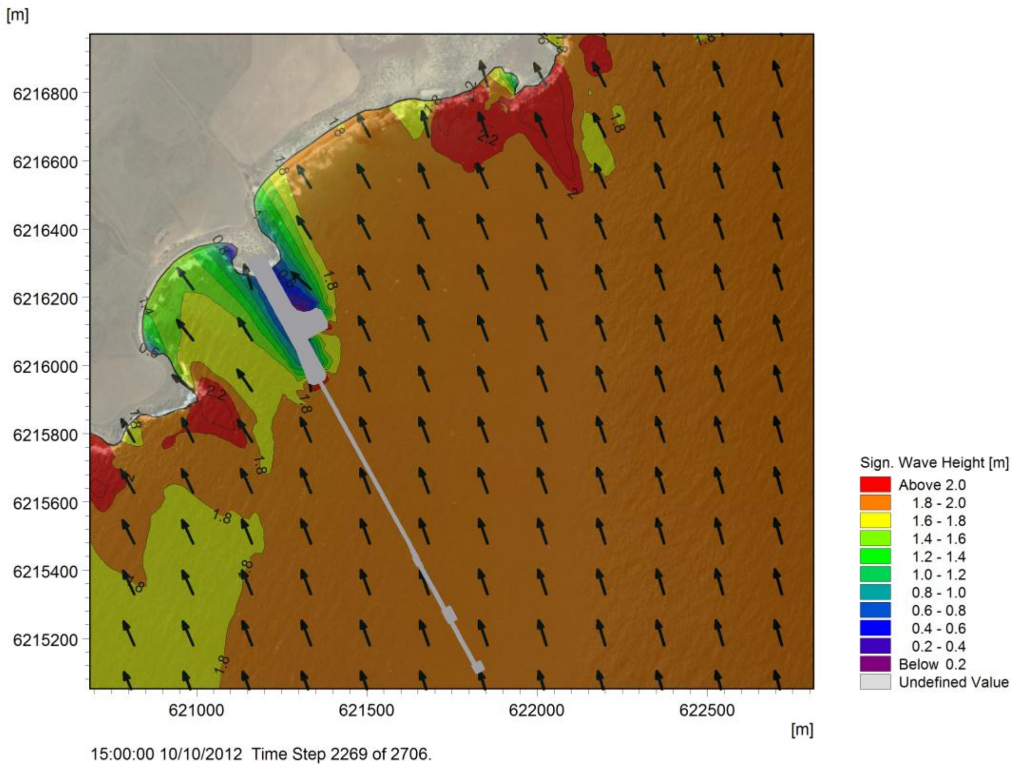

Figure 4-18 High south easterly wave conditions for infrastructure scenario

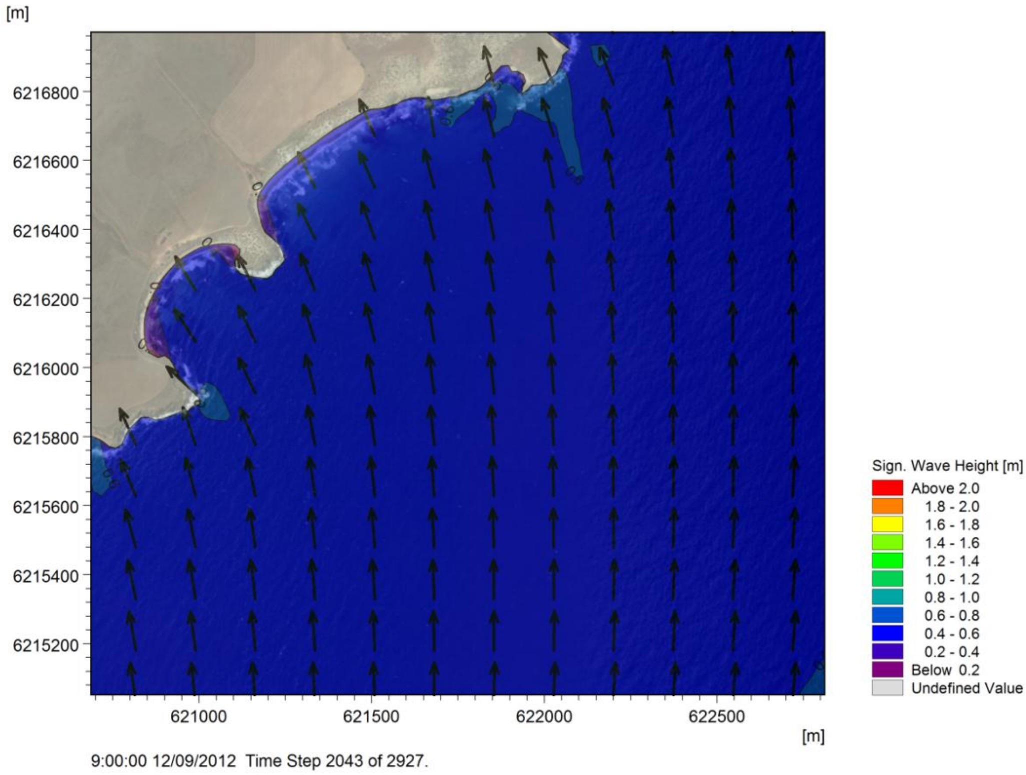

Figure 4-19 Typical southerly wave conditions

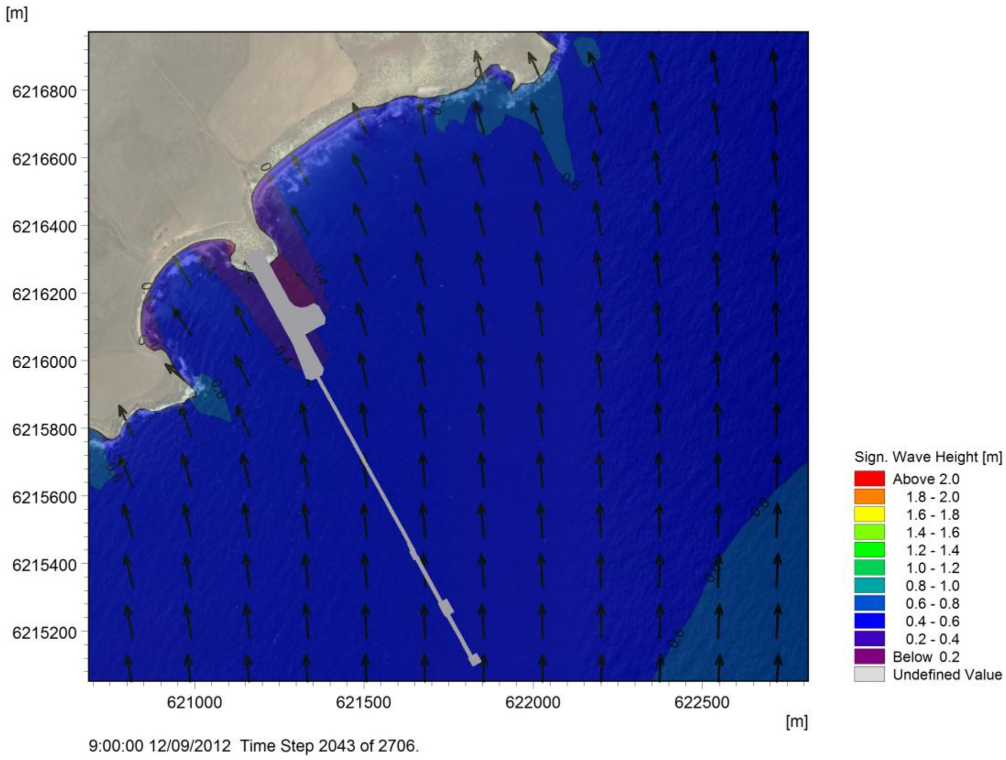

Figure 4-20 Typical southerly wave conditions infrastructure scenario

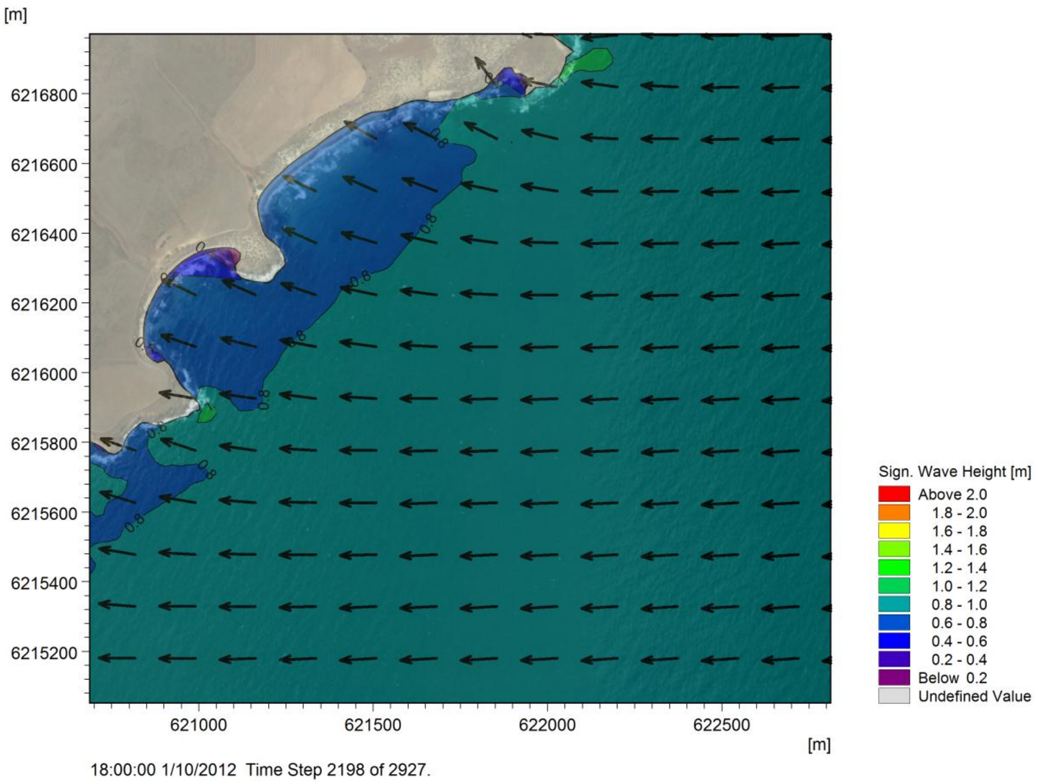

Figure 4-21 Typical easterly wave conditions

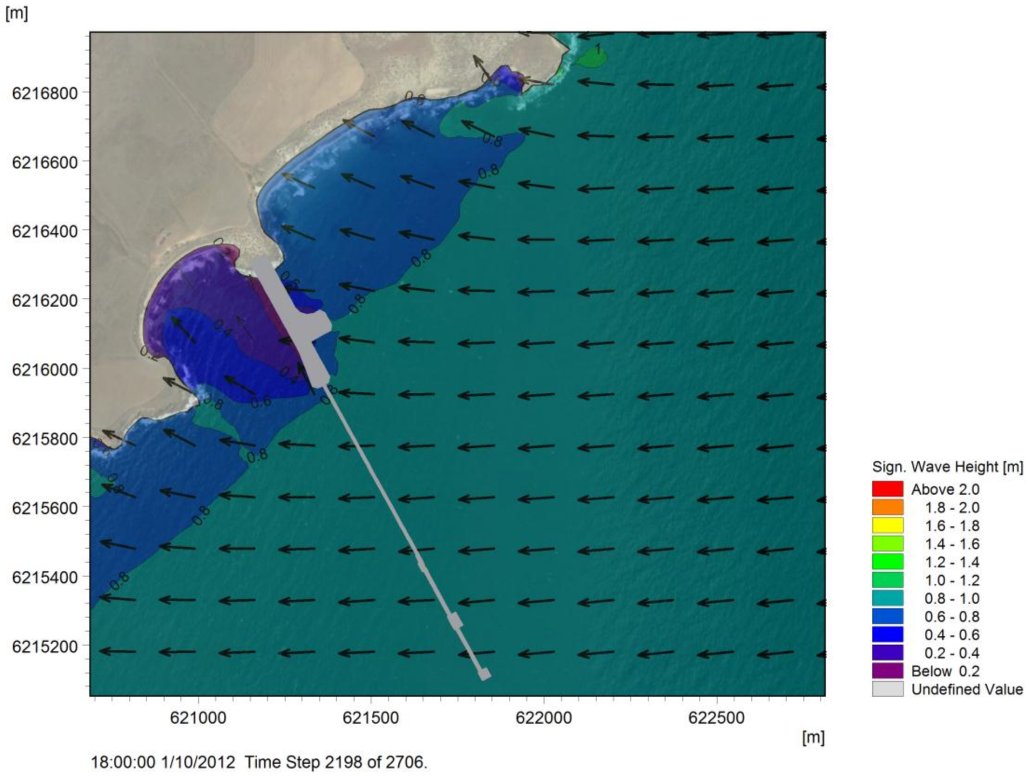

Figure 4-22 Typical easterly wave conditions infrastructure scenario

4.6.3 Wave Climate Comparison Discussion

Typical South Easterly Wave Conditions

Figure 4-16 and Figure 4-16 illustrate the wave height and direction for a typical south easterly wave condition with and without the inclusion of the proposed maritime infrastructure. In general, the resulting wave conditions after construction of the maritime infrastructure are similar to the base case results. The addition of the MOF and causeway structure provides a sheltering effect to the area either side of the middle headland, generally reducing the wave climate to below Hs=0.6m in the lee of the structure.

High South Easterly Wave Conditions

Similar results are observed when the incoming south easterly wave climate is increased to above Hs=1.8m as shown in Figure 4-17 and Figure 4-18. Wave conditions either side of the causeway are reduced due to the sheltering effect of the MOF and causeway. Impacts to the wave climate are localised around the middle headland in the lee of the structure. In general very limited impact of the infrastructure on this wave condition is experienced in the bays and headlands to the north and south of the causeway.

Typical Southerly Wave Conditions

The wave conditions generated for a typical southerly wave climate are shown in Figure 4-19 and in Figure 4-20 for the infrastructure scenario. The offshore wave conditions are similar to those observed for the base case scenario (Figure 4-19). Locations behind the causeway and MOF structures are sheltered from incoming waves, reducing the wave conditions to below Hs=0.4m. Impacts to the wave climate are localised around the middle headland in the lee of the structure.

Typical Easterly Wave Conditions

Figure 4-21 and Figure 4-22 illustrate the changes in wave climate after construction of the proposed infrastructure for a typical easterly wave condition. The proposed causeway infrastructure shelters the southern bay from incoming wave conditions, reducing conditions within the bay to Hs<0.4m. Similarly the significant wave height at the southern headland is reduced by approximately 0.2m. The oblique angle of this wave condition in relation to the infrastructure results in a greater sheltering effect. However, this condition is relatively infrequent and is considered to result in a minimal impact overall.

4.7 Conclusion

A spectral wave model was adopted to evaluate the potential change in wave climate at the site due to the construction of the proposed MOF and causeway infrastructure. The results indicate that:

- The orientation of the causeway provides some protection to the southern bay, particularly for typical easterly wave conditions whereby the incoming wave climate is reduced by approximately 0.4m within the bay. The exception to this is southerly wave conditions whereby the orientation of the causeway has little impact on the incoming wave conditions.
- The orientation of the proposed causeway provides sheltering to the southern headland during incoming easterly wave conditions, reducing the wave height by approximately 0.2m.

Wave conditions in the northerly bay remain relatively unchanged due to the addition of the causeway infrastructure. However, the structure provides a small region of sheltering either side of the middle headland.

5. Bed shear stress analysis

The results of the SKM hydrodynamic and wave model provide information on the relative change in the potential for nearshore sediment deposition and erosion as a result of the construction of the proposed maritime infrastructure at Cape Hardy. Relative changes in the nearshore bed shear stress between the baseline and infrastructure model runs will identify any resultant change in the potential for sediment transport and provide a quantitative assessment of the impact of the proposed maritime infrastructure on the nearshore sediment transport regime. The results of the bed shear stress analysis will inform the EIS.

5.1 Sediment Transport Threshold

The bed shear stress is the frictional force exerted on a unit area of sea bed by current flowing over it, which can be induced by coastal processes such as waves or tidal flow. This is an important quantity when assessing the potential for sediment transport or siltation.

The threshold bed shear stress provides an indication of the stress required for sediment transportation/motion to occur. This can be estimated using the threshold Shields parameter θ_{cr} (Soulsby 1997);

$$\theta_{cr} = \frac{\tau_{cr}}{g(\rho_S - \rho)d}$$

Where	τ_{cr}	=	threshold bed shear-stress	
	g	=	acceleration due to gravity	= 9.81ms^{-1}
	ρ_S	=	grain density	= 2650 kg/m^3
	ρ	=	water density	= 1025 kg/m^3
	d	=	grain diameter	= 4.67 x 10^{-4} m

To determine the threshold bed shear-stress τ_{cr} the threshold Shields parameter θ_{cr} can be estimated using the following equation developed by Soulsby and Whitehouse (1997) (Soulsby 1997);

$$\theta_{cr} = \frac{0.30}{1 + 1.2D_*} + 0.055\left[1 - \exp(-0.020D_*)\right]$$

Where D_* is the dimensionless grain size given by (Soulsby1997);

$$D_* = \left[\frac{g(s-1)}{v^2}\right]^{1/3} d$$

Where v = kinematic viscosity of water = 1.0 x 10^{-6} m^{2}s^{-1} at a water temperature of 22°C

$s = \rho_S/\rho$

The shear stress threshold was calculated for the bed material at the proposed site location, adopting the sediment properties outlined in the sediment sampling report produced by the University of South Australia (Abbott, 2009). The results are summarised below in Table 5-1.

Table 5-1: Critical Bed Shear Stress Threshold

Parameter	Notation	Bed Shear Stress (Nm^{-2})
Bed shear stress threshold	T_{cr}	0.24

5.2 Sediment Transport Potential Assessment

The bed shear stress has been calculated under both wave and current action to assess the potential for sediment transport both prior to and after construction of the proposed maritime infrastructure at Cape Hardy.

5.2.1 Current Induced Shear Stress

Figure 5-1 to Figure 5-8 illustrate the differences in bed shear stress between the base case and infrastructure scenarios under representative current conditions. The plots indicate that the bed shear stress around the site varies from approximately 0N/m^2 to 0.18N/m^2. This falls below the estimated threshold of motion (0.24N/m^2), hence it is unlikely that significant sediment motion due to currents will occur prior to or after construction.

The bed shear stress corresponding to the maximum spring flood currents is shown in Figure 5-1 and Figure 5-2 for the baseline and infrastructure scenarios respectively.

- Both scenarios indicate that a maximum bed shear stress of approximately 0.18N/m^2 is generated at the northern headland. This corresponds to the high current speeds present at this location.
- When considering the infrastructure scenario, there is an increase in bed shear stress of approximately +0.02N/m^2 at the tip of the causeway as currents are diffracted around the structure.
- The causeway also shelters the northern bay from the incoming flood tides, reducing the extent of low bed shear stress (T < 0.02N/m^2).
- High piling density at the berthing dolphins causes a reduction in current speed and hence a reduction in bed shear stress from 0.04-0.06N/m^2 to 0.02-0.04N/m^2.
- The bed shear stress at the southern headland is reduced from 0.06-0.08N/m^2 to 0.04-0.06N/m^2 due to current interaction with the causeway.

Figure 5-3 and Figure 5-4 illustrate the bed shear stress corresponding to the maximum current conditions for the spring ebb tide.

- Areas of increased bed shear stress of approximately 0.18N/m^2 are generated at the northern headland for both the base case scenario and the infrastructure scenario.
- This corresponds to the location of the maximum current speeds. Similarly, the bed shear stress for the infrastructure scenario is reduced to below 0.02N/m^2 at the southern headland as the causeway shelters the headland from the ebb currents.

The bed shear stress corresponding to the maximum neap flood tide is shown in Figure 5-5 and Figure 5-6.

- The bed shear stress offshore of the southern bay is reduced slightly for the infrastructure scenario as a result of the current circulations generated in the southern pocket beach.
- As the currents are directed around the infrastructure, the bed shear stress is increased to 0.2-0.4N/m^2.

- Maximum bed shear stress levels from 0.14-0.16N/m^2 are generated at the northern headland for both the base case and infrastructure scenario.

Bed shear stress levels generated during a neap flood tide are shown in Figure 5-7 and Figure 5-8.

- After construction of the proposed infrastructure, the causeway shelters the southern headland from the prevailing currents, reducing the bed shear stress to below 0.02N/m^2 in this region.
- As the ebb current flows are directed around the tip of the breakwater the bed shear stress is increased from below 0.02N/m^2 to 0.02-0.04N/m^2 due to the increase in current speed.

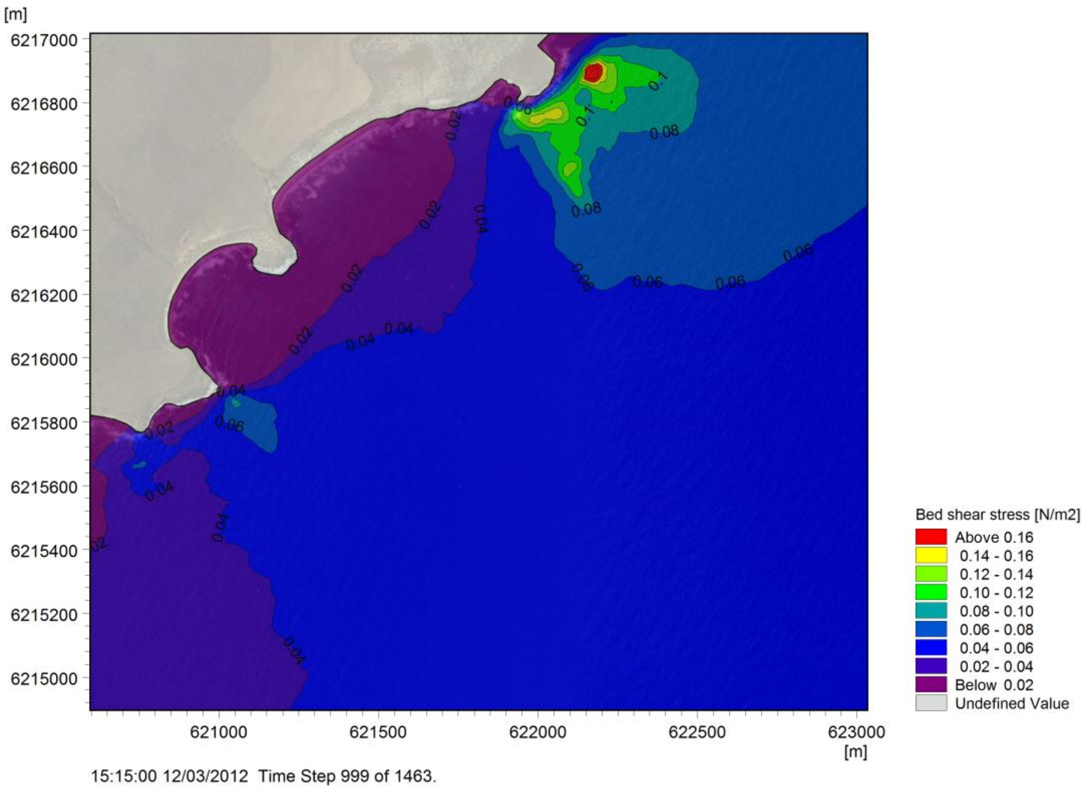

Figure 5-1 Baseline bed shear stress for maximum spring flood current

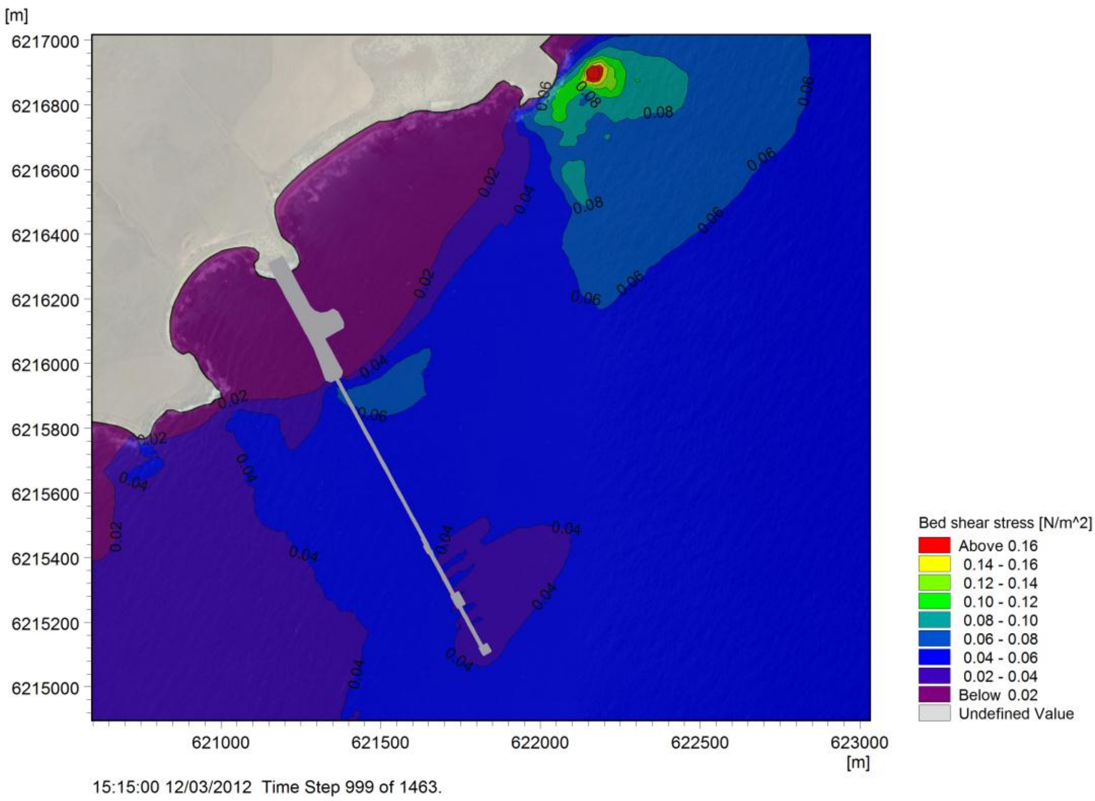

Figure 5-2 Infrastructure scenario bed shear stress for maximum spring flood current

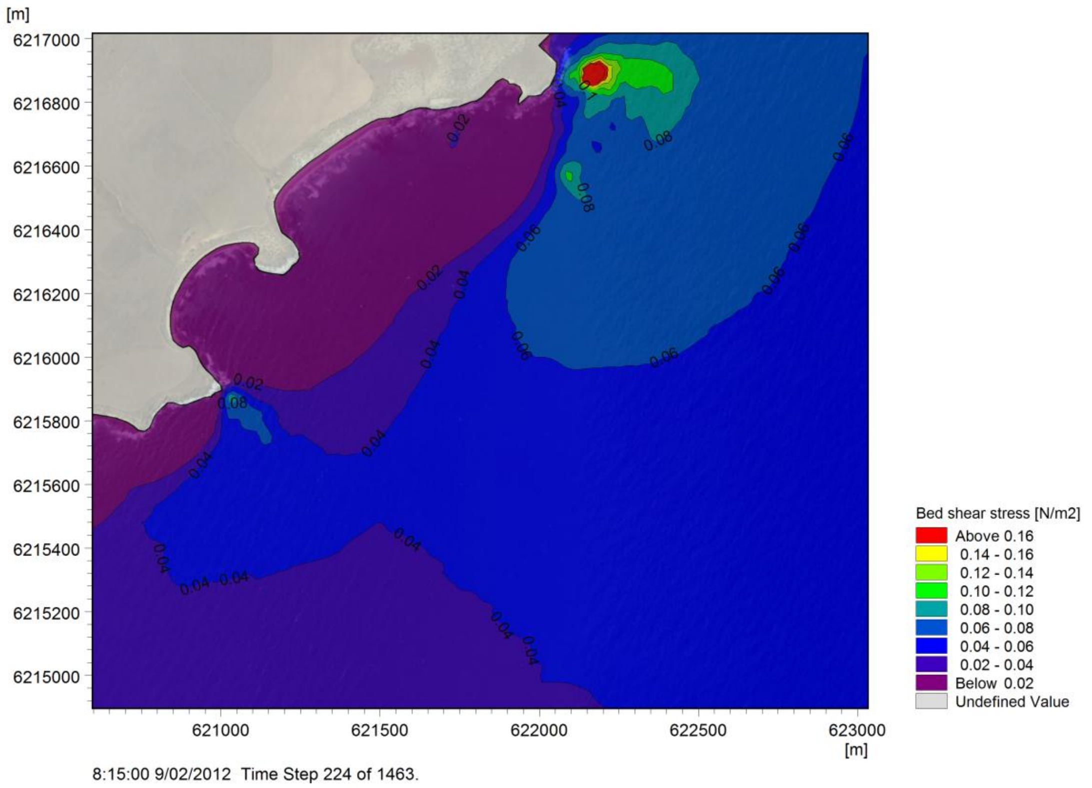

Figure 5-3 Baseline bed shear stress for maximum spring ebb current

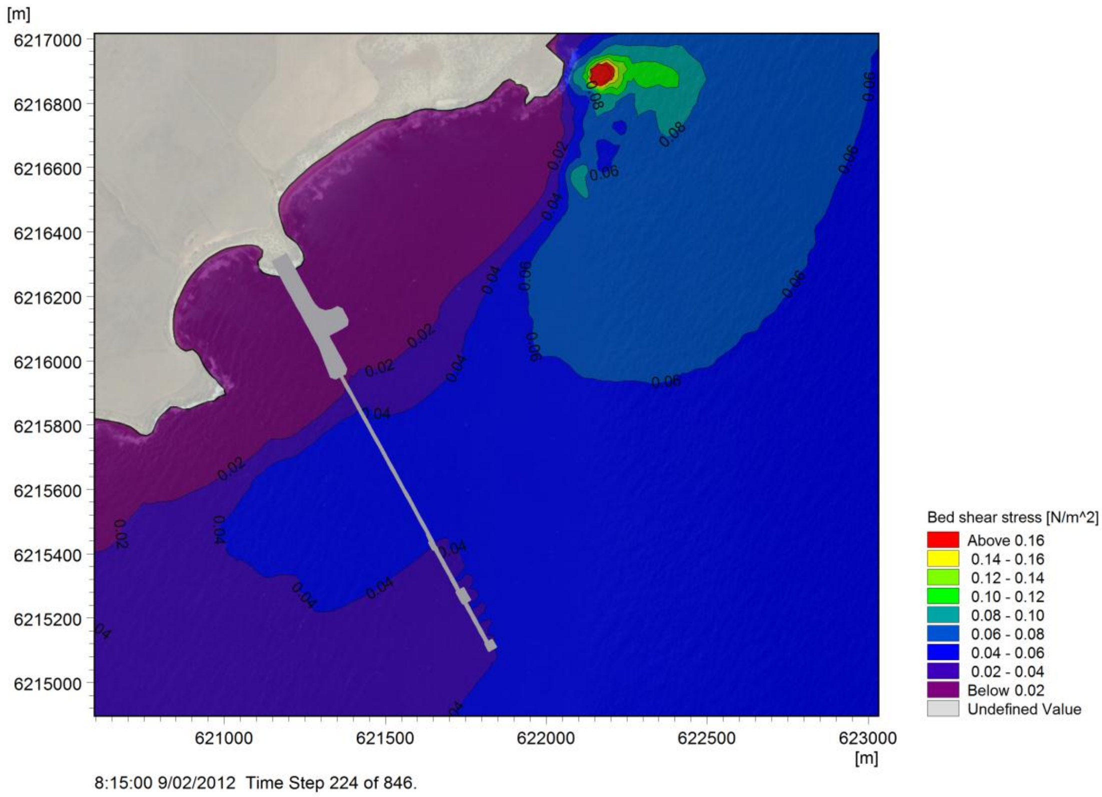

Figure 5-4 Infrastructure scenario bed shear stress for maximum spring ebb current

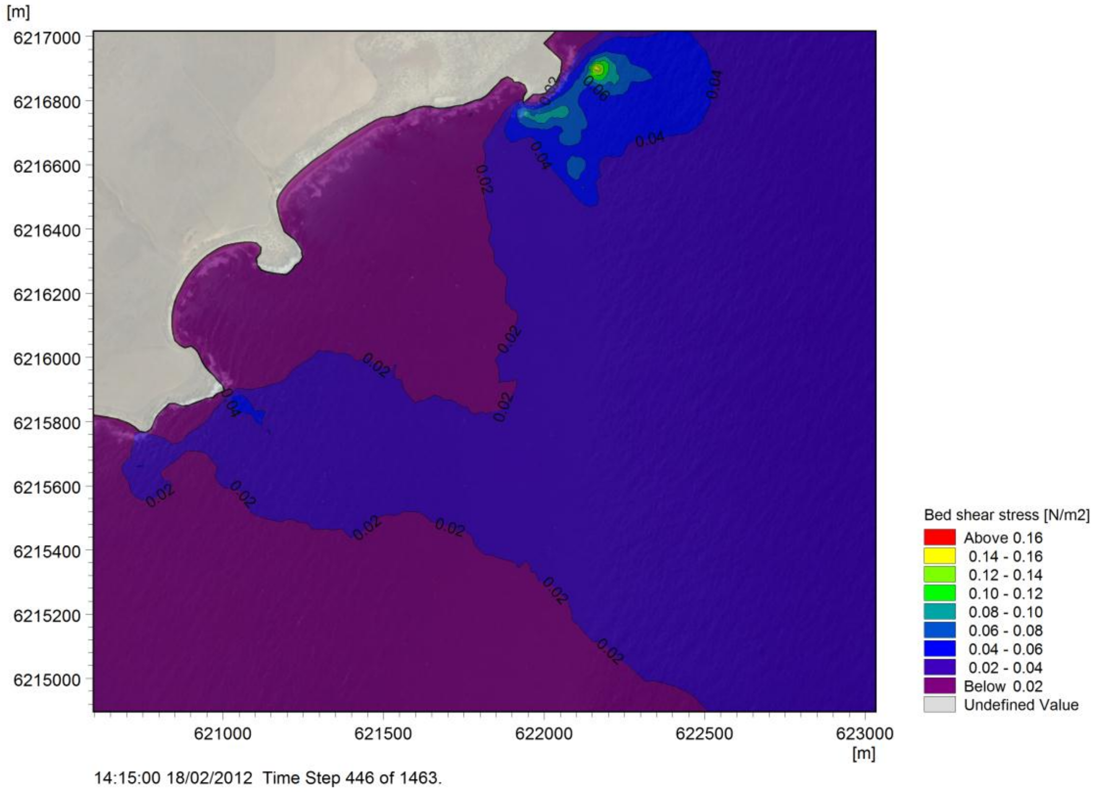

Figure 5-5 Baseline bed shear stress for maximum neap flood current

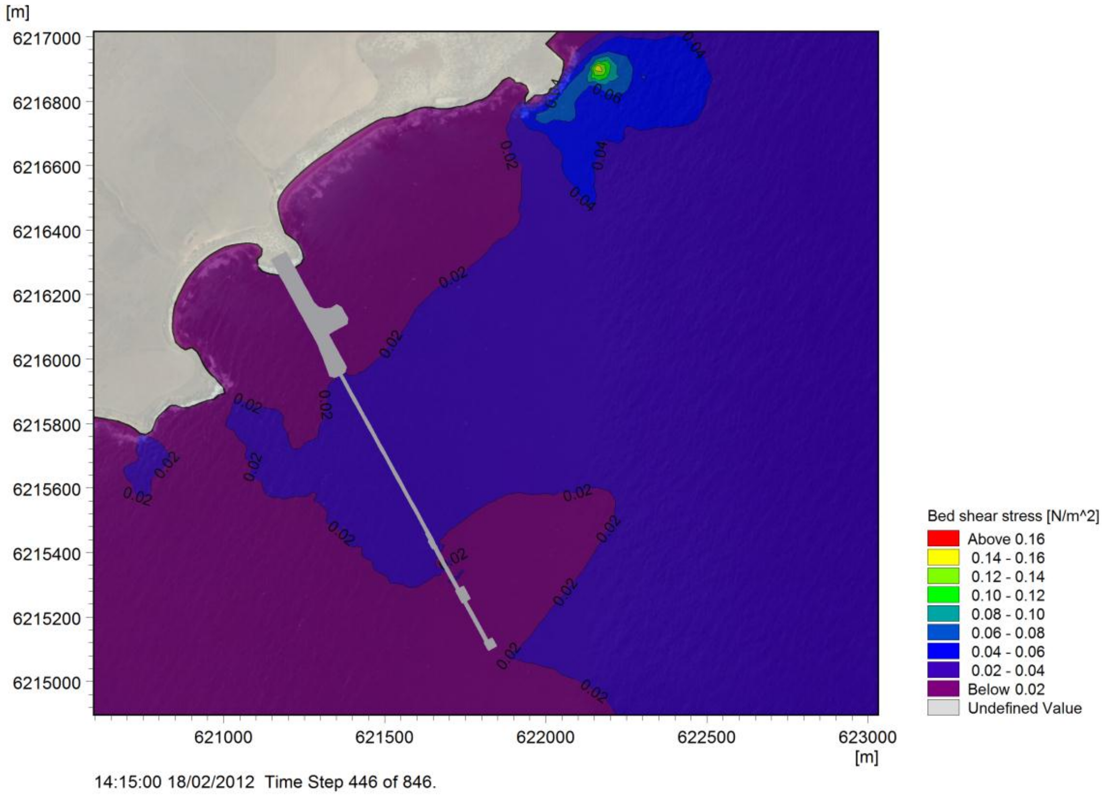

Figure 5-6 Infrastructure scenario bed shear stress for maximum neap flood current

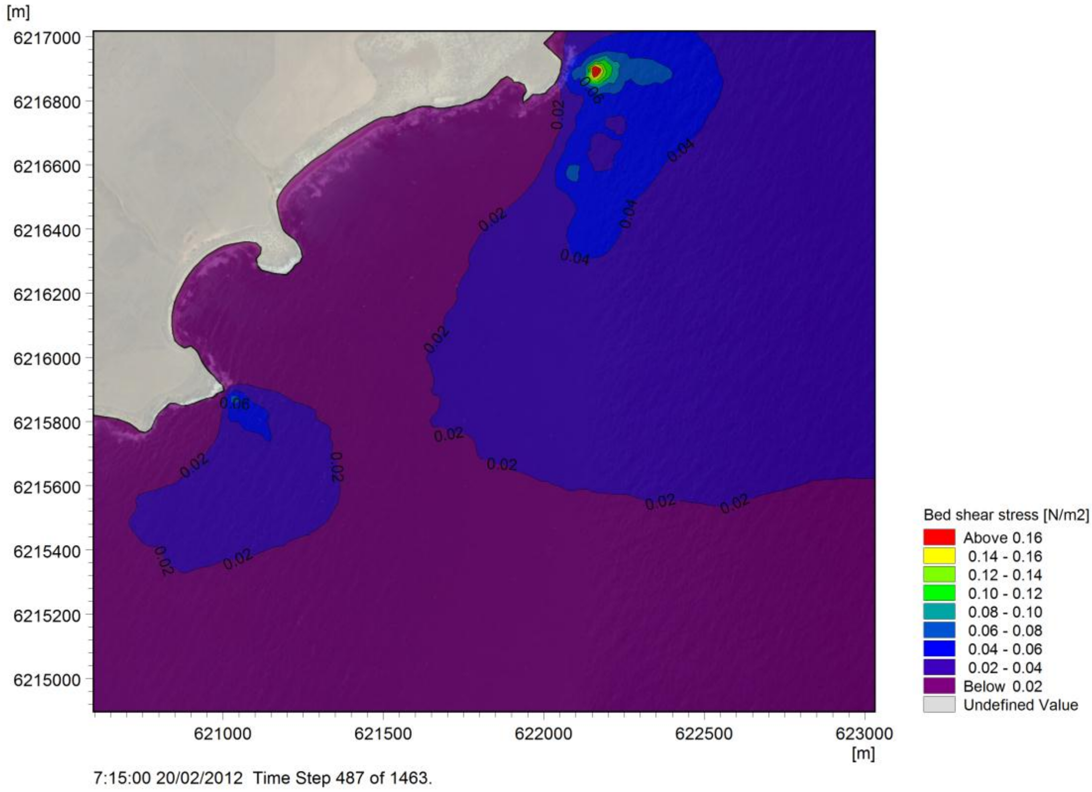

Figure 5-7 Baseline bed shear stress for maximum neap ebb current

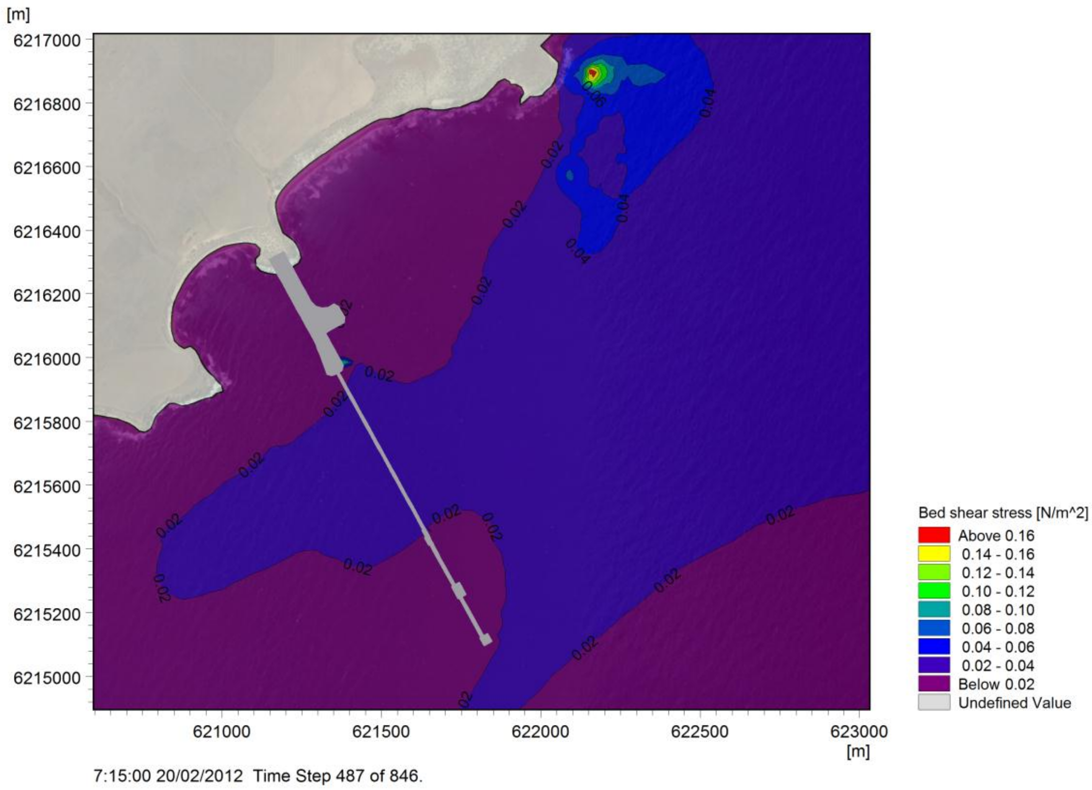

Figure 5-8 Infrastructure scenario bed shear stress for maximum neap ebb current

5.2.2 Wave Induced Shear Stress

A comparison of the wave induced bed shear stress between the base case and the infrastructure scenario is shown in Figure 5-9 to Figure 5-16 for selected key wave conditions.

The bed shear stress for a high occurrence south easterly wave condition is shown in Figure 5-9 (baseline) and Figure 5-10 (infrastructure scenario).

- The base case results indicate minimal wave induced sediment transport in deep water, with bed shear stress levels remaining below the threshold of motion (0.24N/m^2).
- Regions of high bed shear stress are generated at the northern and southern headlands due to the increase in wave conditions (see Figure 4-10).
- The bed shear stress levels along the coastline exceed the threshold of motion, it is expected that sediment transport past the headlands will be restricted due to rocky outcrops along the headland, hence essentially acting as closed cell beaches. This was investigated further and is reported in section 6 of this report.
- The addition of the causeway and MOF results in a reduction in the wave induced bed shear stress to below 0.3N/m^2 behind the structure due to the reduction in wave height.

Figure 5-11 and Figure 5-12 illustrate the bed shear stress expected for large south easterly wave conditions.

- The model run demonstrates that the nearshore sediment is likely to be mobile during large south easterly wave conditions.
- The addition of the causeway will reduce the bed shear stress in regions in close proximity to the structure which are sheltered from the incoming south easterly wave conditions. However, when considering the very low occurrence rate of these wave conditions it is expected that such events will have minimal impact on the annual gross and net sediment transport rates.

The estimated wave induced bed shear stress for typical southerly wave conditions is shown in Figure 5-13 and Figure 5-14.

- High wave conditions at the headlands generate regions of increased bed shear stress, however it is most likely that rocks along the headland will restrict sediment transport. This was investigated further and is reported in section 6 of this report.
- Bed shear stress levels on the northern side of the causeway are reduced due to the sheltering effect provided by the causeway during southerly wave conditions.

The bed shear stress results for typical easterly wave conditions are shown in Figure 5-15 and Figure 5-16.

- The highest potential for wave induced sediment transport is generated at the headlands due to the increase in wave conditions. The presence of rocks at these locations is suspected to restrict sediment transport. It is predicted that the majority of sediment transport will occur within the northern and southern pocket beaches.
- The addition of the causeway structure reduces bed shear stress levels to below 0.1N/m^2 on the southern side of the structure as it shelters the region from the incoming easterly wave conditions.

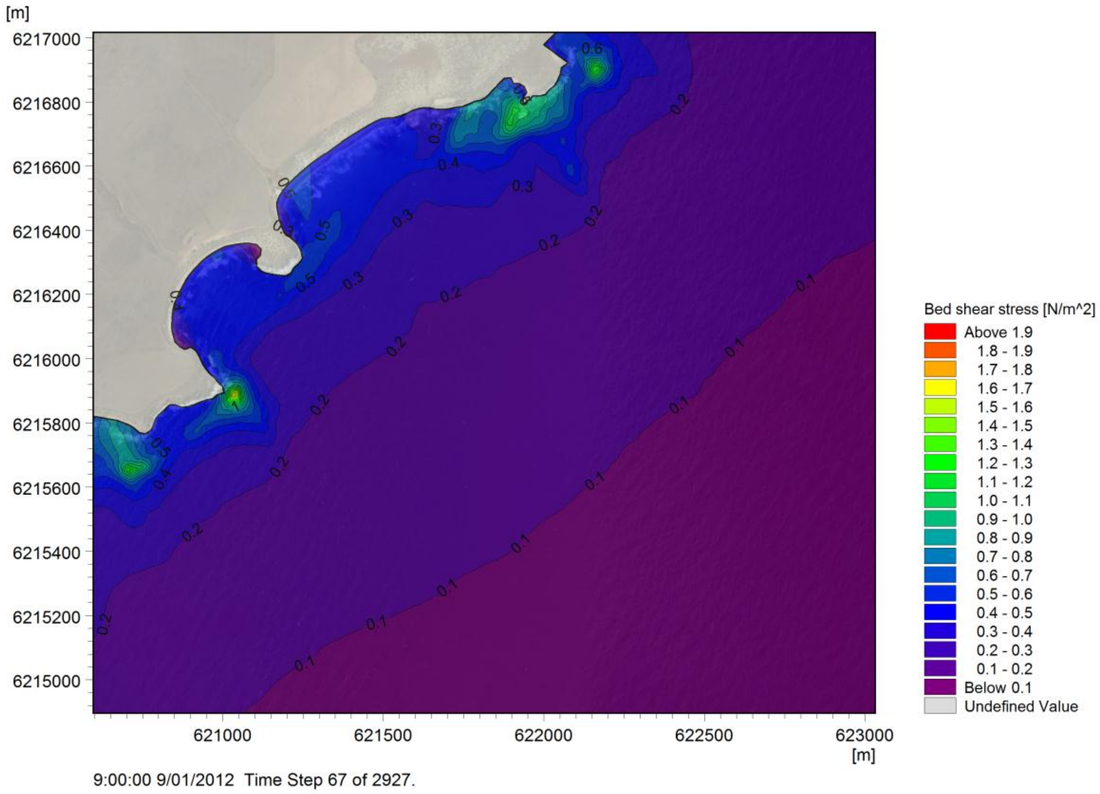

Figure 5-9 Baseline bed shear stress for average south easterly conditions

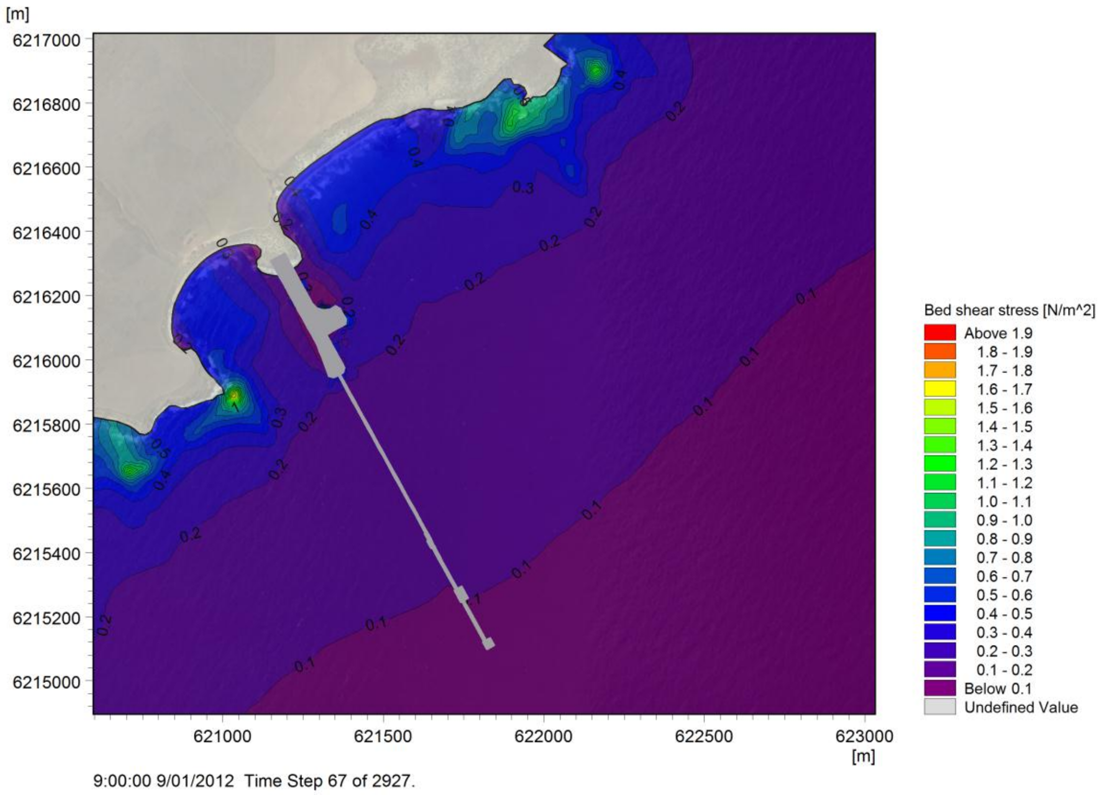

Figure 5-10 Infrastructure scenario bed shear stress for average south easterly conditions

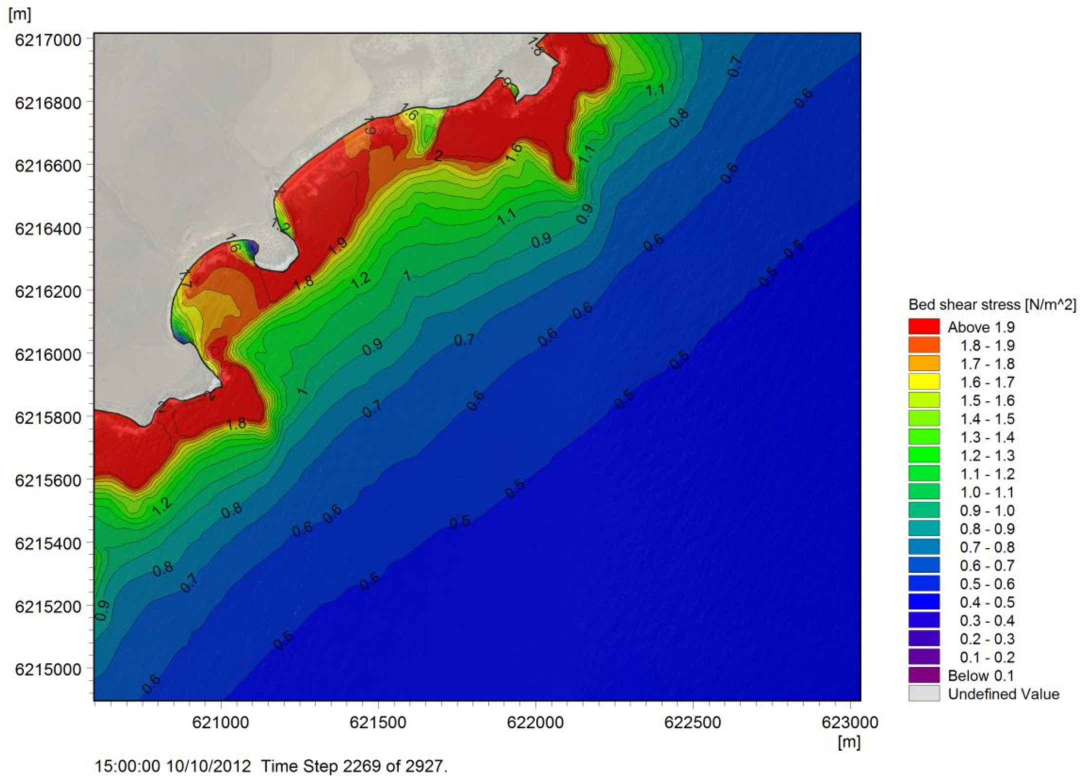

Figure 5-11 Baseline bed shear stress for large south easterly wave conditions

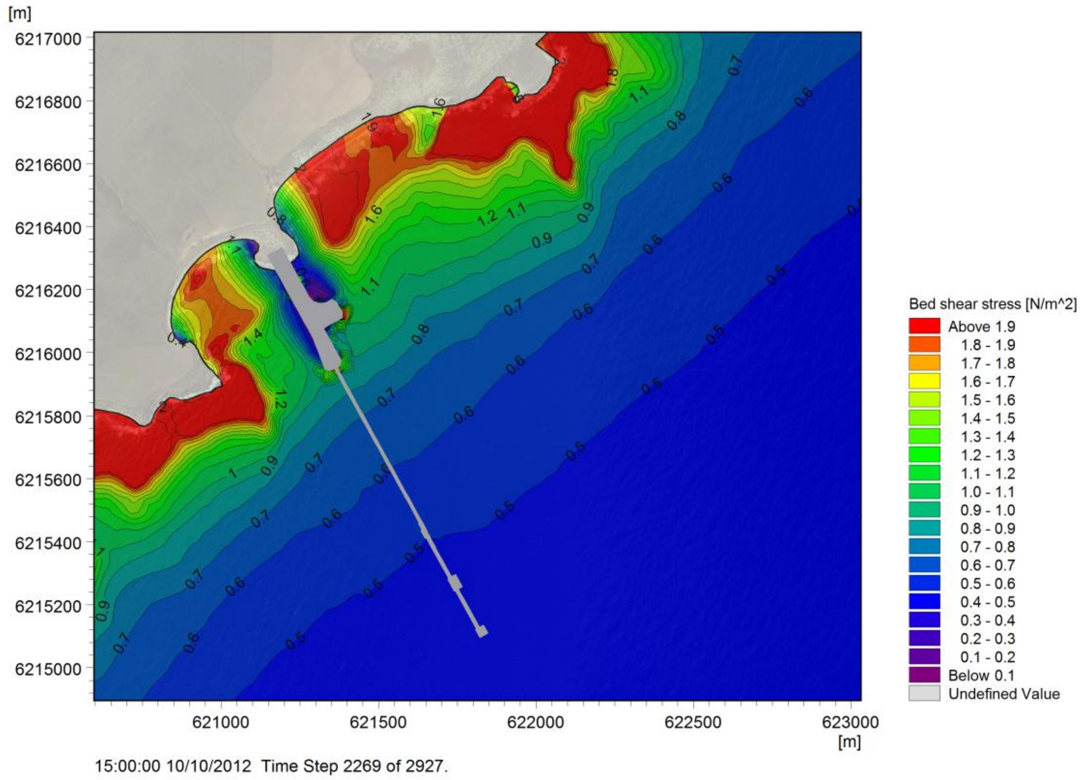

Figure 5-12 Infrastructure scenario bed shear stress for large south easterly wave conditions

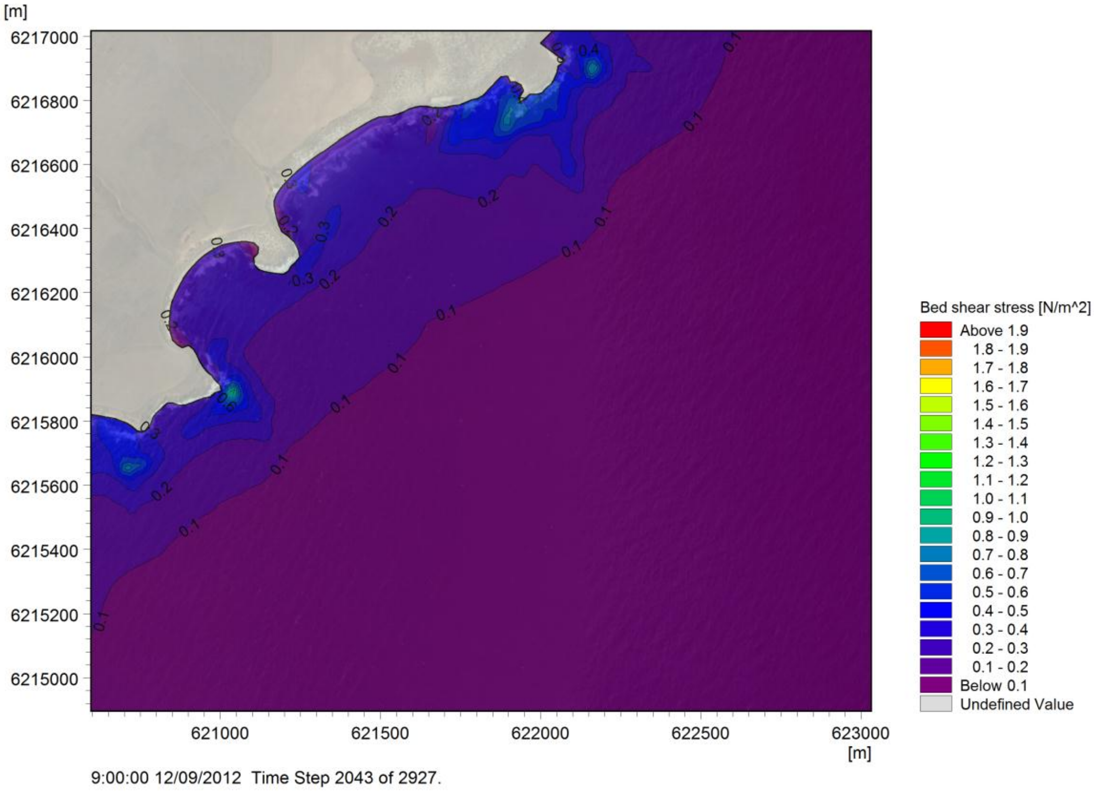

Figure 5-13 Baseline bed shear stress for sample southerly wave conditions

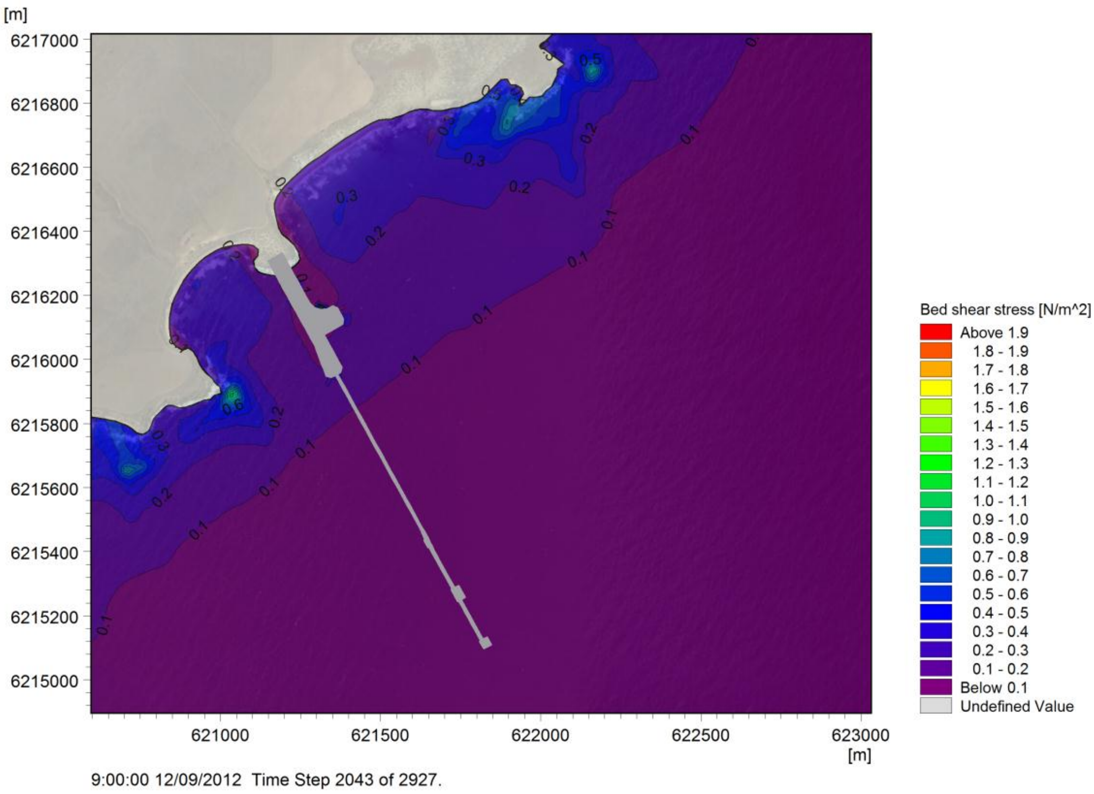

Figure 5-14 Infrastructure scenario bed shear stress for sample southerly wave conditions

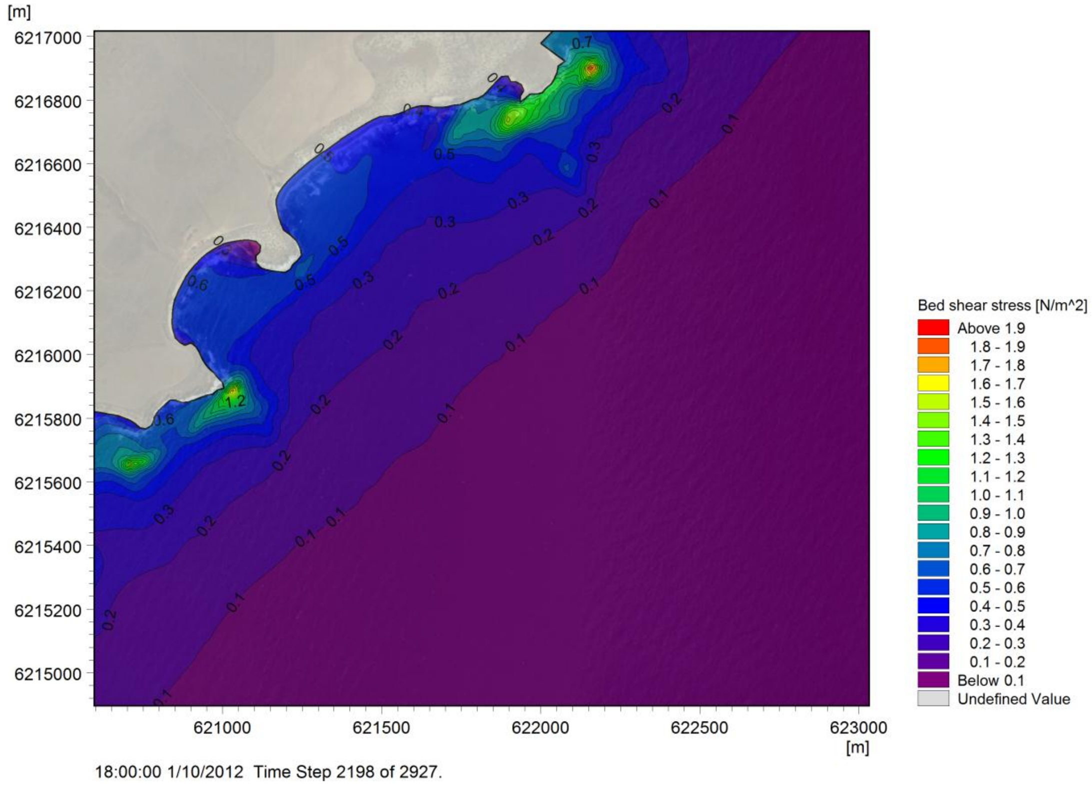

Figure 5-15 Baseline bed shear stress for sample easterly wave conditions

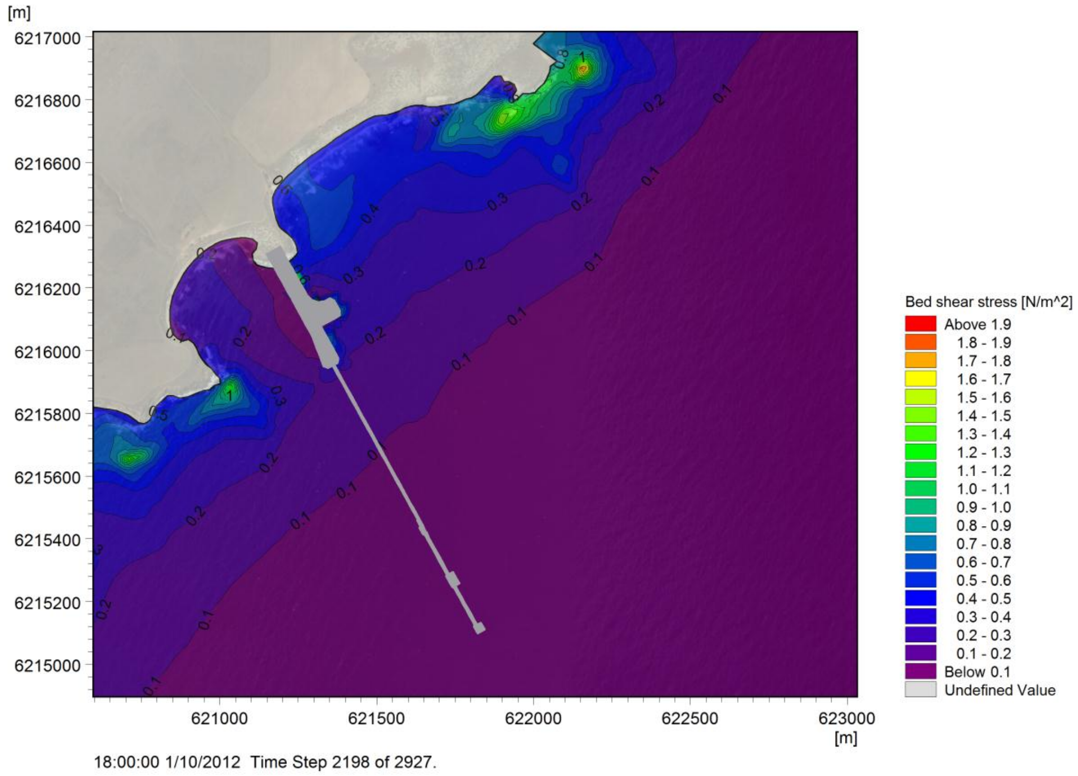

Figure 5-16 Infrastructure scenario bed shear stress for sample easterly wave conditions

5.3 Conclusions

Potential impacts resulting from the construction of the proposed infrastructure on sediment transport at the site location have been assessed in terms of bed shear stress from both currents and waves.

The current induced bed shear stress results indicate that:

- The orientation of the proposed structure leads to a shadowing effect on the southern bay and headland during spring and neap ebb currents, reducing the bed shear stress in these regions. A slight shadowing effect is also observed in the northern bay during spring and neap flood currents.
- However, for both the baseline scenario and the infrastructure scenario, bed shear stress generated during typical neap and spring tides is less than the threshold for motion, $0.24 N/m^2$ and therefore changes to the current regime as a result of the construction of the proposed maritime infrastructure is unlikely to have a significant impact on the sediment transport.

The wave induced bed shear stress results indicate that:

- For both the baseline and infrastructure scenarios, ambient and high wave conditions result in bed shear stress levels above the threshold of motion ($0.24 N/m^2$) for regions along the coast. Hence there is potential for wave induced sediment transport at these locations both prior to and after construction.
- Construction of the proposed MOF and causeway infrastructure leads to some sheltering of the southern bay during typical easterly and south easterly wave conditions, hence reducing bed shear stress levels within the bay.
- The greatest current and wave induced bed shear stress levels occur at the northern and southern headlands due to the increased wave heights at these locations. However, it is assumed that in reality large rock deposits at each of the headlands will restrict sediment transport between adjacent bays.

6. Sediment Transport Assessment

The proposed maritime infrastructure at Cape Hardy includes the construction of a nearshore causeway structure to facilitate tug mooring facilities and a material offload facility (MOF). An investigation was carried out to assess the impact of the proposed infrastructure on the existing shoreline and nearshore sediment transport processes.

6.1 Sediment Transport Processes

Maritime infrastructure constructed in close proximity to a dynamic shoreline can alter and provide shelter from the incoming wave climate. This can result in changes to the longshore drift (littoral sediment transport) regime and subsequent accretion (build-up) or erosion of beach material. The proposed maritime infrastructure includes a solid causeway structure which could arrest the longshore sediment transport in this section of coastline.

An aerial image of the site is shown below in Figure 6-1. Initial assumptions of the sediment transport processes, prior to the construction of any maritime infrastructure, are labelled on the image. The three rock headlands will restrict the sediment transport along the coast, hence creating realtively closed cell northern and southern pocket beaches. This is further illustrated in Figure 6-2 to Figure 6-5 where regions of rock deposits are visible at each of the headlands. Additional photographs of the region are also included in Appendix E for reference.

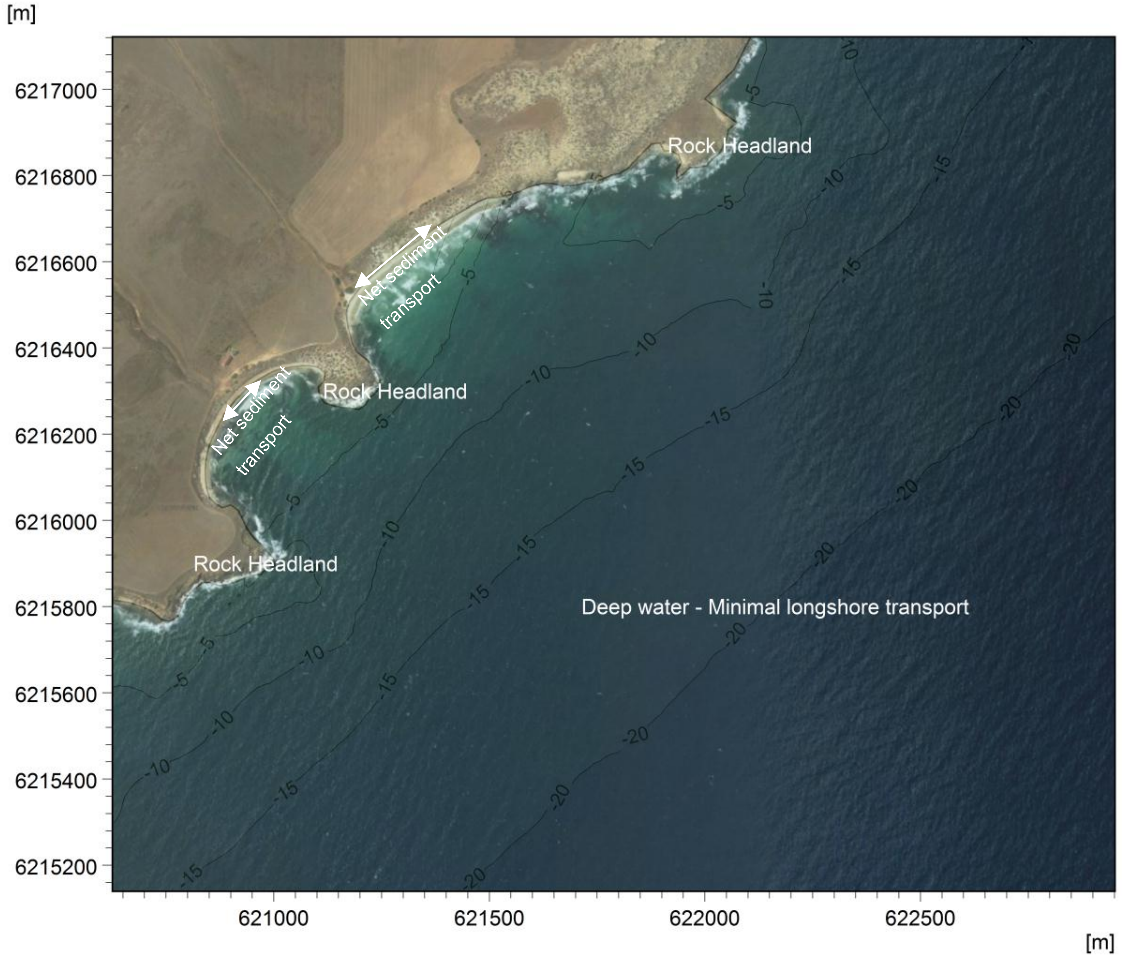

Figure 6-1 Typical sediment transport processes at proposed site location

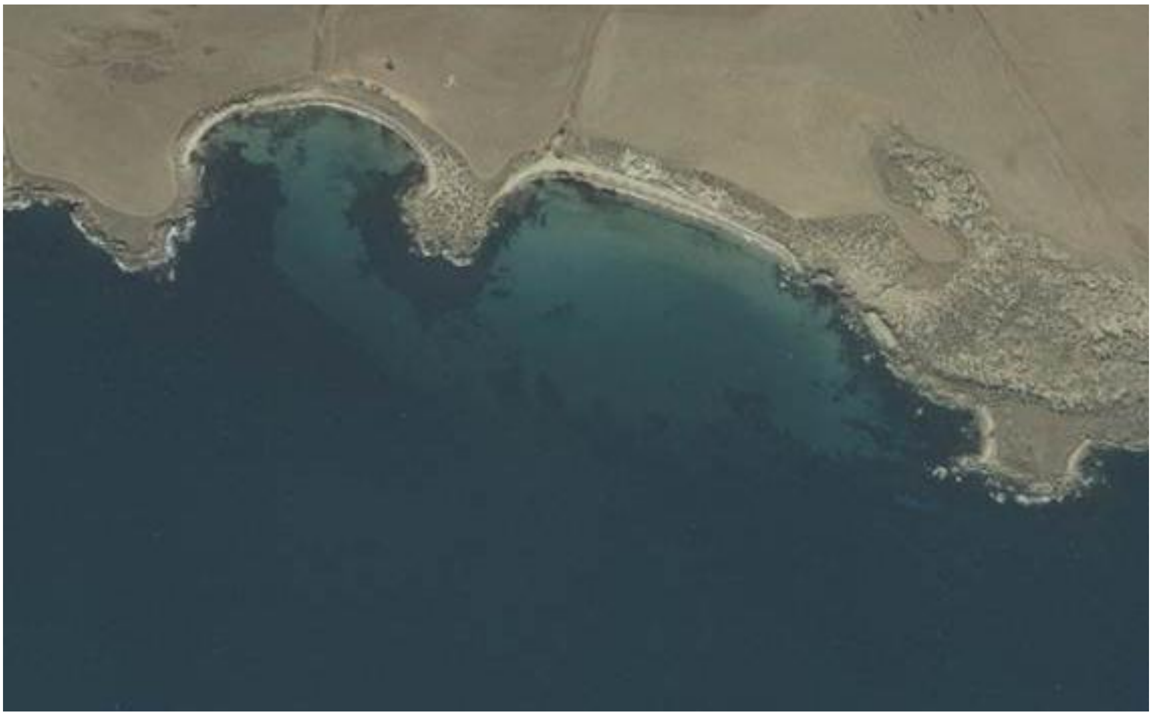

Figure 6-2 Rock deposits at the proposed site location

Figure 6-3 Southern headland

Figure 6-4 Northern headland

Figure 6-5 Middle headland

6.1.1 Depth of Closure

From the photographs and from the bathymetric survey data, it was determined that the rocky headlands extend into relatively deep water. A depth of closure calculation was adopted to provide an estimation of the depth at which sediment transport is initiated. This will provide an indication of whether sediment is mobile at the depths off the headlands which will in turn give an indication of whether beach sediment is bypassing the rocky headlands.

Initial calculations were undertaken adopting empirical formulae from the Shore Protection Manual (SPM 1984) to estimate the average depth of closure. The average depth of closure was estimated to be approximately 8m for typical wave conditions at the site (Hs<1m).

Water depth at the end of the rocky headlands ranges from 6-10mCD. This indicates that only a small amount of sediment is expected to transfer between the pocket beaches. This corresponds to historical aerial photography of the region which illustrates no noticeable change in the coastline which indicates that the shoreline is relatively stable (see Appendix F).

6.2 Longshore Transport Modelling

A longshore sediment transport model was adopted to assess how stable the existing shoreline is and whether the proposed maritime infrastructure will have a significant impact on the longshore sediment transport regime.

The Littoral Drift components of DHI's Littoral Processes FM module were adopted for the purpose of this assessment to simulate the sediment transport for the baseline and infrastructure scenarios. This will provide an indication of any relative change in the nearshore sediment transport processes as a result of the construction of the proposed maritime infrastructure.

6.2.1 Model Description

The Littoral Drift model of DHI's Littoral Processes FM module accounts for wave refraction, shoaling, breaking, and directional spreading, as well as wave setup caused by wave radiation stress, and longshore current. The calculation of littoral transport is composed of two components:

- Longshore current calculation
- Sediment transport calculation

The longshore current model allows for a description of regular and irregular waves as input into the model, as well as the influence of tidal current, non-uniform bottom friction, wave refraction, shoaling and breaking. To determine the cross-shore distribution of longshore current, wave height and wave setup for a coastal profile the longshore and cross-shore momentum balance equations are solved.

Longshore sediment transport is estimated from a Quasi Three-Dimensional Sediment Transport model (STPQ3D), which calculates the instantaneous and time-averaged hydrodynamics and sediment transport in two horizontal directions in a point. These longshore sediment transport rates are then integrated based on the local wave, current and sediment conditions to estimate the total littoral drift across the cross-shore profile.

The model assumes that there is an unlimited supply of sediment to the profile and therefore provides an indication the potential volumes of longshore drift.

6.2.2 Profiles

To investigate the coastal environment cross shore beach profiles were created at increments along the coastline. These profiles were extracted from the high resolution bathymetric survey data. The model domain and corresponding cross shore profile is shown in Figure 6-6. The cross shore profiles were extracted from the -17mCD depth contour to the baseline at 1m increments to ensure that the region of potential sediment transport was well defined.

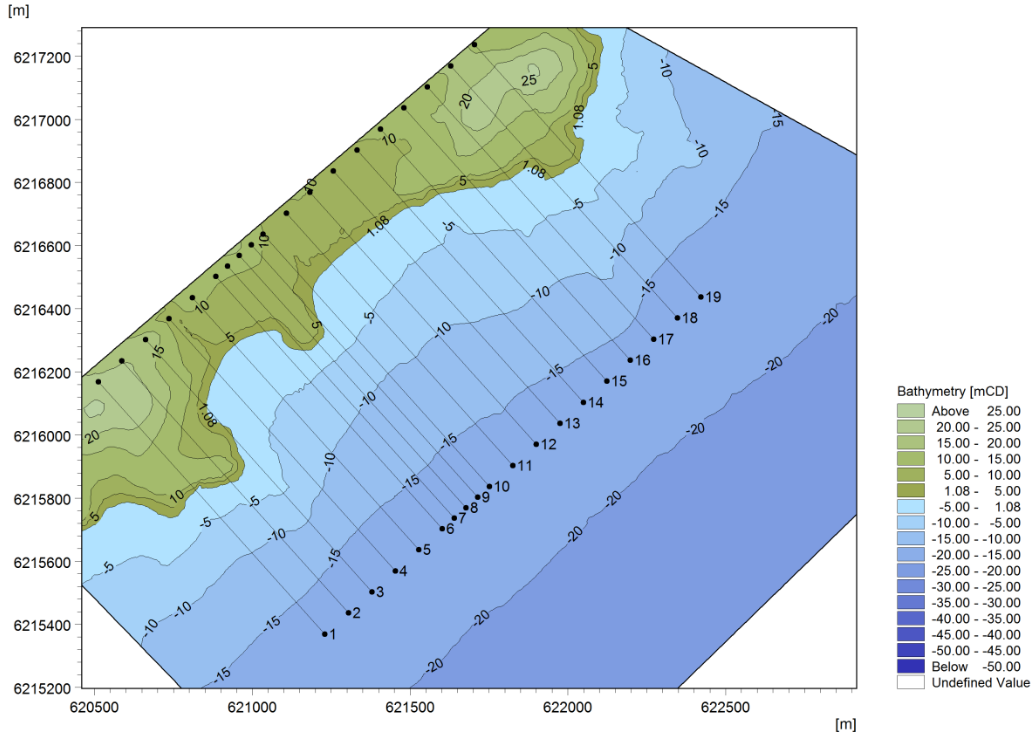

Figure 6-6 Model domain and profile locations

6.2.3 Sediment Characteristics

In addition to bathymetry, the bed roughness, mean grain diameter, and sediment fall velocity were defined for each profile. Sampling that was undertaken by the Ian Wark Research Institute, University of South Australia, indicated a mean grain diameter of 0.476mm for sediment around the site of interest.

The corresponding bed roughness was calculated using the relationship K_N=2.5d_{50}.

The sediment fall velocity was calculated using the following equation (DHI, 2009);

$$\omega = \sqrt{g(s-1)d} \cdot \left(\left(\frac{2}{3} + \frac{36v^2}{g(s-1)d^3} \right)^{1/2} - \left(\frac{36v^2}{g(s-1)d^3} \right)^{1/2} \right)$$

Where;

s = relative sediment density

g = gravity

ν = kinematic viscosity, found using the following equation:

$$v = \left(1.78 - 0.0570812T + 0.00106177T^2 - 8.27141 \cdot 10^{-6} T^3\right) \cdot 10^{-6}$$

Where;

T= water temperature in degrees centigrade

To help define the sediment properties, bed parameters were added as input into the Littoral Drift model. These characteristics included the relative sediment density, porosity, ripple parameters, and critical shields parameter as summarised below in Table 6-1.

Table 6-1 Input sediment characteristics

Sediment Parameter	Model Input
Mean grain diameter	0.476mm
Bed roughness	0.00119m
Sediment density	2650 kg/m^3
Sediment fall velocity	0.059m/s
Relative sediment density	2.59
Porosity	0.4
Ripple parameters	C1 = 0.1 C2 = 2.0 C3 = 16.0 C4 = 3.0
Critical shields parameter	0.045

Rocky outcrops identified in the profiles were specified as land and was assumed to be stable in the model.

6.2.4 Wave Conditions

To simulate the annual sediment drift for each beach profile in the littoral drift model, wave climates were extracted from the baseline 30 year wave model at the relevant offshore profile locations. The extracted wave climates were compared for the various extraction points, with the results indicating that similar wave climates were generated along the coast (see Appendix G). Hence the wave climate extracted offshore at profile 9, located in the middle of the domain, was adopted as a suitable representative climate for all profiles. Extracted parameters used as input into the model included Hrms (Hs/$\sqrt{2}$), Tp, mean wave direction, water level, and percent occurrence. These input wave conditions were developed for a 50 year period and run at varying water levels to take into account tidal variance, i.e. MSL, MHWS, MLWS. Figure 6-7 summarises the wave climate extracted offshore at profile 9.

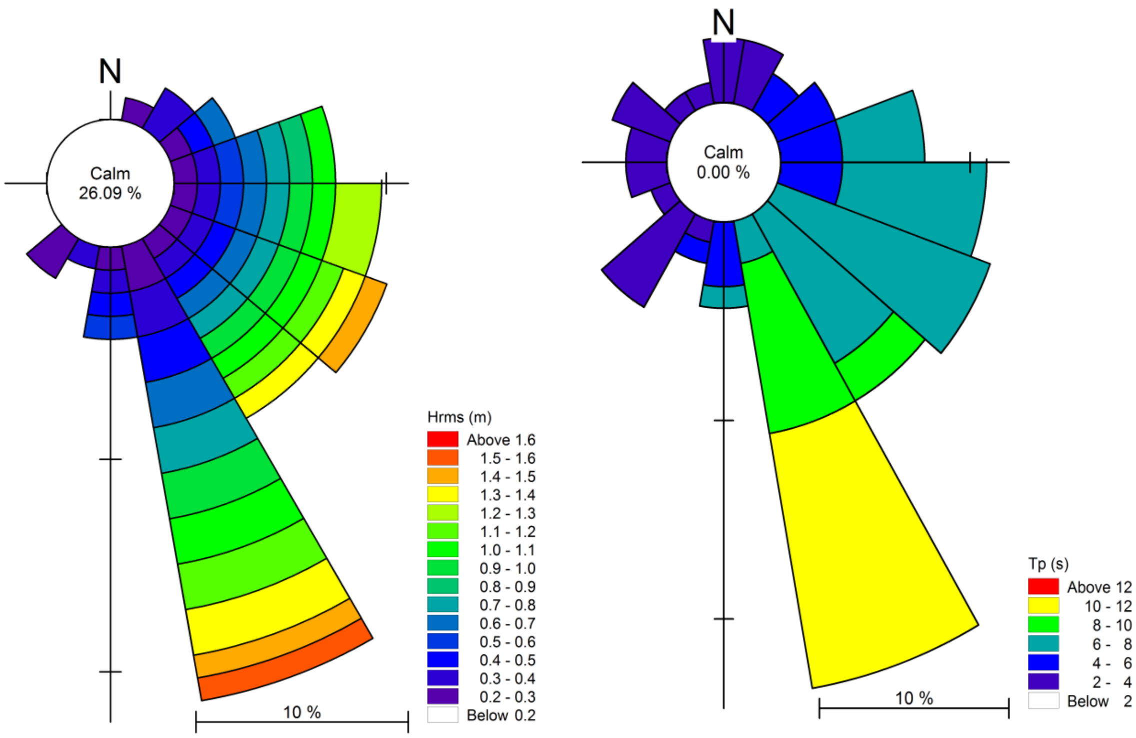

Figure 6-7 Wave rose of Hrms wave height and peak wave period for 50yr period

6.2.5 Model Setup

Longshore sediment transport rates were calculated for five cross shore profiles which represent the various profiles extracted along the shoreline (Figure 6-6). Profile 11 and 5 were selected to represent the cross shore profiles located within the northern and southern bays respectively, and profile 2, 8, and 19 were selected to represent cross shore profiles at each of the headlands. These five profiles are shown below in Figure 6-8.

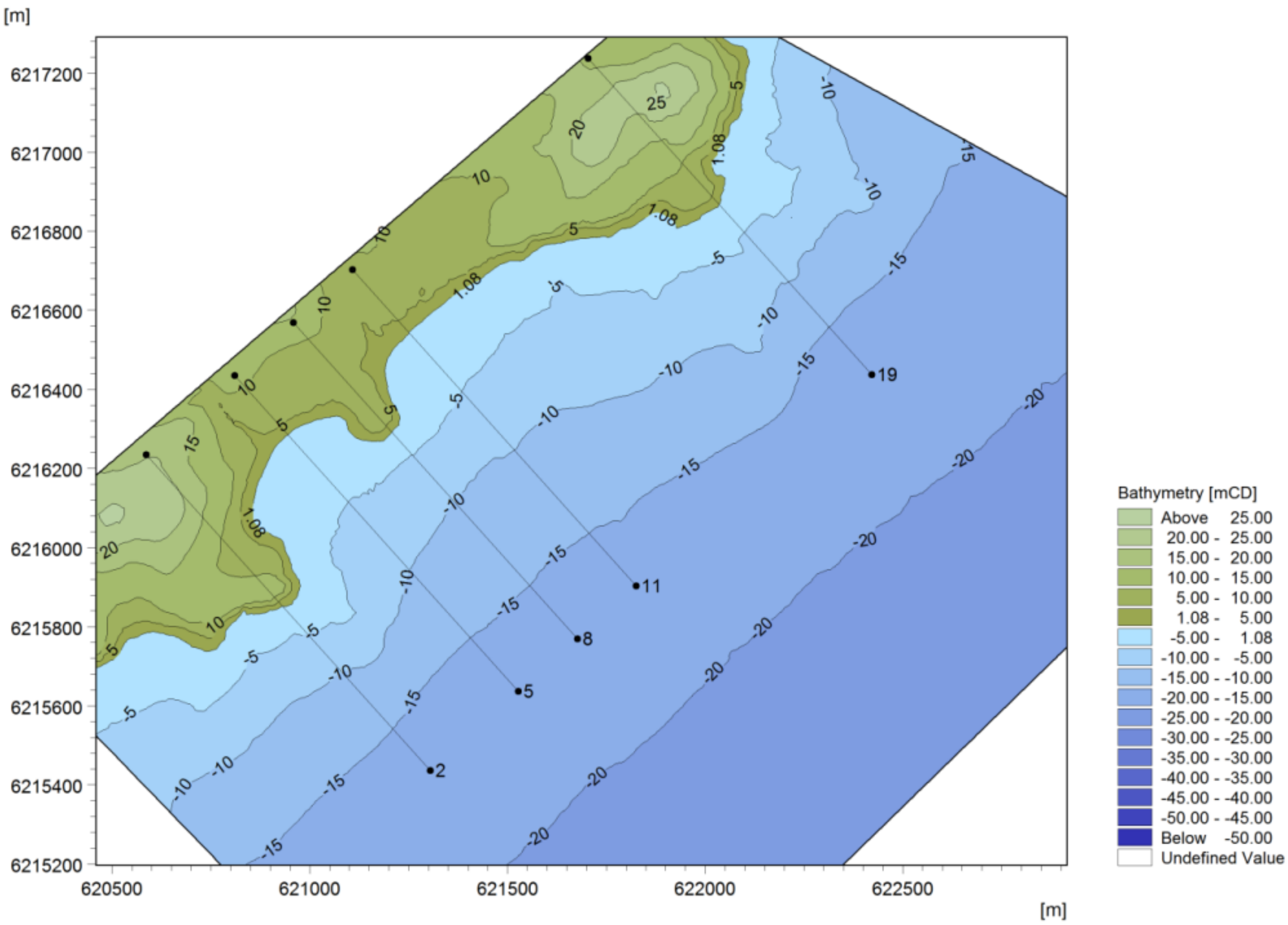

Figure 6-8 Representative cross shore profiles

6.2.6 Model Verification

The empirical Kamphius longshore transport equation, as shown in Appendix H, was adopted to verify the model outputs. Table 6-2 displays a comparison of these results for profile 11. Calculated estimates for the gross longshore transport are within the same order of magnitude to those predicted using the Littoral Drift model, with the Kamphius results correlating well to the gross transport rates estimated from the model.

Table 6-2 Longshore transport rates

Q_{LS}	Gross (m^3/yr)
$Q_{KAMPHIUS}$	220255
$Q_{MODELLED}$	238800

6.2.7 Model Results (Basecase)

The modelled gross and net longshore drift rates for profile 11 are shown in Figure 6-9. The profile cross section is comprised of fine sediment (d_{50}=0.476mm) offshore which continues to approximately +5mCD whereby it is then stabilised by dune vegetation. The littoral drift begins at the maximum water level run in the model (MHWS=1.82mCD) and ends at approximately -7mCD, which corresponds to the calculated depth of closure of 8m. The modelling results show a relatively large gross longshore drift within the northern bay (approximately 238800m^3/yr) demonstrating that the beach material is relatively mobile. The net drift (approximately 26990m^3/yr) is a low volume in comparison to the gross volume which demonstrates that the beach is relatively stable with a slight net northern drift.

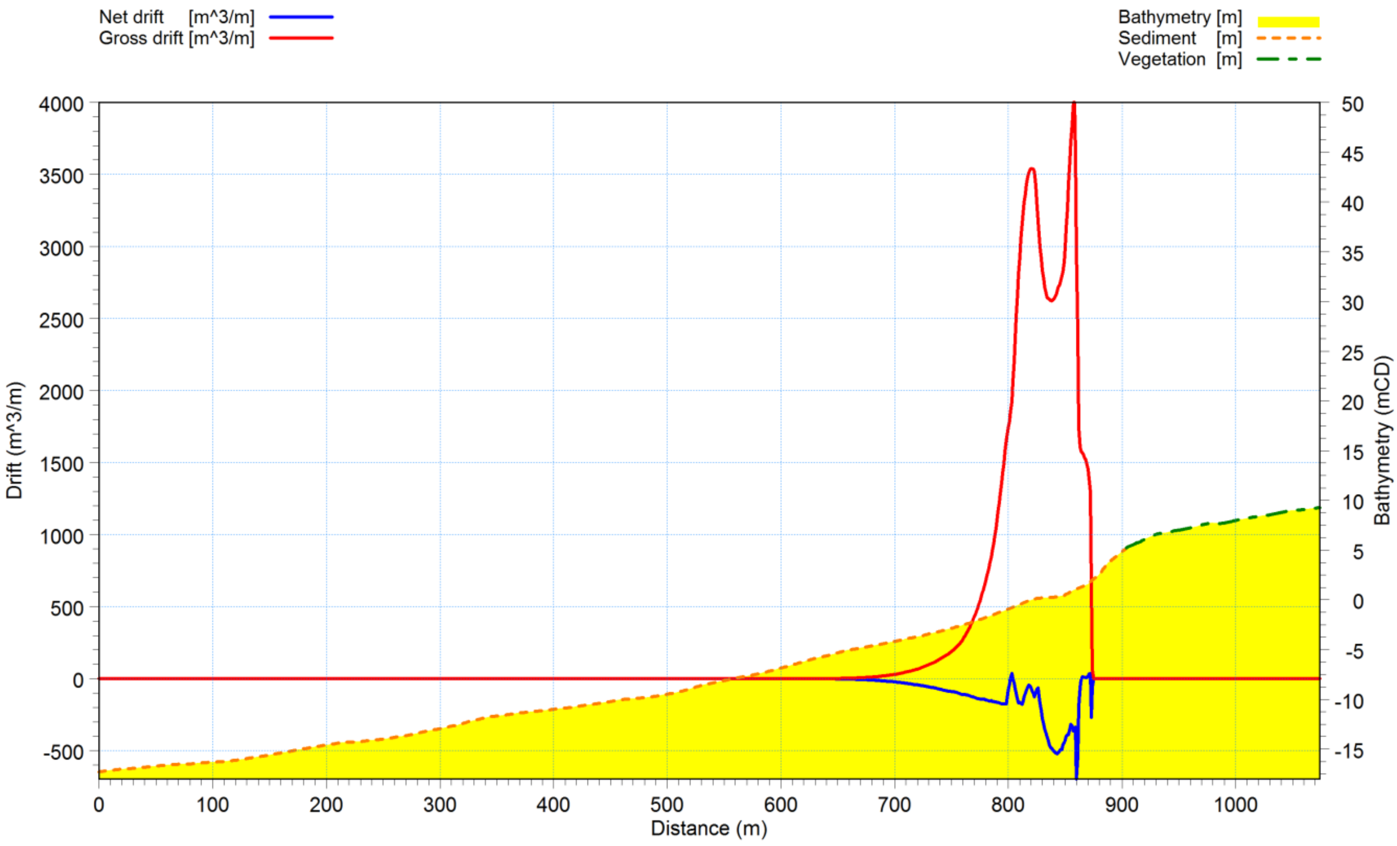

Figure 6-9 Annual gross and net longshore drift rates for profile 11 (northern bay)

Figure 6-10 shows the estimated longshore drift for the southern bay (profile 5). The drift rates indicate that the southern bay is also relatively stable, with a net transport rate of 27720m^3/yr to the north and a gross transport rate of 209200m^3/yr.

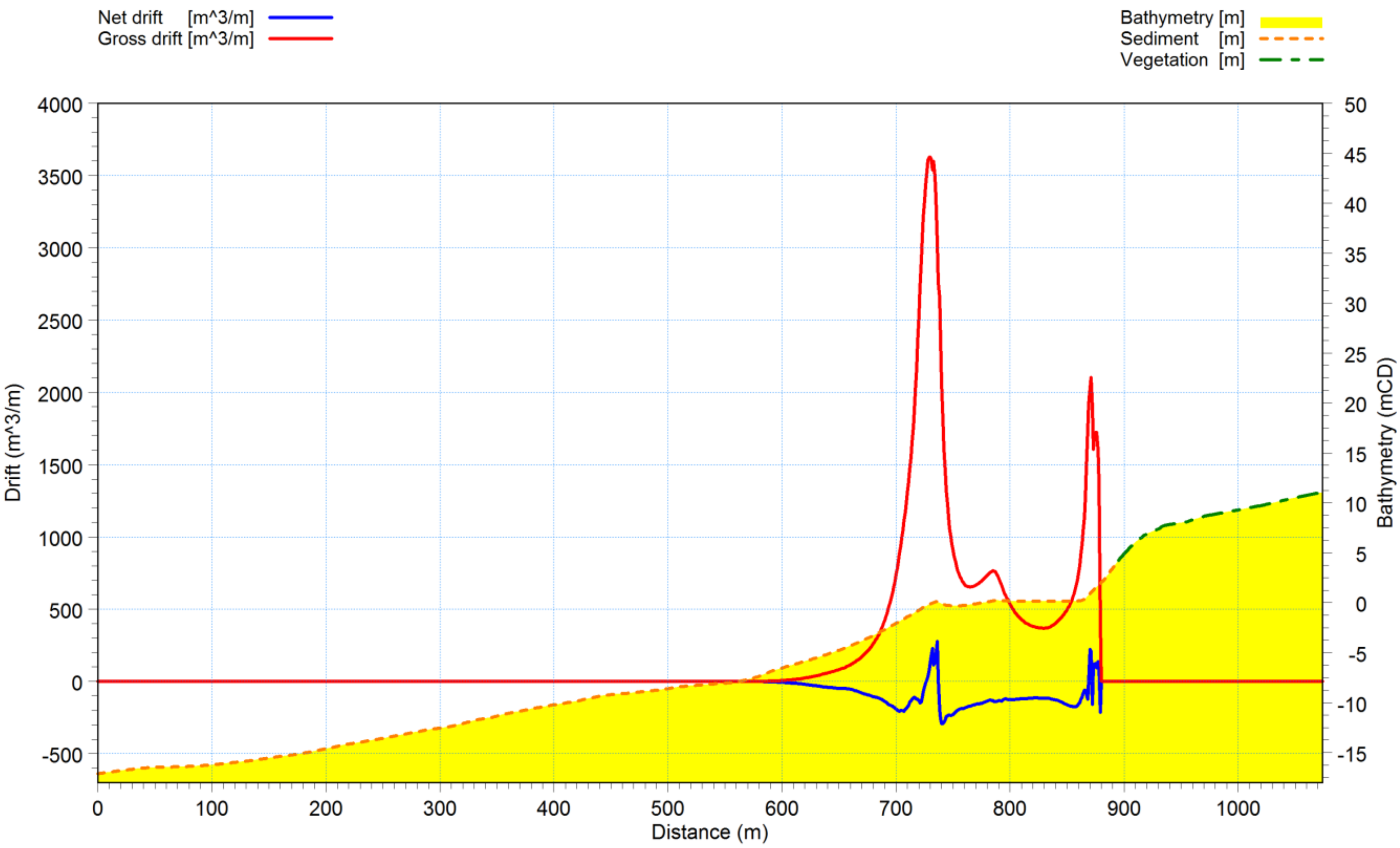

Figure 6-10 Annual gross and net longshore drift rates for profile 5 (southern bay)

The model results within the bays (profile 5 and 11) demonstrate that the bays are relatively stable showing a low net in relation to the gross longshore drift. This corresponds to the historic aerial photographic records which show limited shoreline changes over time. Although the overall net drift is shown to be south to north the volumes are relatively small in comparison to the overall gross drift and may vary from year to year. There is not a substantial build-up of sediment on the southern side of any of the headlands which implies that the net drift could be over predicted by the modelling.

The estimated net and gross longshore drift across the southern headland (profile 2) is shown in Figure 6-11. The rocky headland stabilises the the cross shore profile for approximately 600m, resulting in very little (if any) sediment drift over this region. Minimal sediment drift rates were predicted by the model showing a gross transport of 6157m^3/yr and a net northerly drift of 2480m^3/yr. These volumes are very low in comparison to the gross drift estimated in the embayments showing a significant restriction in sediment supply. The extent of the rocky headland has been estimated from aerial photography and bathymetric data, and could in fact extend further seaward which would cut off even more longshore sediment transport from entering the bay. Therefore taking into account the conservative representation of the headland and the level of accuracy of the model it is likely that the headland acts as terminal groyne, minimising longshore drift entering and leaving the southern bay.

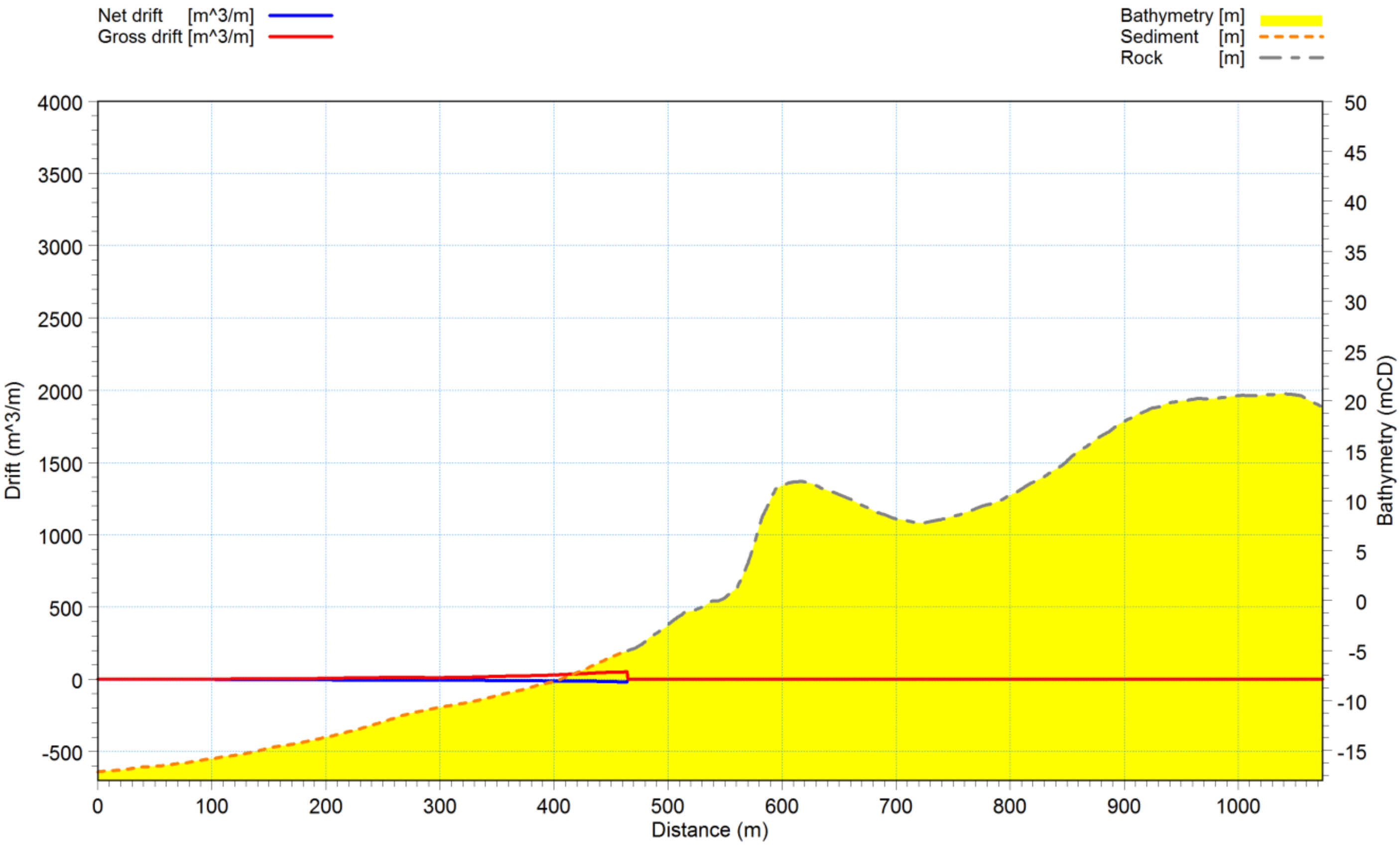

Figure 6-11 Annual gross and net longshore drift rates for profile 2 (southern headland)

The littoral drift for the northern headland (profile 19) is shown in Figure 6-12. Again it has been assumed that the rocky headland is extends 600m from the baseline. This results in minimal sediment entering or leaving the system with the headland essentially acting as a terminal groyne. The annual drift rates predicted by the model estimate a gross longshore transport of 6757m^3/yr and a net northerly transport of 2783m^3/yr past the northern headland. Again taking into account the conservative representation of the headland and the level of accuracy of the model it is likely that the headland acts as terminal groyne, minimising longshore drift entering and leaving the northern bay.

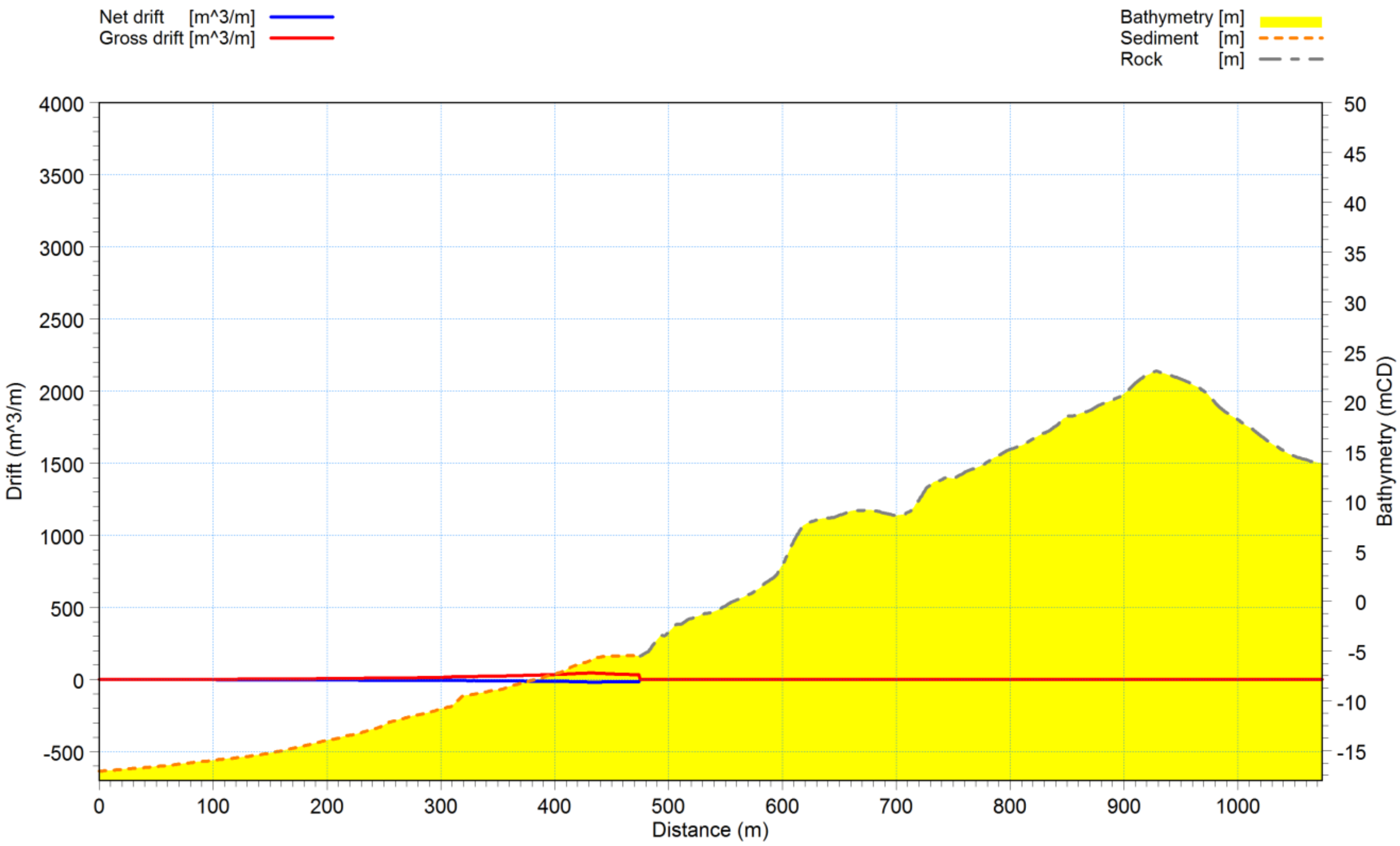

Figure 6-12 Annual gross and net longshore drift rates for profile 19 (northern headland)

Figure 6-13 shows the net and gross longshore drift across the middle headland (profile 8). It has been estimated from aerial photography and topographic data that the rocky headland extends out from the baseline approximately 450m. The longshore drift further offshore is marginally greater than that for the northern and southern headlands, however overall this is still a reasonably small volume of longshore drift. The model outputs indicate a gross transport of 6993m^3/yr and a net northerly drift of 2588m^3/yr. Hence it can be assumed that there is minimal sediment transport between the bays.

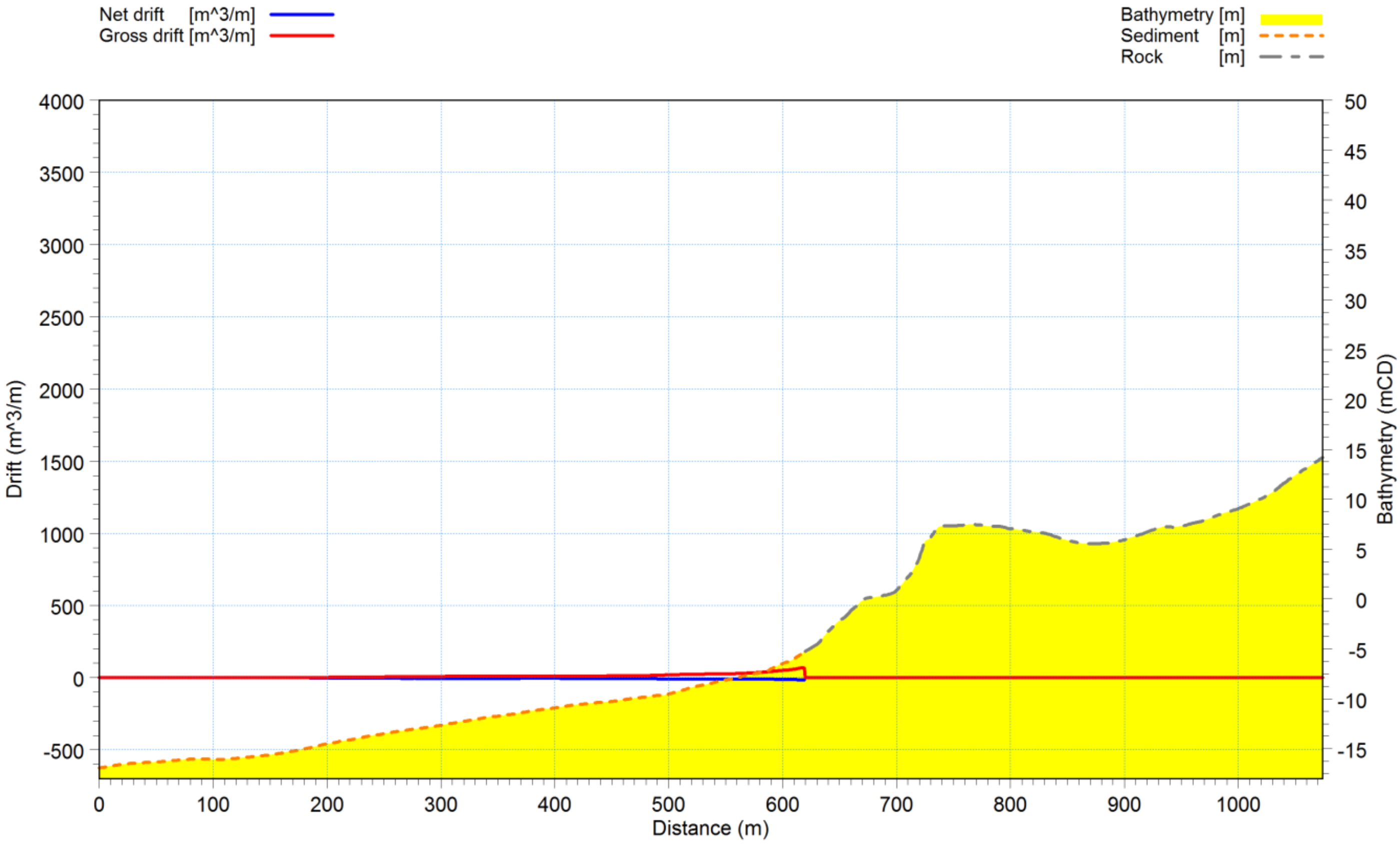

Figure 6-13 Annual gross and net longshore drift rates for profile 8 (middle headland)

6.2.8 Model Results (Development scenario)

The addition of the proposed reclaimed causeway and MOF facility essentially extends the headland further seaward, further restricting the sediment drift between the northern and southern bays. Figure 6-14 shows the extent of the proposed infrastructure plotted alongside the existing sediment drft volumes currently bypassing the middle headland. The plot shows that the addition of the proposed infrastructure will essentially prevent sediment from passing between the two bays. The model results have predicted that the gross drift bypassing the headland will be reduced from a volume of 6993m^3/yr to 1080m^3/yr. This could result in a build-up of sand in close proximity to the proposed structure.

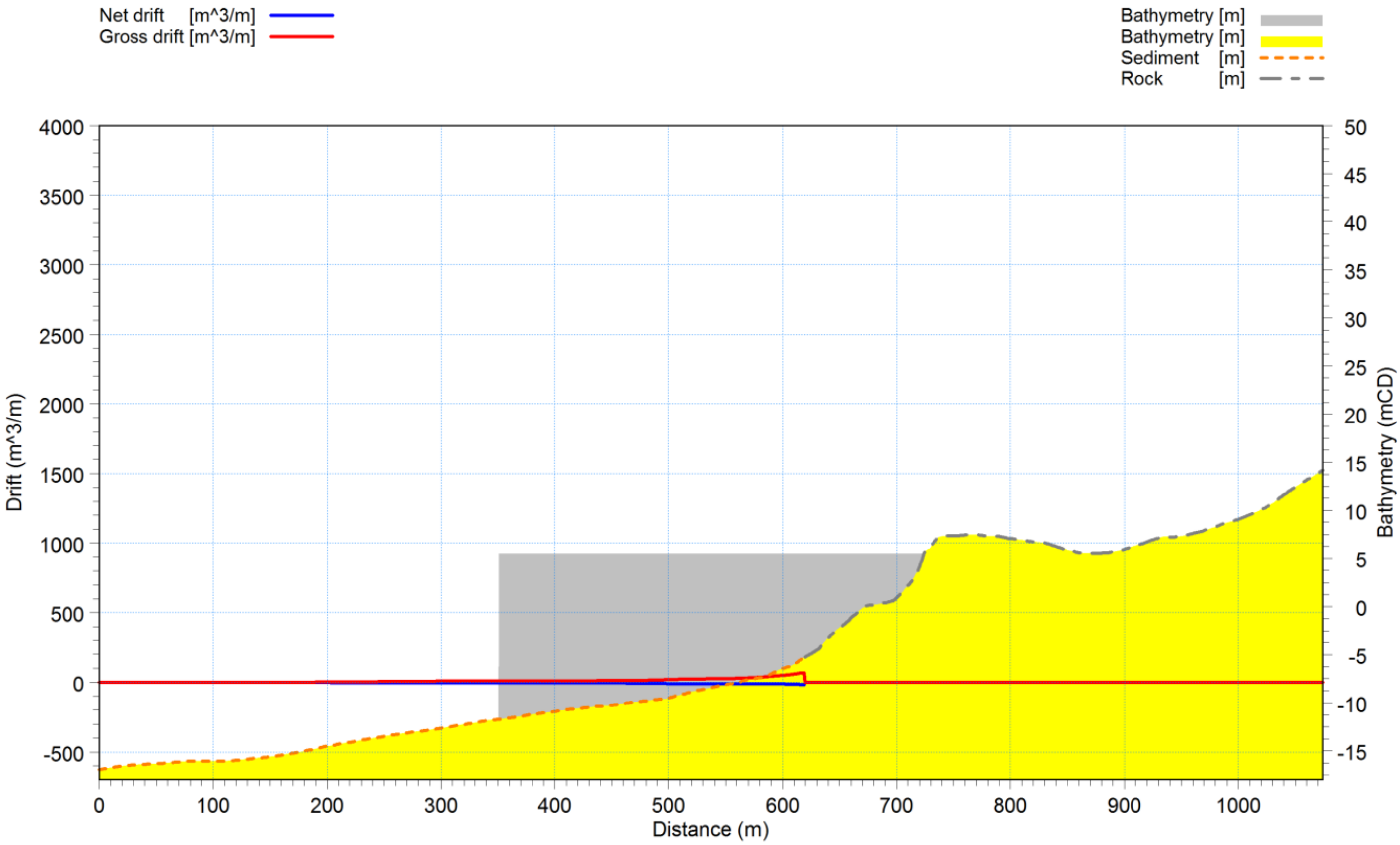

Figure 6-14 Causeway impact on longshore littoral drift rates (profile 8)

6.3 Conclusions

Littoral drift models have been run to assess the potential impacts of the causeway structure on the longshore sediment drift regime at the site. The results indicate that:

- A northerly net drift rate is observed along the coastline, corresponding to the predominant south easterly wave climate at Cape Hardy.
- Sediment drift across the headlands is restricted, with minimal net and gross longshore drift rates calculated for the corresponding cross shore profiles. This indicates that the headlands significantly restrict the sediment transport past the headlands into the adjacent bays.
- The construction of the causeway structure at the central headland is likely to accentuate the effects of the headland, further restricting the net and gross sediment drift past this point.

- Due to the low volumes of sediment passing the headlands, it is assumed that the northern and southern bays essentially act as closed cell beaches whereby the majority sediment transport is primarily restricted to within the bays.

Overall it is considered that the construction of the causeway and MOF infrastructure will further restrict the sediment transport between the northern and southern bays which may result in localised accretion and erosion, however the low net volumes bypassing the existing headlands implies that impacts will be minor.

7. Summary

Numerical modelling has been undertaken to assess the potential impacts associated with the proposed maritime infrastructure for the Central Eyre Iron Project. This infrastructure includes a reclaimed causeway with a Module Offload Facility, a tug mooring facility, as well as a jetty and wharf structure.

Numerical modelling has been undertaken using DHI MIKE21 models to assess the hydrodynamic and wave climate prior to and after construction. Similarly, the DHI MIKE Littoral Processes FM model has been used to assess any potential impacts on the longshore sediment transport in the region. Results from these models indicate the current, wave climate, and sediment transport regimes are impacted as follows:

- **Currents:** Changes to the nearshore and offshore current regimes are minor and localised. Any changes in the nearshore currents are predominately caused by the construction of the proposed causeway and MOF infrastructure, whilst offshore currents are predominately affected by the piling density along the wharf, jetty, and berthing dolphins.
- **Wave climate:** The orientation of the proposed causeway results in the wave climate at the northern bay remaining relatively unchanged after construction of the infrastructure. The wave climate within the southern bay is reduced by up to 0.4m due to the sheltering effect of the structure. Offshore wave conditions remain largely unchanged.
- **Nearshore sediment transport:** Bed shear stress calculations indicate that any nearshore sediment transport is a result of the prevailing wave climate at the site, with the wave induced bed shear stress above the 0.24N/m^2 threshold of motion. The current induced bed shear stress is below this threshold; hence it is unlikely that the currents will have a significant impact on sediment transport at the site.
- **Longshore sediment transport:** Overall it is considered that the construction of the causeway and MOF infrastructure will further restrict the sediment transport between the northern and southern bays which may result in localised accretion and erosion, however the low net volumes bypassing the existing headlands implies that there won't be a significant impact on the longshore sediment transport regime as the bays are already acting as closed cell systems impacts will be minor.

8. References

Abbott (2012), *Laser diffraction particle sizing of 15 marine sediment samples,* Ian Wark Research Institute, University of South Australia, Adelaide

DHI (2009), *LITSTP User Guide - Noncohesive Sediment Transport in Currents and Waves*, DHI, Denmark.

DHI (2009), *Littoral Processes FM – Scientific Documentation*, DHI, Denmark.

DHI (2009), *MIKE 21 SW User Guide – Spectral Waves FM Module*, DHI, Denmark.

DHI (2011), *MIKE 21 & MIKE 3 FLOW MODEL FM Hydrodynamic Module Short Description*, DHI, Denmark.

Soulsby (1997), *Dynamics of marine sands*, Thomas Telford Services Limited, London.

U.S. Army Corps of Engineers (1984), *Shore Protection Manual – Volume I*, U.S. Army Engineer Waterways Experiment Station Coastal Engineering Research Center, Vicksburg

Appendix A. Auswave model Wind Data summary

Table A-1 Wind speed/wind direction joint occurrence summary table for 2012 extracted from the BOM AUSWAVE model

Wind Speed (m/s)	Wind Direction (degrees)																		
	0-20	20-40	40-60	60-80	80-100	100-120	120-140	140-160	160-180	180-200	200-220	220-240	240-260	260-280	280-300	300-320	320-340	340-360	Grand Total
0-2	0.03%	0.14%	0.20%	0.14%	0.24%	0.24%	0.07%	0.10%	0.14%	0.07%	0.17%	0.14%	0.14%	0.17%	0.14%	0.10%	0.10%	0.14%	2.46%
2-4	0.61%	0.75%	0.99%	0.96%	1.02%	1.30%	1.20%	1.09%	0.96%	0.72%	0.48%	0.65%	0.31%	0.44%	0.48%	0.14%	0.38%	0.48%	12.94%
4-6	0.99%	1.13%	1.61%	1.71%	1.64%	1.81%	1.84%	2.29%	2.80%	1.95%	1.98%	1.26%	0.99%	0.96%	0.48%	0.61%	0.38%	0.51%	24.93%
6-8	1.30%	1.26%	1.23%	0.65%	1.20%	1.30%	1.54%	2.60%	1.98%	1.57%	2.66%	1.91%	1.61%	1.02%	1.16%	0.72%	0.51%	0.55%	24.76%
8-10	1.47%	0.55%	0.34%	0.55%	0.58%	0.75%	1.81%	2.70%	1.09%	0.82%	1.23%	1.88%	1.67%	0.99%	1.26%	0.31%	0.48%	0.38%	18.85%
10-12	0.89%	0.34%	0.07%	0.14%	0.10%	0.03%	0.58%	1.33%	0.31%	0.55%	1.06%	1.09%	0.65%	0.61%	0.58%	0.48%	0.27%	0.34%	9.43%
12-14	0.17%	0.14%	-	-	-	0.03%	0.17%	0.34%	0.34%	0.10%	0.38%	0.48%	0.44%	0.68%	0.41%	0.24%	0.10%	0.14%	4.17%
14-16	-	0.03%	-	-	-	-	0.10%	0.10%	0.10%	0.14%	0.17%	0.24%	0.24%	0.10%	0.27%	0.17%	-	-	1.67%
16-18	-	-	-	-	-	-	-	-	0.03%	0.03%	0.03%	0.07%	0.14%	0.20%	-	-	-	0.03%	0.55%
18-20	-	-	-	-	-	-	-	-	-	-	0.03%	-	-	0.03%	0.03%	0.03%	-	-	0.14%
20-22	-	-	-	-	-	-	-	-	-	-	-	0.03%	-	-	0.07%	-	-	-	0.10%
Grand Total	5.46%	4.34%	4.44%	4.13%	4.78%	5.46%	7.31%	10.55%	7.75%	5.94%	8.20%	7.75%	6.18%	5.23%	4.88%	2.80%	2.22%	2.56%	100.00%

Appendix B. ADCP data

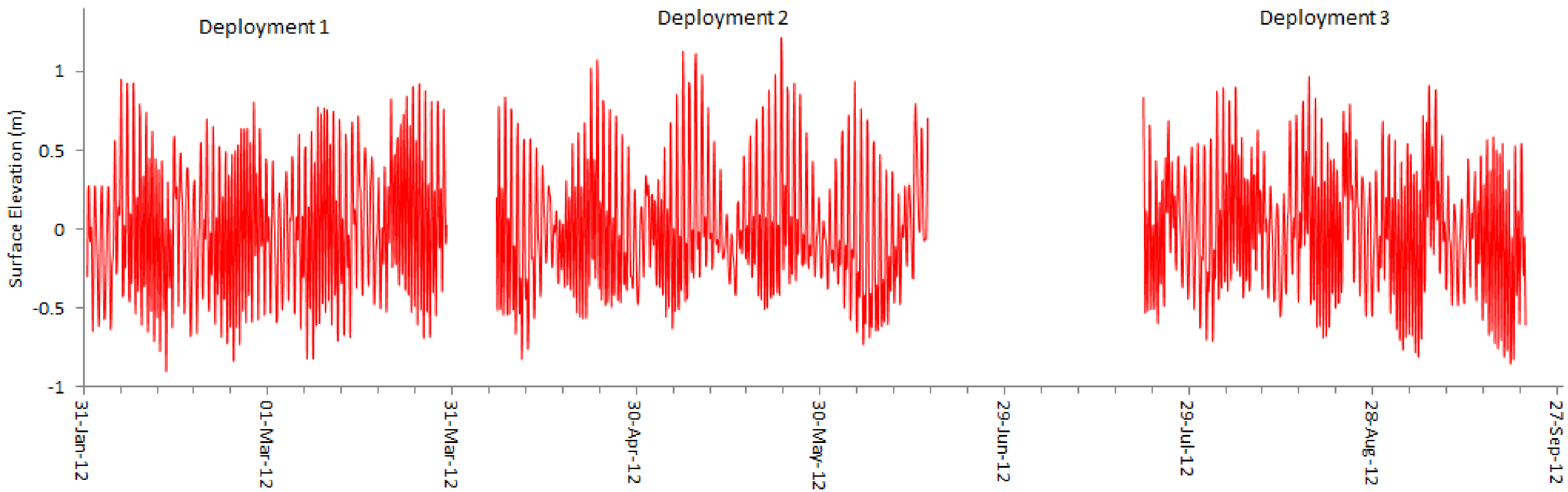

Figure B-1 ADCP measured surface elevation from 31/01/2012 to 21/09/2012

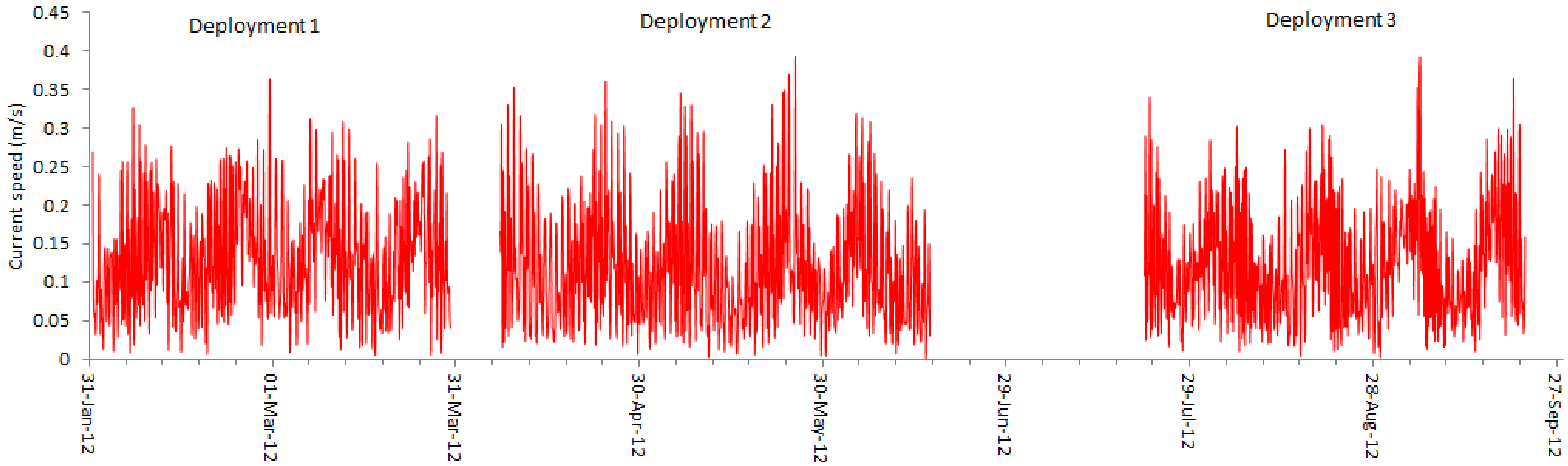

Figure B-2 ADCP measured current speed from 31/01/2012 to 21/09/2012

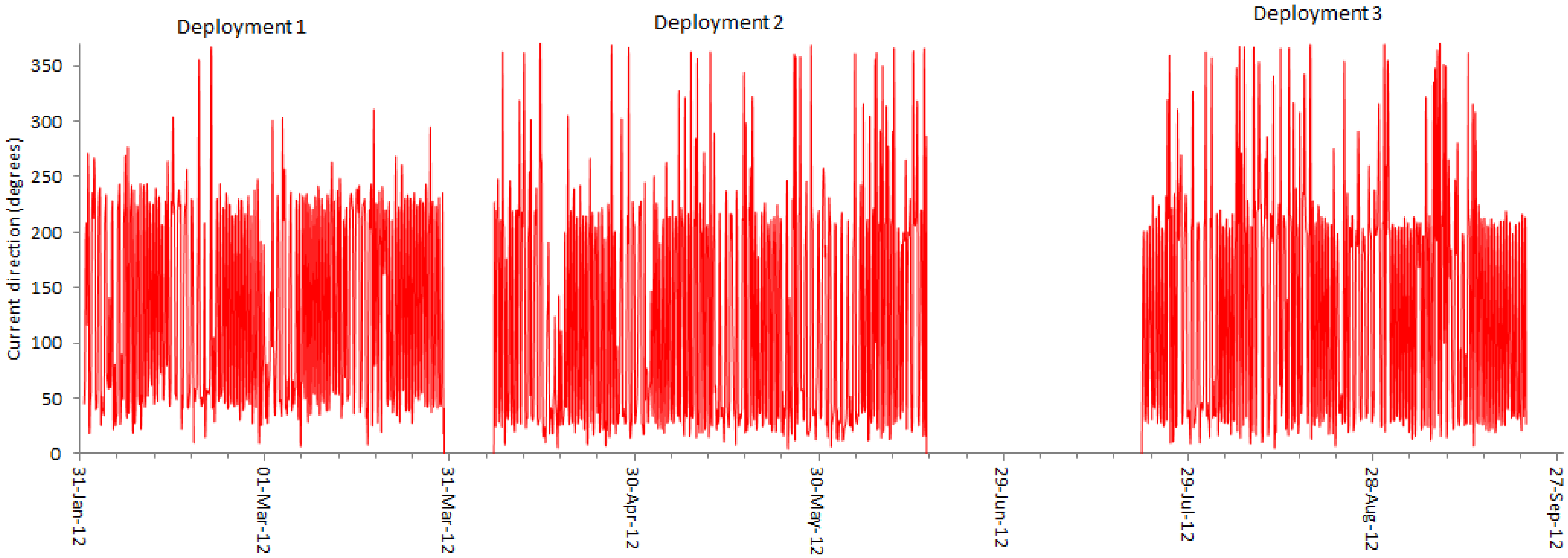

Figure B-3 ADCP measured current direction from 31/01/2012 to 21/09/2012

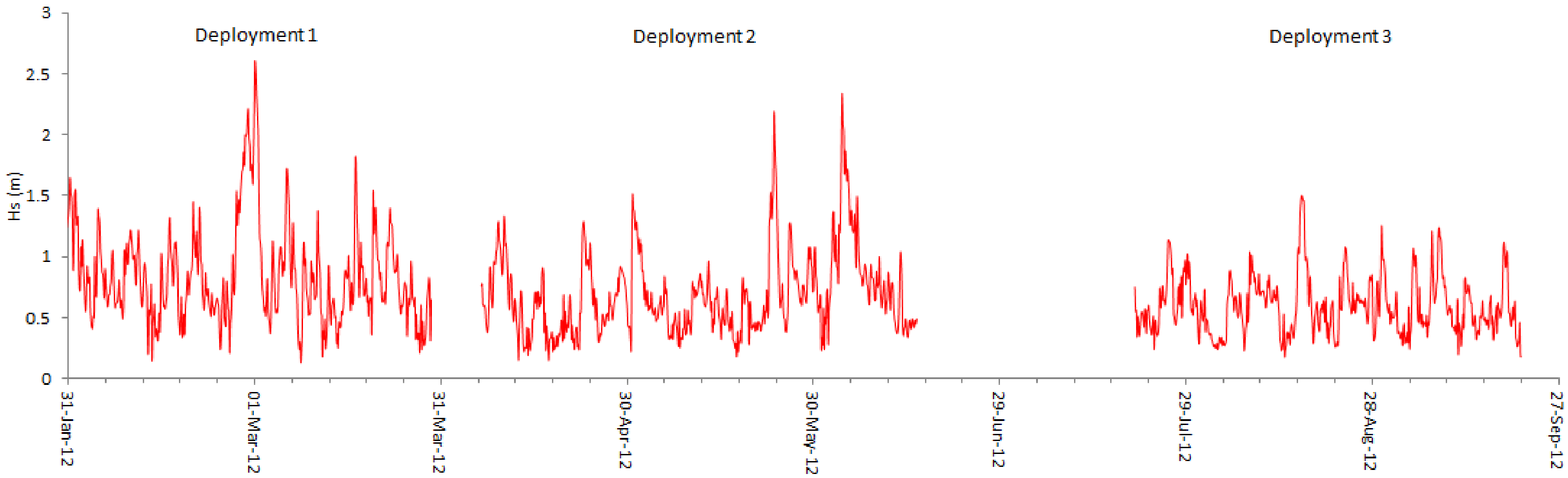

Figure B-4 ADCP measured significant wave height from 31/01/2012 to 21/09/2012

Figure B-5 ADCP measured peak wave period from 31/01/2012 to 21/09/2012

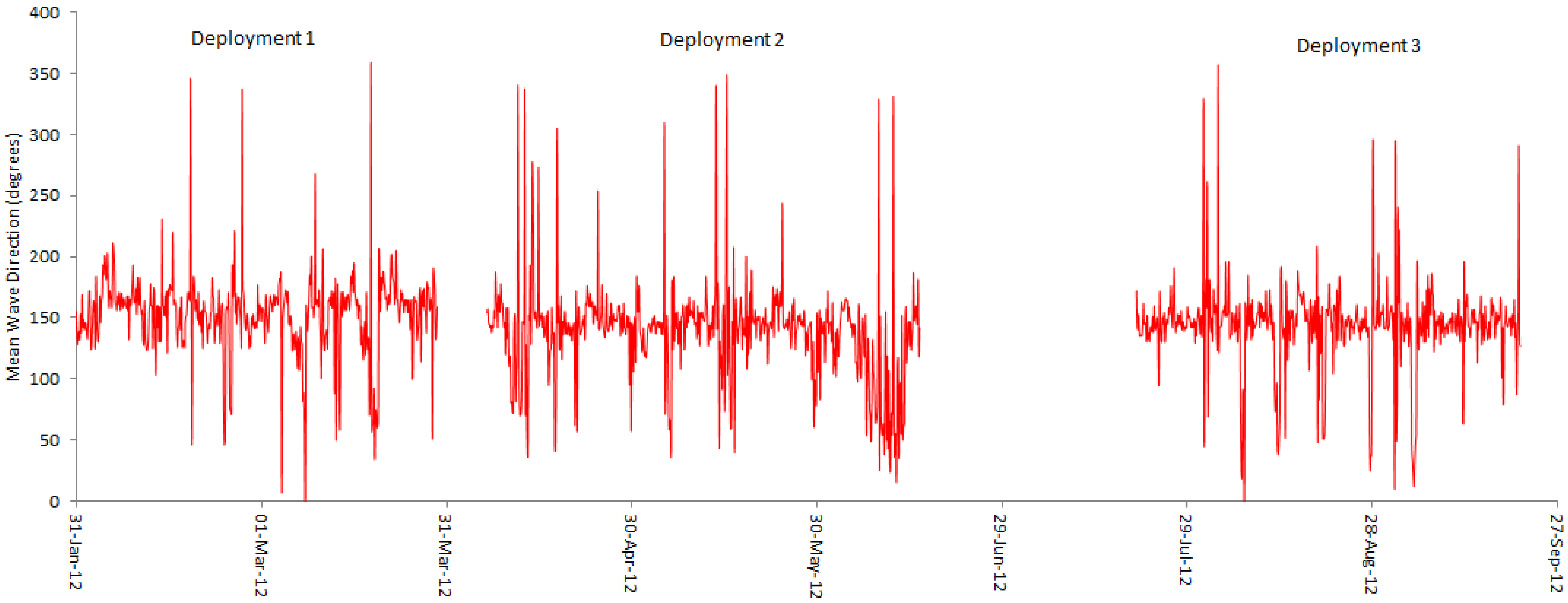

Figure B-6 ADCP mean wave direction from 31/01/2012 to 21/09/2012

Appendix C. Wave Dataset Summary

A.1 2012 Wave Dataset

An annual wave dataset was extracted from the BOM AUSWAVE model for the year 2012. Data was extracted from the model at the location shown in Figure C-1. Wave direction, wave period, and significant wave height data was extracted from the model and is summarised in the wave height and wave period directional rose plots in Figure C-2 and Figure C-3 respectively.

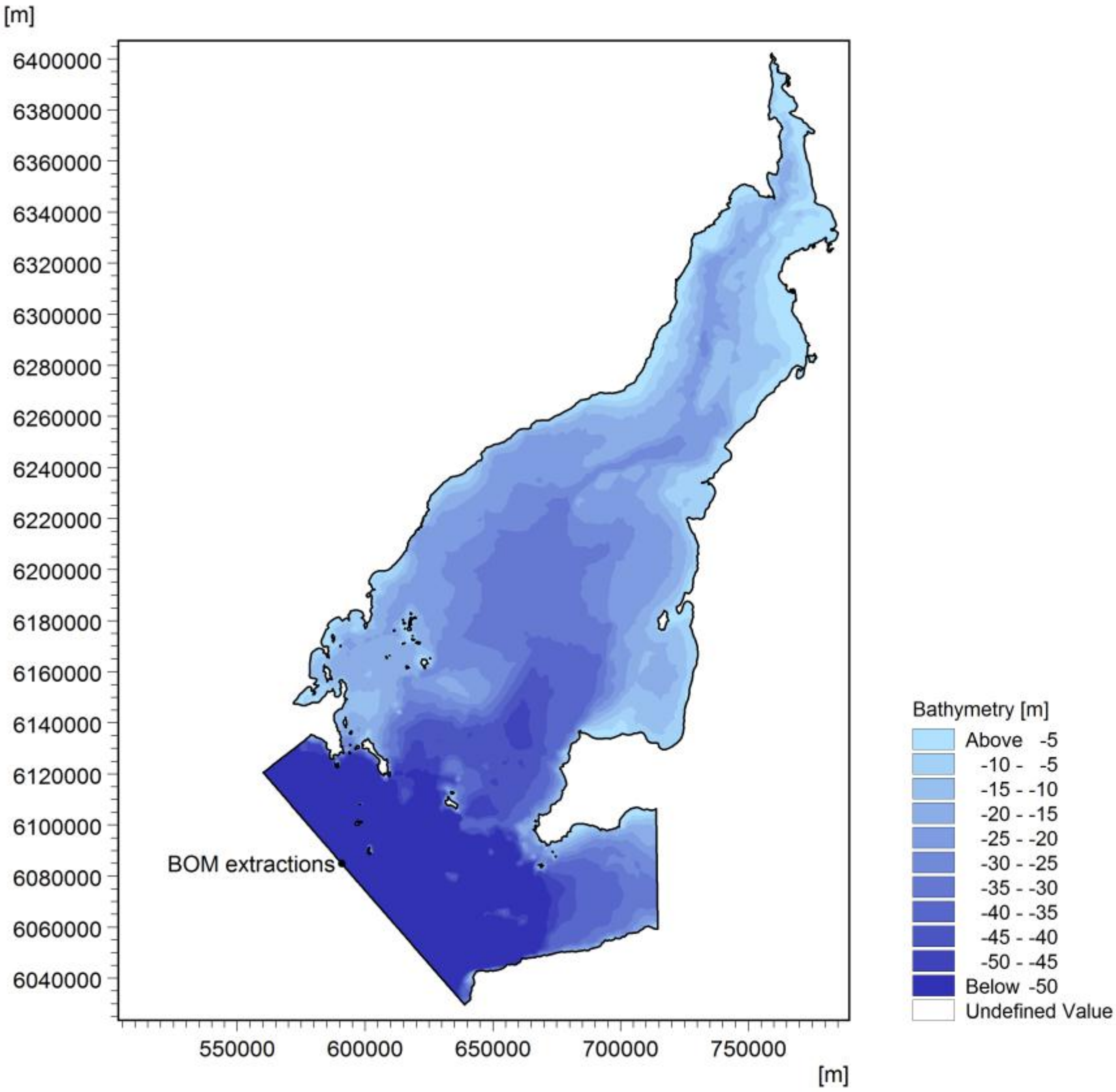

Figure C-1 AUSWAVE Extraction location

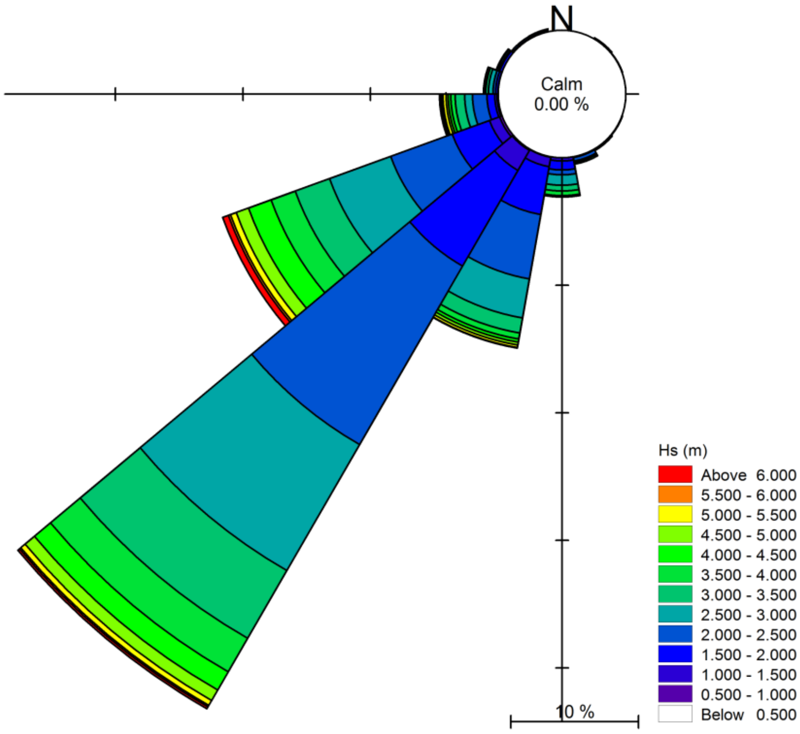

Figure C-2 Wave rose for Hs and mean wave direction for the year 2012 (BOM AUSWAVE)

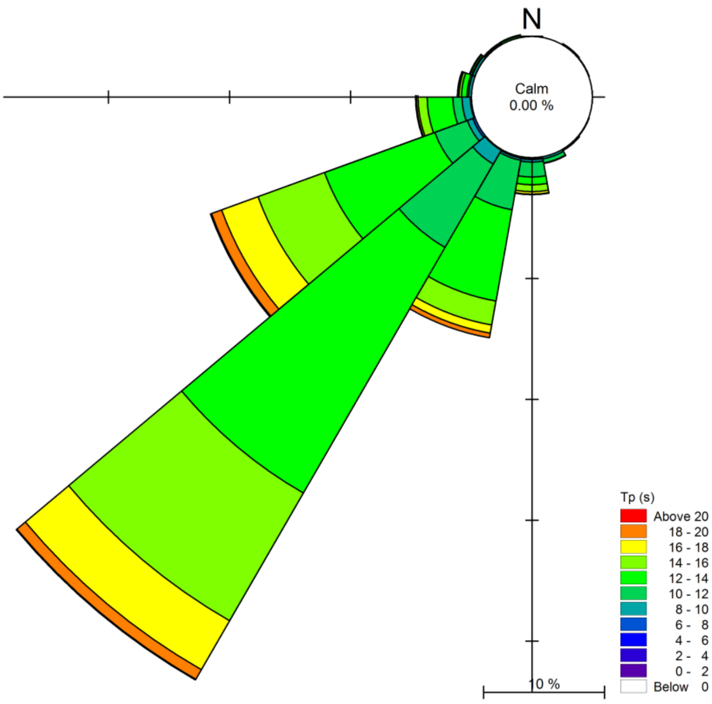

Figure C-3 Wave Rose for Tp and mean wave direction for the year 2012 (BOM AU SWAVE)

A.2 Long Term Wave Dataset

Significant wave height, wave period, and wave direction were also extracted from the BOM WAVEWATCH III model. This data is summarised below in Figure C-4 and Figure C-5.

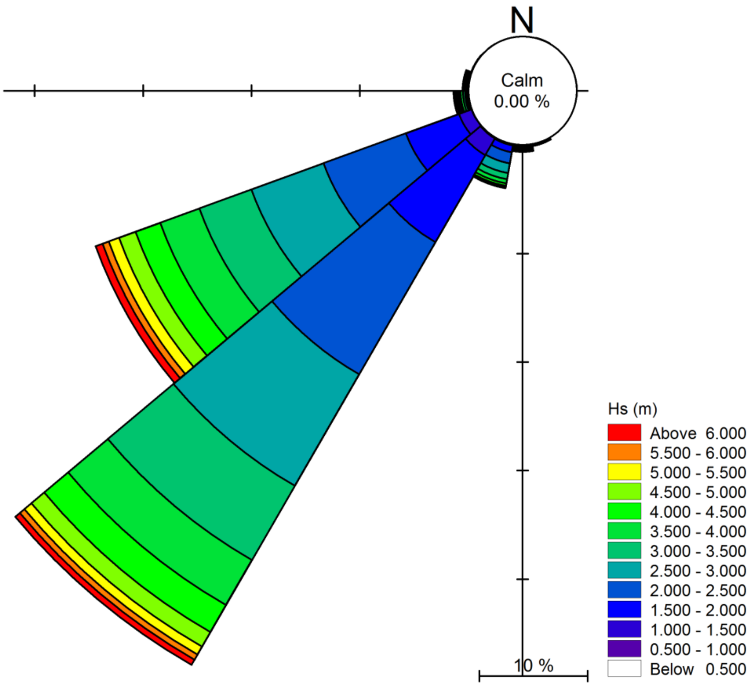

Figure C-4 Wave rose for Hs and peak wave direction for 1979–2009 (BOM WAVEWATCH III)

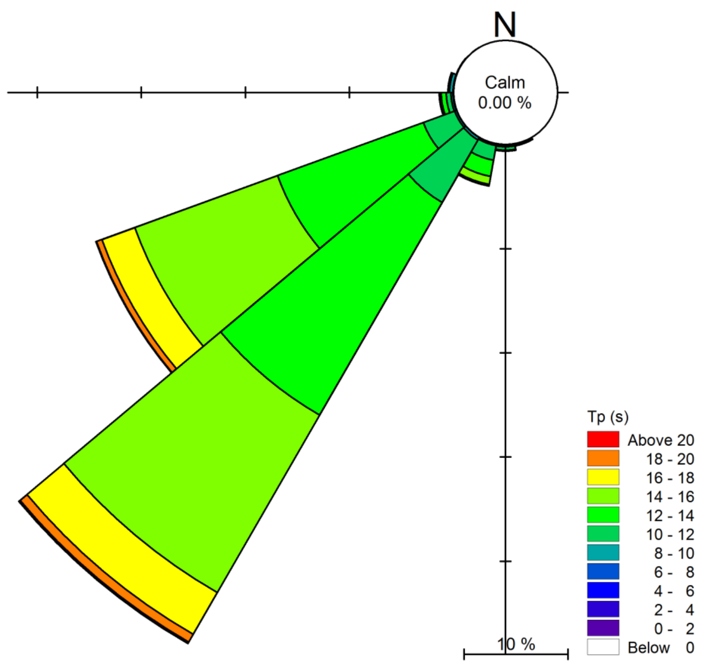

Figure C-5 Wave rose for Tp and peak wave direction for 1979-2009 (BOM WAVEWATCH |||)

A.3 Offshore Wave Condition Summary

Offshore waves are dominated by swell waves generated in the Southern ocean. Offshore peak wave periods are generally greater than 10s and less than 18s. The ocean swell is predominantly approaches from the south westerly quadrant between 200 and 240degTN. Significant wave heights are generally greater than 1m and less than 5m.

Appendix D. 30 year wave model summary

Table D-8-1 30 year wave height and directional occurrence table at site location

Hs (m)	Mean Wave Direction (degrees)																		
	0-20	20-40	40-60	60-80	80-100	100-120	120-140	140-160	160-180	180-200	200-220	220-240	240-260	260-280	280-300	300-320	320-340	340-360	Grand Total
0-0.2	-	-	-	-	-	-	0.01%	0.10%	0.04%	0.02%	0.01%	0.02%	0.02%	0.02%	0.02%	0.02%	0.01%	0.01%	0.31%
0.2-0.4	0.03%	0.07%	0.03%	0.04%	0.07%	0.17%	0.72%	4.56%	1.12%	0.15%	0.18%	0.12%	0.06%	0.02%	0.02%	0.01%	0.02%	0.03%	7.41%
0.4-0.6	-	0.02%	0.06%	0.31%	0.73%	1.10%	2.34%	15.76 %	2.46%	0.23%	0.10%	0.00%	-	-	-	-	-	-	23.11%
0.6-0.8	-	-	0.03%	0.87%	1.78%	2.07%	3.40%	16.54 %	1.70%	0.07%	-	-	-	-	-	-	-	-	26.47%
0.8-1	-	-	0.02%	0.84%	2.50%	2.54%	3.80%	10.81 %	0.91%	0.01%	-	-	-	-	-	-	-	-	21.42%
1-1.2	-	-	-	0.35%	1.38%	2.17%	3.54%	5.17%	0.35%	-	-	-	-	-	-	-	-	-	12.96%
1.2-1.4	-	-	-	0.08%	0.46%	1.01%	2.24%	2.00%	0.13%	-	-	-	-	-	-	-	-	-	5.93%
1.4-1.6	-	-	-	0.01%	0.10%	0.27%	0.79%	0.63%	0.04%	-	-	-	-	-	-	-	-	-	1.84%
1.6-1.8	-	-	-	-	0.02%	0.05%	0.17%	0.19%	0.00%	-	-	-	-	-	-	-	-	-	0.43%
1.8-2	-	-	-	-	-	0.01%	0.02%	0.06%	0.01%	-	-	-	-	-	-	-	-	-	0.10%
2-2.2	-	-	-	-	-	-	-	0.02%	-	-	-	-	-	-	-	-	-	-	0.02%
2.2-2.4	-	-	-	-	-	-	-	-	-	-	-	-	-	-	-	-	-	-	0.00%
Grand Total	0.03%	0.09%	0.14%	2.50%	7.05%	9.40%	17.02 %	55.84 %	6.75%	0.47%	0.28%	0.14%	0.08%	0.04%	0.05%	0.03%	0.03%	0.04%	100.00%

Table D-8-2 30 year wave period and directional occurrence table at site location

Tp (s)	Mean Wave Direction (degrees)																	
	0-20	20-40	40-60	60-80	80-100	100-120	120-140	140-160	160-180	180-200	200-220	220-240	240-260	260-280	280-300	300-320	320-340	340-360	Grand Total
0-2	-	-	-	-	-	-	-	-	-	-	-	-	0.01%	0.02%	0.03%	0.01%	0.01%	-	0.06%
2-4	0.03%	0.08%	0.04%	0.01%	0.00%	0.00%	0.01%	0.01%	0.03%	0.08%	0.27%	0.14%	0.07%	0.03%	0.02%	0.02%	0.02%	0.04%	0.91%
4-6	-	0.01%	0.10%	2.09%	3.78%	2.85%	1.18%	0.27%	0.64%	0.39%	0.01%	-	-	-	-	-	-	-	11.32%
6-8	-	-	-	0.40%	3.27%	6.49%	13.14%	5.63%	2.89%	0.01%	-	-	-	-	-	-	-	-	31.83%
8-10	-	-	-	-	-	0.06%	2.67%	17.06%	3.16%	-	-	-	-	-	-	-	-	-	22.95%
10-12	-	-	-	-	-	-	0.02%	22.67%	0.03%	-	-	-	-	-	-	-	-	-	22.72%
12-14	-	-	-	-	-	-	-	9.15%	-	-	-	-	-	-	-	-	-	-	9.15%
14-16	-	-	-	-	-	-	-	0.96%	-	-	-	-	-	-	-	-	-	-	0.96%
16-18	-	-	-	-	-	-	-	0.09%	-	-	-	-	-	-	-	-	-	-	0.09%
18-20	-	-	-	-	-	-	-	-	-	-	-	-	-	-	-	-	-	-	-
Grand Total	0.03%	0.09%	0.14%	2.50%	7.05%	9.40%	17.02%	55.84%	6.75%	0.47%	0.28%	0.14%	0.08%	0.04%	0.05%	0.03%	0.03%	0.04%	100.00%

Appendix E. Site photographs

Figure E-1 Southern headland

Figure E-2 Northern headland

Figure E-3 Northern headland taken from middle headland

Figure E-4 Southern headland taken from middle headland

Figure E-5 Southern headland

Figure E-6 Southern headland

Appendix F. Aerial photography

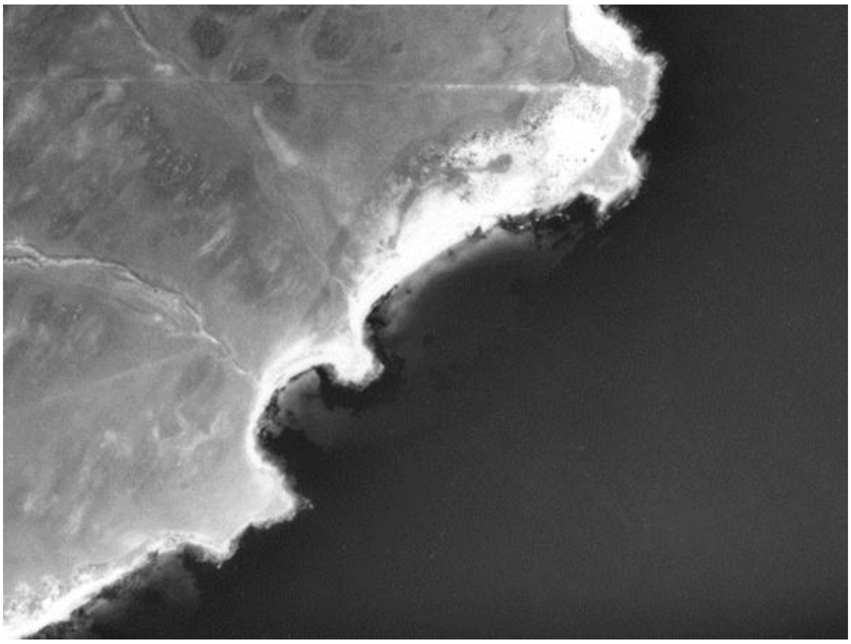

Figure F-1 Aerial photograph taken 1973

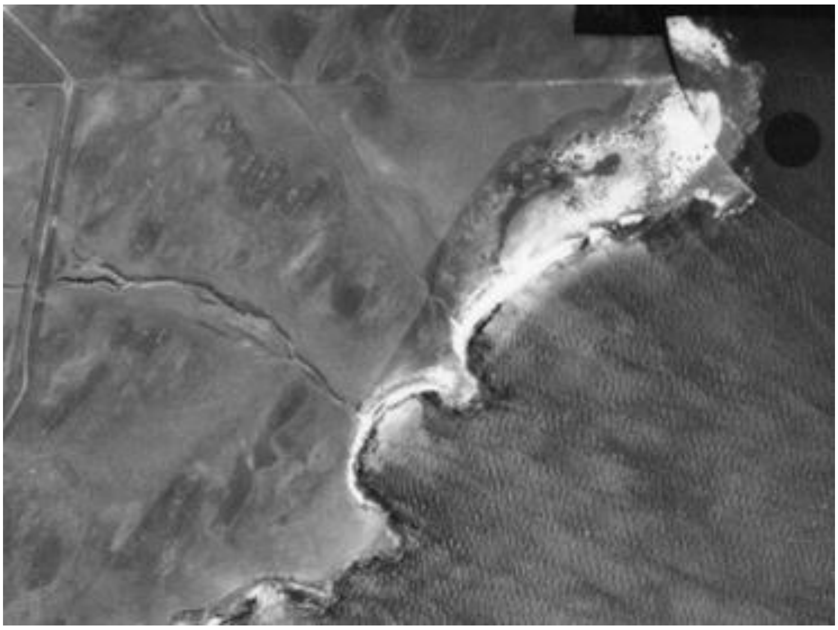

Figure F-2 Aerial photograph taken 1973

Figure F-3 Aerial photograph taken 1986

Figure F-4 Aerial photograph taken 1992

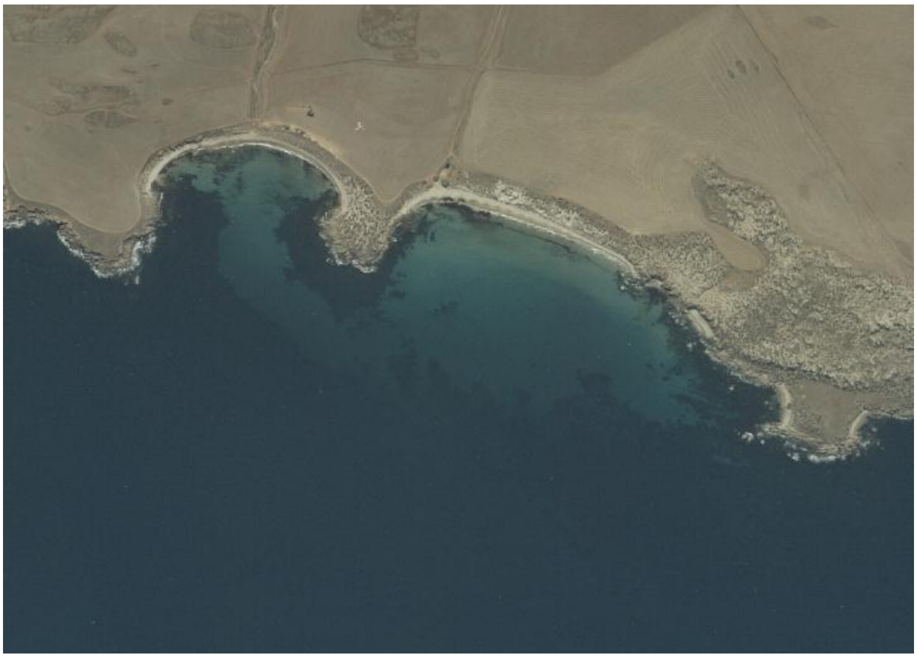

Figure F-5 Aerial photograph 2004

Figure F-6 Aerial Photography January 2012

Appendix G. Comparison of extracted wave climates

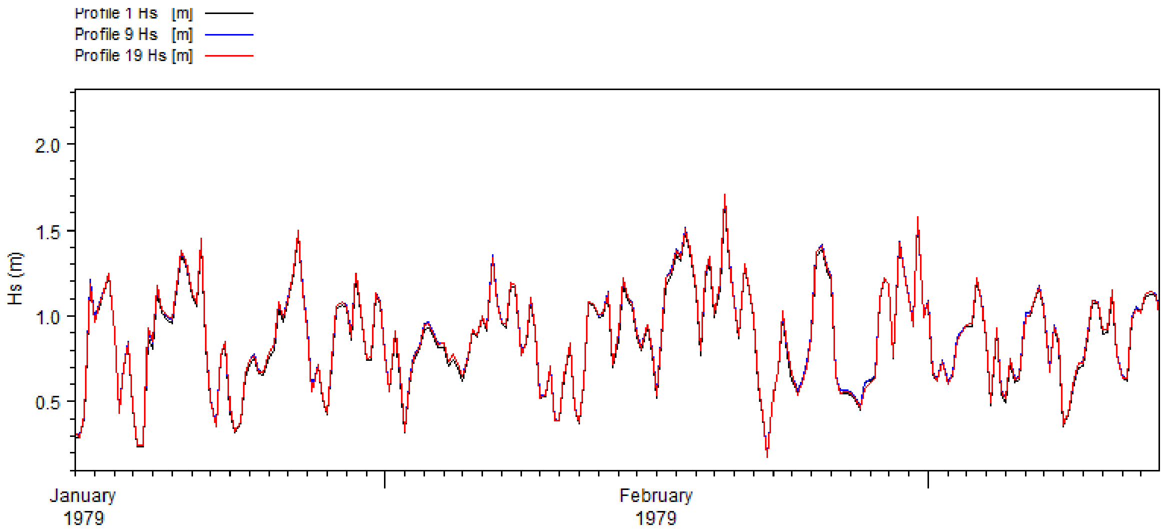

Figure G-1 Extracted wave heights for profiles 1 (south), 9 (middle), and 19 (north)

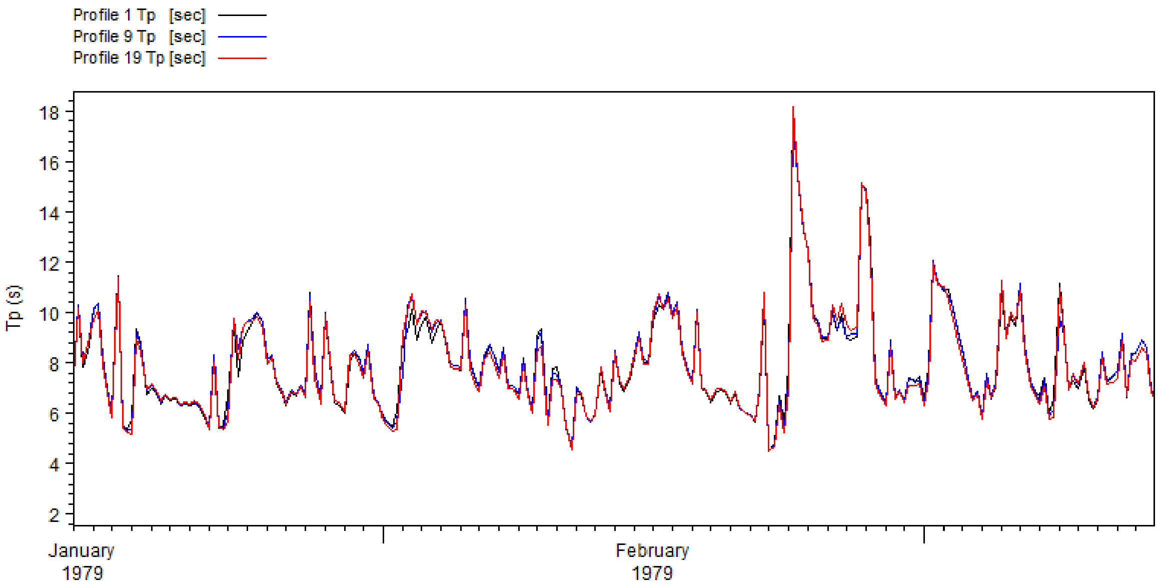

Figure G-2 Extracted wave periods for profiles 1 (south), 9 (middle), and 19 (north)

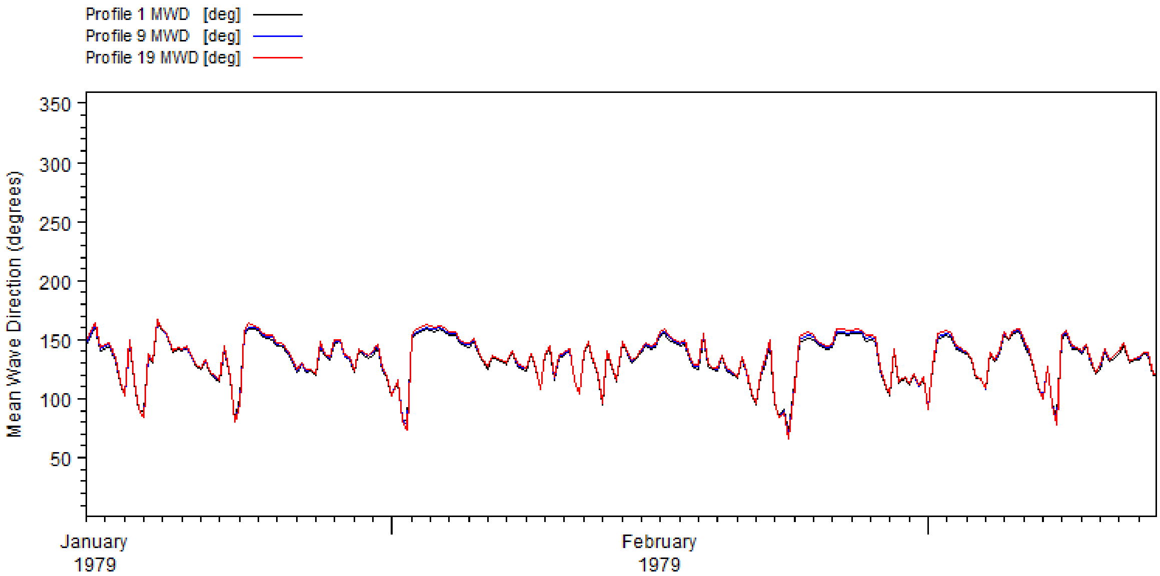

Figure G-3 Extracted mean wave directions for profiles 1 (south), 9 (middle), and 19 (north)

Appendix H. Longshore sediment transport equation

Kamphius Formula (USACE, 2002)

$$Q = 6.4 \times 10^{4} H_{sb}^{2} T_{p}^{1.5} m^{0.75} d^{-0.25} \sin^{0.6}\left(2\theta_{b}\right)$$

Where;

m = beach slope

d = sediment grain size

H_{sb} = significant breaking wave height

θ_b = breaker wave angle